

Enhanced damage modelling for fracture and fatigue

Citation for published version (APA):

Peerlings, R. H. J. (1999). *Enhanced damage modelling for fracture and fatigue*. [Phd Thesis 1 (Research TU/e / Graduation TU/e), Mechanical Engineering]. Technische Universiteit Eindhoven.
<https://doi.org/10.6100/IR520108>

DOI:

[10.6100/IR520108](https://doi.org/10.6100/IR520108)

Document status and date:

Published: 01/01/1999

Document Version:

Publisher's PDF, also known as Version of Record (includes final page, issue and volume numbers)

Please check the document version of this publication:

- A submitted manuscript is the version of the article upon submission and before peer-review. There can be important differences between the submitted version and the official published version of record. People interested in the research are advised to contact the author for the final version of the publication, or visit the DOI to the publisher's website.
- The final author version and the galley proof are versions of the publication after peer review.
- The final published version features the final layout of the paper including the volume, issue and page numbers.

[Link to publication](#)

General rights

Copyright and moral rights for the publications made accessible in the public portal are retained by the authors and/or other copyright owners and it is a condition of accessing publications that users recognise and abide by the legal requirements associated with these rights.

- Users may download and print one copy of any publication from the public portal for the purpose of private study or research.
- You may not further distribute the material or use it for any profit-making activity or commercial gain
- You may freely distribute the URL identifying the publication in the public portal.

If the publication is distributed under the terms of Article 25fa of the Dutch Copyright Act, indicated by the "Taverne" license above, please follow below link for the End User Agreement:

www.tue.nl/taverne

Take down policy

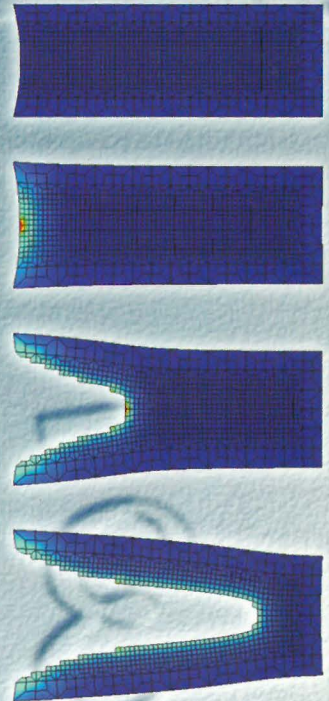
If you believe that this document breaches copyright please contact us at:

openaccess@tue.nl

providing details and we will investigate your claim.

APA
99
PEE

Enhanced damage modelling for fracture and fatigue



R.H.J. Peerlings

Enhanced damage modelling for fracture and fatigue

Enhanced damage modelling for fracture and fatigue

Proefschrift

ter verkrijging van de graad van doctor
aan de Technische Universiteit Eindhoven,
op gezag van de Rector Magnificus, prof.dr. M. Rem,
voor een commissie aangewezen door het College voor Promoties
in het openbaar te verdedigen op
dinsdag 23 maart 1999 om 16.00 uur

door

Ronnie Henricus Johannes Peerlings

geboren te Weert

CIP-DATA LIBRARY TECHNISCHE UNIVERSITEIT EINDHOVEN

Peerlings, Ron H.J.

Enhanced damage modelling for fracture and fatigue / by Ron H.J. Peerlings. – Eindhoven :
Technische Universiteit Eindhoven, 1999.

Proefschrift. – ISBN 90-386-0930-2

NUGI 834

Trefwoorden: breuk / vermoeiing / schade / materiaalmodellen / eindige-elementenmethode
/ localisering

Subject headings: fracture / fatigue / damage / material models / finite element method /
localisation

Druk: Universiteitsdrukkerij TU Eindhoven, Eindhoven, The Netherlands

Dit proefschrift is goedgekeurd door de promotoren:

prof.dr.ir. R. de Borst
prof.dr.ir. M.J.W. Schouten

Copromotor:

dr.ir. W.A.M. Brekelmans

Contents

Summary	vii
1 Introduction	1
1.1 Background and motivation	1
1.2 Scope and outline	3
2 Elasticity based damage mechanics	5
2.1 Concepts of damage mechanics	5
2.2 Elasticity based damage	7
2.3 Quasi-brittle damage	9
2.4 High-cycle fatigue damage	14
3 Localisation and mesh sensitivity	19
3.1 Localisation of deformation and damage	19
3.2 Quasi-brittle fracture	25
3.3 Fatigue	27
3.4 Regularisation methods	29
4 Nonlocal and gradient-enhanced damage	31
4.1 Nonlocal damage mechanics	32
4.2 Gradient formulations	34
4.3 Boundary conditions	37
4.4 Crack initiation	39
4.5 Crack growth	46
4.6 Discussion	52
5 Finite element implementation	53
5.1 Spatial discretisation	53
5.2 Temporal discretisation	57
5.3 Iterative procedure	63
5.4 Crack growth	65

6 Applications	67
6.1 Concrete fracture	67
6.2 Composite fracture	81
6.3 Metal fatigue	86
7 Conclusion	93
Bibliography	97
Samenvatting	107
Dankwoord	109
Curriculum vitae	111

Summary

The nucleation of cracks and their subsequent growth can be described in a unified fashion using continuum damage mechanics. A field variable is introduced which represents the development of microstructural material damage in a continuum sense. At a certain critical level of this damage variable all strength is locally lost and a crack is thus initiated. Under continued loading the completely damaged zone (i.e., the continuum damage representation of the crack) propagates by a process of damage growth and stress redistribution. The rate of propagation and its direction are governed by the damage growth in a relatively small process zone in front of the crack instead of by the separate fracture criteria used in fracture mechanics.

Numerical analyses based on standard damage models, however, are often found to depend heavily on the spatial discretisation. The growth of damage tends to localise in the smallest band that can be captured by the spatial discretisation. As a consequence, increasingly finer discretisation grids lead to crack initiation earlier in the loading history and to faster crack growth. In the limit of an infinite spatial resolution, the predicted damage band has a thickness zero and the crack growth becomes instantaneous. The response is then perfectly brittle, i.e., no work is needed to complete the fracture process. This nonphysical behaviour is caused by the fact that the localisation of damage in a vanishing volume is no longer consistent with the concept of a continuous damage field which forms the basis of the continuum damage approach.

The origins of the pathological localisation of damage have been studied for elasticity-based damage models of quasi-brittle fracture and high-cycle fatigue. Two mechanisms play an important role in it. Firstly, the set of partial differential equations which govern the rate of deformation may locally lose ellipticity at a certain level of accumulated damage. Discontinuities may then arise in the displacement solution, which result in a singular damage rate. This damage rate singularity in turn leads to the instantaneous initiation of a crack. Secondly, when a crack has been initiated, either prematurely as a result of displacement discontinuities or because the damage variable has become critical in a stable manner, the damage rate singularity at the crack tip results in instantaneous failure of the material in front of the crack tip. Since the damage rate singularity is preserved as the crack propagates, the remaining cross section is traversed instantaneously.

Displacement discontinuities and damage rate singularities can be avoided by adding non-locality to the damage model. In nonlocal damage theory spatially averaged quantities are used for this purpose. The enhanced continuum description which is thus obtained results in smooth damage fields, in which the localisation of damage is limited to the length scale

introduced by the averaging. As a consequence, premature initiation of cracks is avoided and predicted crack growth rates remain finite.

A similar effect can be achieved by including higher-order deformation gradients in the constitutive model. Two of these gradient enhancements have been considered, which can both be derived as approximations of the nonlocal model. In the first approach second-order strain gradients explicitly enter the stress-strain relations. In the second approach the dependence on strain gradients follows implicitly from a partial differential equation which must be solved in addition to the equilibrium equations. Particularly the implicit approach is equivalent to the nonlocal model in many respects. Indeed, implicit gradient models can be shown to contain the same long-range spatial interactions which are characteristic of nonlocal models.

The implicit gradient damage model can be fitted with relative ease into a standard nonlinear finite element formulation. Crack growth is simulated by removing completely damaged elements from the discretisation. This remeshing is necessary to avoid nonphysical damage growth at the crack faces as a result of interactions between the crack and the remaining continuum.

The finite element formulation has been used to simulate quasi-brittle fracture and high-cycle fatigue fracture. The damage bands obtained in these analyses have a finite width which depends on the intrinsic length introduced by the gradient enhancement. The quasi-brittle model shows a stable softening response, which compares well with experimental data. The fatigue model results in a finite crack initiation life and a finite crack growth rate. For both phenomena results are no longer sensitive to the spatial discretisation.

Chapter 1

Introduction

1.1 Background and motivation

Preventing failure of mechanical systems has been an important issue in engineering design ever since the early stages of the industrial era. Each individual component of these systems must be dimensioned such that it can resist the forces to which it will be subjected during normal service. Additionally, safety factors can be applied to account for unforeseen loadings or material flaws. For standard design purposes the yield limit is often used as a failure criterion, which means that the component will never undergo permanent deformation under design loads. However, when safety and reliability are critical (e.g., in nuclear installations) or when the added weight and cost of overdimensioning cannot be tolerated (aircraft), more accurate predictions are needed for the onset of failure, as well as of the fracture process itself (crack paths, residual strength, remaining service life, etc.). These issues have traditionally been addressed using fracture mechanics. Starting from the assumption of an idealised, dominant flaw, fracture mechanics theory provides conditions for the growth of a crack from this flaw. Additional criteria have been developed for the crack growth direction, growth rates under dead loads (creep) or repeated loading (fatigue) and other aspects of the fracture process, see for instance Broek (1986) for a review of these techniques.

The advent of digital computing technology has greatly extended the practical relevance of fracture mechanics. Where a large degree of simplification used to be necessary, accurate numerical analyses can nowadays be performed for arbitrary geometries and loading conditions (Atluri, 1986; Aliabadi and Rooke, 1991). Furthermore, the ability to numerically solve complex mathematical problems has inspired extensions of the classical, linear theory with nonlinear material behaviour (e.g., Kanninen and Popelar, 1985; Aliabadi et al., 1992). Under the influence of these developments, a second, fundamentally different type of modelling has emerged, in which fracture is considered as the ultimate consequence of a material degradation process. Instead of separately defining constitutive relations and a fracture criterion, this loss of mechanical integrity is accounted for in the constitutive model. Crack initiation and growth then follow naturally from the standard continuum mechanics theory. This concept can be implemented for instance in standard plasticity by assuming a decrease of the yield stress with increasing deformation (strain softening) after a certain amount of plastic flow (Pietruszczak and Mróz, 1981; Feenstra and de Borst, 1996).

However, the most distinct exponent of continuum approaches towards fracture is continuum damage mechanics. It introduces a set of field variables (damage variables) which explicitly describe the local loss of material integrity. The notion of a continuous representation of – intrinsically discontinuous – material damage stems from the work of Kachanov (1958) on tertiary creep and was further developed by Rabotnov (1969). But it was not before the mid-1970s that it was realised that the theory could be used to describe not only the formation, but also the growth of macroscopic cracks (Hayhurst et al., 1975). A crack is then represented by that part of the material domain in which the damage has become critical, i.e., where the material cannot sustain stress anymore. Redistribution of stresses results in the concentration of deformation and damage growth in a relatively small region in front of the crack tip. It is the growth of damage in this process zone which determines in which direction and at what rate the crack will propagate, hence the term ‘local approach to fracture’ which is sometimes used for this type of crack modelling (Lemaitre, 1986; Chaboche, 1988).

The very fact that damage mechanics and related models use a continuous representation of cracks renders them particularly suitable for numerical simulations. Damage formulations can be fitted into nonlinear finite element algorithms and implemented in simulation codes with relative ease and they do not rely on the special discretisation and remeshing techniques used in numerical fracture mechanics. It is an essential requirement of finite element formulations that the approximate solutions provided by them converge to the actual solution of the boundary value problem when the discretisation is refined. In the early 1980s, however, it was found that finite element solutions of softening damage and plasticity problems do not seem to converge upon mesh refinement (e.g., Pietruszczak and Mróz, 1981; Bažant et al., 1984; Schreyer and Chen, 1986). As a matter of fact, they do converge to a solution, but this solution is physically meaningless. Accordingly, the mesh sensitivity of the analyses is not caused by the numerical methods which are used, but by the fact that the underlying continuum model does not properly describe the physical phenomena that take place (Bažant et al., 1984; Triantafyllidis and Aifantis, 1986; de Borst et al., 1993).

The failure of continuum damage models in describing fracture processes can be understood if one realises that the concept of a continuous damage variable presumes a certain local homogeneity – or at least smoothness – of the microstructural damage distribution. But the continuum models based on this concept allow for discontinuous solutions, in which the development of damage localises in a surface while the surrounding material remains unaffected. This localisation of damage is in contradiction with the supposed smoothness of the damage field and thus affects the physical relevance of the model. Two possible ways out of this conflict present themselves: either the smoothness requirement must somehow be eased, or the continuum formulation must be modified in such a way that a larger degree of smoothness is ensured.

The cohesive zone models of Dugdale (1960) and Barenblatt (1962) and the fictitious crack model proposed by Hillerborg et al. (1976) can be considered as examples of the first category. They assume that the nonlinearity is concentrated in a plane in front of the actual, discrete crack. The faces of this fictitious crack can still transfer stresses, with a magnitude which is a function of their separation. More recent studies have shown how such functions can be derived from continuum models (Simo et al., 1993; Larsson and Runesson, 1994;

Oliver, 1996). Notice that this approach is also closely related to (nonlinear) fracture mechanics, since it assumes a discrete crack.

The second strategy concentrates on preventing the so-called pathological localisation of damage and deformation. Stability and bifurcation analyses of plasticity and damage formulations have provided a reasonable understanding of the origins of the behaviour and the conditions under which it occurs (Hill, 1962; Rudnicki and Rice, 1975; Rice, 1976; Benallal et al., 1989). A range of extensions to the conventional damage and plasticity models have been proposed in order to regularise the localisation of deformation (see for instance de Borst et al. (1993) for a review). Among them, the most promising is perhaps the class of nonlocal and gradient models. Both approaches introduce spatial interaction terms in the constitutive model, either using integral (nonlocal) relations (Bažant et al., 1984; Pijaudier-Cabot and Bažant, 1987; Tvergaard and Needleman, 1995) or gradients of some constitutive variable (Aifantis, 1984; Coleman and Hodgdon, 1985; Lasry and Belytschko, 1988; Mühlhaus and Aifantis, 1991; de Borst and Mühlhaus, 1992). The additional terms have a smoothing effect on the deformation (and damage) fields, and thus preclude localisation in a plane. From a physical standpoint, the presence of spatial interactions can be motivated by microstructural considerations for some classes of materials (e.g., Aifantis, 1984; Bažant, 1991; Fleck and Hutchinson, 1993; Geers, 1997).

The past decade has provided us with some understanding of the mathematical implications of the nonlocal and gradient enhancement, particularly in avoiding pathological localisation. But fundamental questions still remain. For example, the role of the enhancement in crack growth modelling and the associated treatment of boundaries have not yet been fully clarified. Furthermore, nonlocal and gradient models are known to be closely related, but may nevertheless behave quite differently. In fact, very similar gradient formulations have been observed to lead to remarkably different localisation properties. It is therefore believed that these and other issues need to be further resolved in order to fully exploit the potential of nonlocal and gradient formulations.

1.2 Scope and outline

The aim of this thesis is to provide a deeper insight into the mathematical and numerical aspects of continuum models of damage and fracture, and to develop a consistent, continuum description of these processes. Continuum damage mechanics will serve as the conceptual framework of these developments. In order not to obscure the key issues with needless complexity, the damage model which is used has been kept as simple as possible: it essentially consists of linear elasticity extended with an isotropic damage mechanism. The lack of permanent deformations in this constitutive model limits its practical relevance to quasi-brittle fracture and high-cycle fatigue. Although these phenomena can be treated in the same elasticity based damage framework, the damage models which describe them are quite different in some respects. Both models will therefore be used as examples throughout this thesis.

Chapter 2 introduces the general concepts of damage mechanics. Constitutive relations of elasticity based damage are first developed in a general format. These relations are then

particularised for quasi-brittle fracture and fatigue, respectively. The shortcomings of the classical theory are demonstrated in Chapter 3. The origins of the pathological localisation are first shown in a one-dimensional setting. The general, three-dimensional case is analysed by considering the rate equilibrium problem. Examples are given of the resulting mesh sensitivity in quasi-brittle and fatigue damage. At the end of the chapter a brief overview is given of existing methods to overcome these difficulties. The discussion then focuses on nonlocal and gradient-enhanced damage formulations (Chapter 4). It is shown that nonlocality may be introduced at the macroscopic level to represent the influence of the microscopic material structure on damage processes. Gradient formulations are derived as approximations of the nonlocal theory, and the mathematical consequences of both enhancements in crack initiation and crack growth are discussed.

In Chapter 5 finite element formulations of the gradient damage models for quasi-brittle and fatigue fracture are developed. For the high-cycle fatigue model the time integration of the damage growth relation is reformulated such that large numbers of cycles can be simulated without needing an excessive number of increments. A consistent Newton-Raphson solution scheme is developed for the discretised equations. Special attention is given to the numerical treatment of crack growth. In Chapter 6, examples of the application of the numerical models are given. The quasi-brittle model has been applied to concrete fracture and to fracture of a short fibre reinforced polymer. The fatigue model has been used to simulate the initiation and growth of fatigue cracks in a low-strength steel. Emphasis is on demonstrating the mesh objectivity of these simulations, but where possible the results are compared with experimental data from the literature. Chapter 7, finally, gives a brief summary of conclusions and discusses perspectives for continuum damage modelling of fracture.

Chapter 2

Elasticity based damage mechanics

Three decades of research have provided us with a wealth of damage models for virtually any combination of material behaviour and fracture mechanism. However, since our primary interest is understanding the behaviour of classical and enhanced damage formulations in mathematical terms, the complexity of the damage modelling is reduced here as much as possible. Thermal and other nonmechanical influences are left out of consideration and strains and rotations are assumed to be small. Furthermore, viscous effects and permanent deformations are neglected and the material behaviour is assumed to be linear elastic in the absence of damage growth. The remaining class of models basically consists of linear elasticity extended with a damage mechanism and is therefore often called elasticity based damage or damage coupled with elasticity (Lemaitre and Chaboche, 1990; Lemaitre, 1996).

Applications of elasticity based damage mechanics are limited to phenomena in which the growth of material defects is the predominant dissipation mechanism and plastic deformations remain negligible. Although particularly the latter condition imposes a severe limitation, two important fracture mechanisms remain: quasi-brittle fracture and high-cycle fatigue. Both phenomena involve a high degree of microstructural change before complete fracture occurs, and therefore lend themselves well for a description in a damage mechanics framework. After the introduction of some concepts and definitions of classical damage mechanics in general (Section 2.1) and elasticity based damage in particular (Section 2.2), constitutive models of quasi-brittle damage and high-cycle fatigue are discussed in detail in Sections 2.3 and 2.4, respectively.

2.1 Concepts of damage mechanics

The basic premise of continuum damage mechanics is that microstructural defects (microcracks, microvoids) in a material can be represented by a set of continuous damage variables. An illustration of this concept is given in Figure 2.1: the value of the damage variable D in a certain point of the continuum is a measure of the number and size of defects in a small volume at this point. Several definitions of damage variables in terms of measurable, physical quantities exist, see for instance Lemaitre and Chaboche (1990). However, for macroscopic

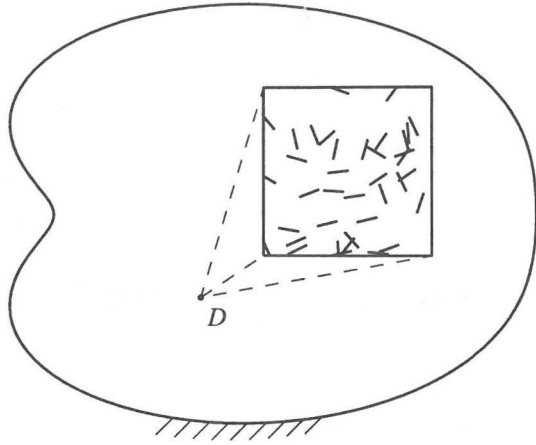


Figure 2.1: Damage variable as a representation of microstructural defects.

modelling purposes the precise physical interpretation of the damage variables is often less relevant. A precise definition is therefore not given at this point.

It is assumed in the sequel that the development of damage does not introduce anisotropy into the material behaviour and that a single, scalar damage variable suffices to describe the local damage state. In the more general, anisotropic case, a set of damage variables (or a tensor) must be used (Krajcinovic and Fonseka, 1981; Lemaitre and Chaboche, 1990; Fichant et al., 1995). The damage variable D is defined such that $0 \leq D \leq 1$, where $D = 0$ represents the initial, undamaged material and $D = 1$ represents a state of complete loss of integrity. Strictly speaking, the initial material always contains some defects, but it is assumed that these are accounted for in the virgin material properties, so that the initial damage can be set to zero.

After a certain amount of loading, three regions can generally be distinguished in the material domain Ω (Figure 2.2). No damage may have developed at all in a part Ω_0 . The damage variable still has its initial value $D = 0$ in this region and the material properties are those of the virgin material. In a second region Ω_d , some development of damage has occurred, but the damage is not yet critical ($0 < D < 1$). The limiting value $D = 1$ has been reached in the third region Ω_c , i.e., the mechanical integrity and strength have been completely lost in this region.

The completely damaged region Ω_c is the continuum damage representation of a crack. It is important to realise that the local, complete loss of strength in Ω_c implies that stresses are identically zero for arbitrary deformation fields. The equilibrium equations are meaningless in this region (see the next section for an example) and it must therefore be excluded from the equilibrium problem by introducing an internal boundary, on which the condition of zero stress is imposed as a boundary condition. A free boundary problem is thus obtained, in which the position of the internal boundary (the crack front and crack faces) follows from the growth of damage.

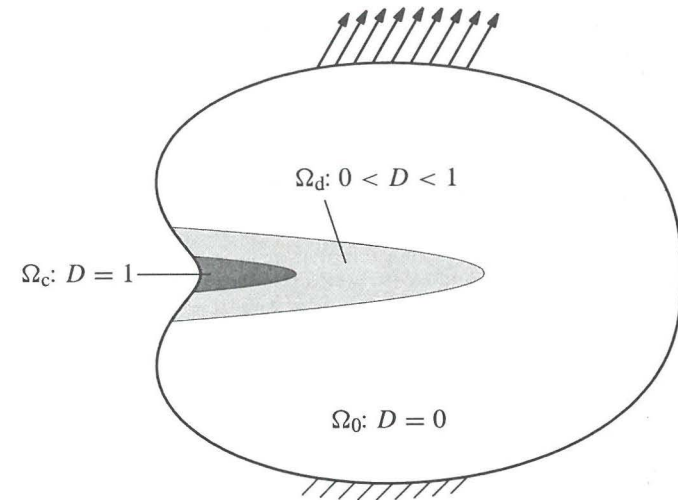


Figure 2.2: Damage distribution in a continuum.

2.2 Elasticity based damage

The classical stress-strain relation of elasticity based damage mechanics reads (see for instance Lemaitre and Chaboche, 1990)

$$\sigma_{ij} = (1 - D) C_{ijkl} \varepsilon_{kl}. \quad (2.1)$$

Einstein's summation convention has been used in this relation; σ_{ij} ($i, j = 1, 2, 3$) denotes the Cauchy stress components and ε_{kl} ($k, l = 1, 2, 3$) the linear strains

$$\varepsilon_{kl} = \frac{1}{2} \left(\frac{\partial u_k}{\partial x_l} + \frac{\partial u_l}{\partial x_k} \right), \quad (2.2)$$

where u_k are the displacement components with respect to the Cartesian coordinates $\mathbf{x} = [x_1, x_2, x_3]^T$. The reference configuration ($u_k = 0$) is assumed to be stress-free. The elastic constants C_{ijkl} are given by

$$C_{ijkl} = \lambda \delta_{ij} \delta_{kl} + \mu (\delta_{ik} \delta_{jl} + \delta_{il} \delta_{jk}), \quad (2.3)$$

with δ the Kronecker delta and λ and μ Lamé's constants. The latter can be expressed in terms of Young's modulus E and Poisson's ratio ν according to

$$\lambda = \frac{E\nu}{(1+\nu)(1-2\nu)}, \quad \mu = \frac{E}{2(1+\nu)}. \quad (2.4)$$

Relation (2.1) shows that the damage variable acts as a stiffness reduction factor. For increasing damage, the effective stiffness moduli $(1 - D)C_{ijkl}$ decrease, until they become zero for

$D = 1$. When all stiffness has vanished, no stresses can be transferred ($\sigma_{ij} = 0$), so that we indeed have a stress-free situation for $D = 1$.

Substitution of (2.1) and (2.2) into the standard equilibrium equations

$$\frac{\partial \sigma_{ij}}{\partial x_i} = 0 \quad (2.5)$$

and making use of the right minor symmetry of the elasticity tensor (i.e., $C_{ijkl} = C_{ijlk}$) gives the system of second-order partial differential equations

$$(1 - D) C_{ijkl} \frac{\partial^2 u_k}{\partial x_i \partial x_l} - \frac{\partial D}{\partial x_i} C_{ijkl} \frac{\partial u_k}{\partial x_l} = 0. \quad (2.6)$$

For a given damage field $D(\mathbf{x}) < 1$, the displacement components u_k can be determined from this differential system and the corresponding kinematic and dynamic boundary conditions. In a crack however, where $D \equiv 1$, both terms in the differential equations vanish. Consequently, the differential system degenerates and the boundary value problem becomes ill-posed. As discussed in Section 2.1, this situation must be avoided by limiting the equilibrium problem to the subdomain $\tilde{\Omega} = \Omega_0 \cup \Omega_d$ where $D < 1$ and applying the natural boundary condition $n_i \sigma_{ij} = 0$ at the boundary between crack and remaining material.

The stress-strain relation (2.1) defines the effect of the damage variable on stresses and – through the equilibrium equations – on the deformation field. At the same time, however, the damage variable may increase under the influence of stresses and strains. Whether damage growth is possible is decided on the basis of a damage loading function in terms of the strain components:

$$f(\tilde{\epsilon}, \kappa) = \tilde{\epsilon} - \kappa, \quad (2.7)$$

with $\tilde{\epsilon}$ a positive equivalent measure of the strain state and κ a threshold variable. The equation $f = 0$ defines a loading surface in strain space (cf. the elastoplastic yield surface in stress space). The shape and size of the loading surface are determined by the definition of the equivalent strain $\tilde{\epsilon}$ in terms of the strain components and by the threshold variable κ , respectively. For strain states within the loading surface ($f < 0$) there is no growth of damage and the material behaviour is elastic. The damage variable can only increase when the equivalent strain reaches the threshold value κ , i.e., when $f \geq 0$. The precise conditions for damage growth are different for the quasi-brittle and fatigue models; they are given in Sections 2.3 and 2.4, respectively.

When the appropriate conditions are satisfied, the growth of damage is governed by an evolution law which reads in its most general form

$$\dot{D} = g(D, \tilde{\epsilon}) \dot{\tilde{\epsilon}}, \quad (2.8)$$

where a superimposed dot denotes differentiation with respect to time. Notice that the dependence of the damage growth rate on the equivalent strain rate is linear in order to avoid rate effects. Specific expressions for the evolution function $g(D, \tilde{\epsilon})$ and the equivalent strain $\tilde{\epsilon}$ for quasi-brittle damage and fatigue are given in the following sections.

2.3 Quasi-brittle damage

Quasi-brittle fracture is a collective noun for fracture processes which are not accompanied by large-scale plastic flow, but nevertheless take significantly more energy than needed for the creation of the crack surface. Fracture is not the consequence of the growth of one dominant crack, but rather of a process of nucleation, growth and coalescence of microscopic defects in a volume which is much larger than that occupied by the final, macroscopic crack. As a consequence, a gradual decrease of the deformation resistance is usually observed instead of the sudden loss of strength in perfectly brittle fracture. Examples of materials which exhibit quasi-brittle fracture are concrete, rock, ceramics and some fibre reinforced composites.

Figure 2.3 shows the stress-strain response which is typically observed in tensile tests of concrete specimens if the load is removed at regular intervals (e.g., Mazars and Pijaudier-Cabot, 1989; Shah and Maji, 1989). It should be mentioned that the strain in this diagram is actually an average strain since it is usually obtained by dividing the relative displacement of two points (e.g., the supports) by their distance. For small strains the response is practically linear. When the deformation increases, however, the slope of the stress-strain curve decreases, until it becomes zero at the fracture strength. After having reached the fracture strength, the stress decreases gradually for increasing strain. In this softening stage the load was removed from the specimen at four different stress levels. The slope of the corresponding unloading loops in the diagram becomes smaller for each following unloading-reloading sequence – that is, the elastic stiffness of the material decreases as the damage process continues, as predicted by elasticity based damage. However, a considerable amount of deformation remains at zero stress, which cannot be described by standard elastic damage models. These permanent deformations can be taken into account by adding inelastic terms to the constitutive

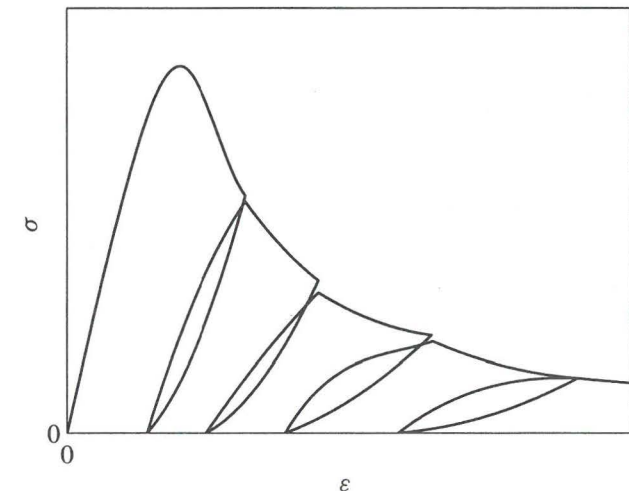


Figure 2.3: Stress-strain response of concrete in tension.

tive model (e.g., Lubliner et al., 1989; Mazars and Pijaudier-Cabot, 1989), but this extension will not be considered here for simplicity.

It can also be observed from Figure 2.3 that when the deformation is increased again after unloading, damage growth starts approximately at the point where the unloading started. In terms of the damage model of Section 2.2 this means that the elastic domain in strain space must grow for increasing damage, such that the strain state remains on the loading surface ($f = 0, \dot{f} = 0$; cf. elastoplasticity). This implies that the damage threshold κ is always equal to the largest value of the equivalent strain $\tilde{\varepsilon}$ which was locally attained during the loading history. Mathematically, this condition can be formulated by the set of Kuhn-Tucker relations

$$f \dot{\kappa} = 0, \quad f \leq 0, \quad \dot{\kappa} \geq 0, \quad (2.9)$$

which must be supplemented by an initial value $\kappa = \kappa_0$ in order to define the initial elastic domain.

The damage growth relation can now be written as

$$\dot{D} = \begin{cases} g(D, \tilde{\varepsilon}) \dot{\tilde{\varepsilon}} & \text{if } f = 0 \text{ and } \dot{f} = 0 \text{ and } D < 1, \\ 0 & \text{else,} \end{cases} \quad (2.10)$$

where the condition $D < 1$ reflects the fact that the damage cannot grow beyond the critical value $D = 1$. Since $\dot{D} > 0$ if and only if $f = 0$ and $\dot{\tilde{\varepsilon}} > 0$, and thus $\dot{\kappa} > 0$, and since both D and κ are semi-monotonic, a one to one relation exists between these two internal variables: $D = D(\kappa)$. This relation can be obtained from (2.10) by integration and use of the consistency relation $\dot{f} = 0$, but it is usually specified directly for quasi-brittle damage models. In the latter case the corresponding evolution function $g(D, \tilde{\varepsilon})$ can be obtained by differentiation with respect to κ .

For theoretical developments the evolution of damage is often defined as

$$D = \begin{cases} \frac{\kappa_c}{\kappa} \frac{\kappa - \kappa_0}{\kappa_c - \kappa_0} & \text{if } \kappa < \kappa_c, \\ 1 & \text{if } \kappa \geq \kappa_c. \end{cases} \quad (2.11)$$

This relation has been plotted in Figure 2.4(a). In a uniaxial stress situation, and assuming that $\tilde{\varepsilon}$ equals the axial strain ε , (2.11) results in linear softening, followed by complete loss of stiffness at $\varepsilon = \kappa_c$, see Figure 2.4(b).

Softening in real materials is usually nonlinear, with a relatively steep initial stress drop followed by a more moderate decrease (cf. Figure 2.3). An exponential softening law is sometimes used for concrete (Mazars and Pijaudier-Cabot, 1989; Peerlings et al., 1998a):

$$D = 1 - \frac{\kappa_0}{\kappa} (1 - \alpha + \alpha e^{-\beta(\kappa - \kappa_0)}). \quad (2.12)$$

This expression and the corresponding stress-strain relation have also been plotted in Figure 2.4. Notice that the damage variable approaches $D = 1$ asymptotically, which means that there will never be complete fracture (Figure 2.4(c)). For $\varepsilon \rightarrow \infty$ the uniaxial stress

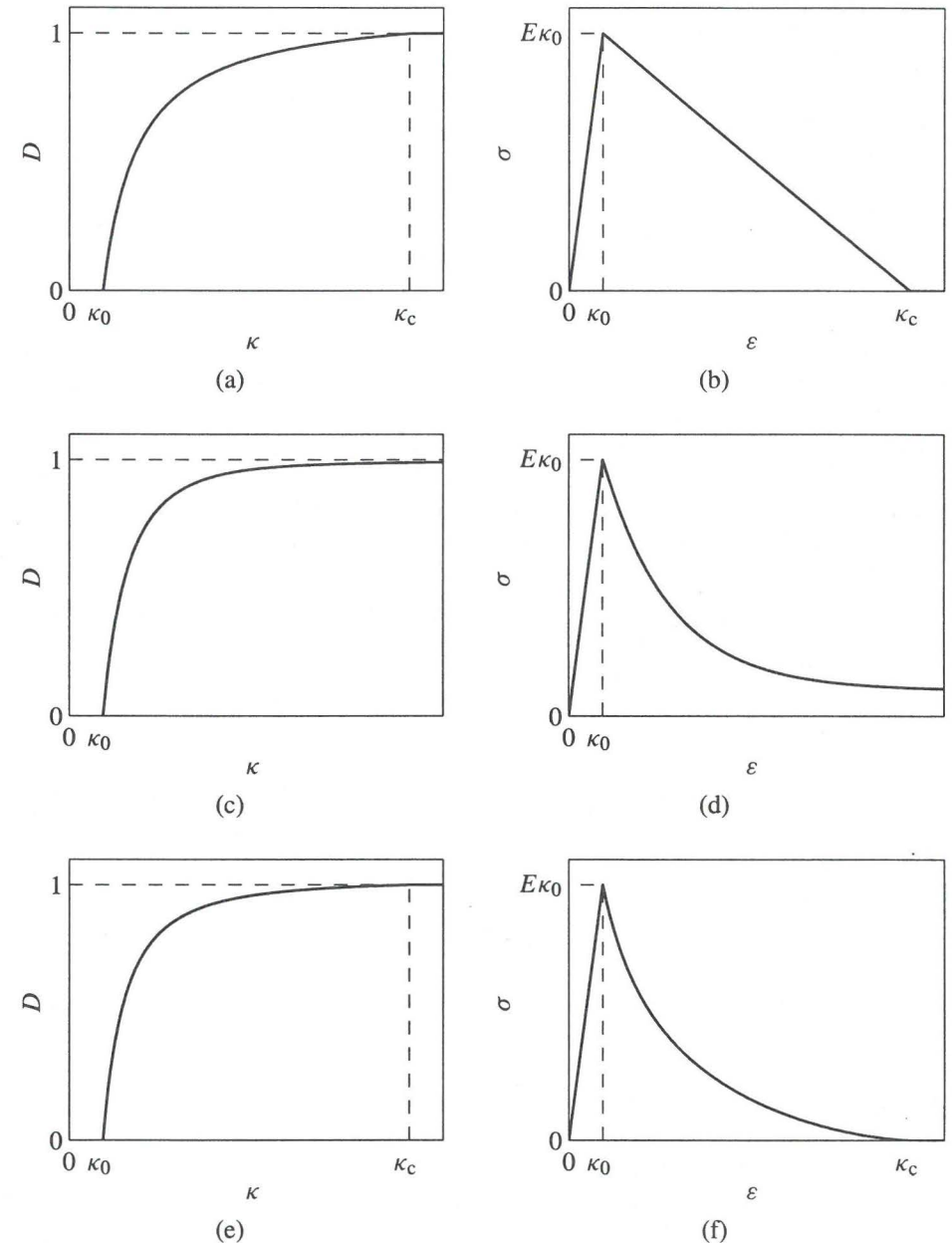


Figure 2.4: Damage growth and corresponding uniaxial stress-strain response for (a,b) linear softening case (2.11), (c,d) exponential softening (2.12) and (e,f) modified power law (2.13).

σ approaches $(1 - \alpha)E\kappa_0$ (Figure 2.4(d)); this asymptote represents the long tail of experimentally obtained load-displacement diagrams, which is the result of crack bridging (e.g., Hordijk, 1991). The parameter β in (2.12) determines the rate at which the damage grows. A higher value results in a faster growth of damage and thus in a more brittle response.

Geers (1997) has proposed a so-called modified power law to describe fracture of short glass-fibre reinforced polymers:

$$D = \begin{cases} 1 - \left(\frac{\kappa_0}{\kappa}\right)^\beta \left(\frac{\kappa_c - \kappa}{\kappa_c - \kappa_0}\right)^\alpha & \text{if } \kappa < \kappa_c, \\ 1 & \text{if } \kappa \geq \kappa_c. \end{cases} \quad (2.13)$$

This relation results in complete fracture ($D = 1$) for $\kappa = \kappa_c$ (Figure 2.4(e,f)). The parameter β in (2.13) mainly influences the initial rate of damage growth, whereas α determines the final softening stage, close to complete failure (Geers, 1997).

Apart from the evolution law for the damage variable, the equivalent strain $\tilde{\epsilon}$ must be defined in order to have a complete quasi-brittle damage model. The equivalent strain definition maps the strain components onto a scalar variable. It must therefore reflect the different effects of the strain components on damage growth by weighting these components appropriately. If the constitutive relations are derived within the framework of thermodynamics of irreversible processes, damage evolution is usually related to the energy release rate associated to the damage variable, which for elasticity based damage is given by (Lemaitre and Chaboche, 1990)

$$Y = \frac{1}{2} \epsilon_{ij} C_{ijkl} \epsilon_{kl}. \quad (2.14)$$

The energy release rate depends only on the strain components and can thus be regarded as an equivalent strain measure which uses the elastic moduli to weight the different strain components. In fact, if the equivalent strain is taken as $\tilde{\epsilon} = Y$, the damage formulation which is used here coincides with the classical model based on thermodynamics.

The slightly modified expression

$$\tilde{\epsilon} = \sqrt{\frac{1}{E} \epsilon_{ij} C_{ijkl} \epsilon_{kl}} \quad (2.15)$$

is more natural in the sense that $\tilde{\epsilon}$ is dimensionless and equals the axial strain for the uniaxial tensile stress case. Definition (2.15) is represented graphically in Figure 2.5(a), which shows a constant- $\tilde{\epsilon}$ curve in the principal strain space. The diagram has been scaled such that $\tilde{\epsilon} = 1$. A plane-stress situation has been assumed and Poisson's ratio has been set equal to $\nu = 0.2$. The dashed lines in the diagram represent uniaxial stress paths.

Figure 2.5(a) shows that the normalised energy release rate definition (2.15) lacks the ability to distinguish between tension and compression. Under uniaxial loading the energy release rate model predicts damage initiation and failure at the same load levels in compression and tension. For engineering materials, however, the compressive strength is often higher than the tensile strength. For instance, the compressive strength of concrete is ten to twenty

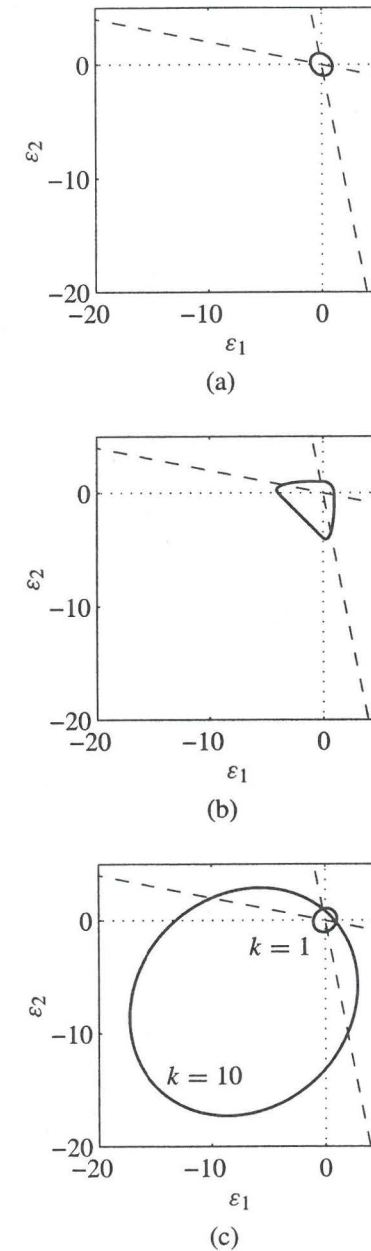


Figure 2.5: Equivalent strain definitions in principal strain space (plane-stress): (a) normalised energy release rate (2.15), (b) Mazars (2.16), (c) modified von Mises (2.17).

times the tensile strength. This difference can be accounted for in the damage model by using an equivalent strain measure which is more sensitive to positive strains than to negative strains. A widely used definition is (Mazars and Pijaudier-Cabot, 1989)

$$\tilde{\varepsilon} = \sqrt{\sum_{i=1}^3 \langle \varepsilon_i \rangle^2}, \quad (2.16)$$

with ε_i ($i = 1, 2, 3$) the principal strains and $\langle \cdot \rangle$ the McAuley brackets: $\langle x \rangle = \frac{1}{2}(x + |x|)$. The contour $\tilde{\varepsilon} = 1$ associated to relation (2.16) has been plotted in Figure 2.5(b). The dependence on solely the positive principal strains indeed renders the equivalent strain more sensitive to tensile strains than to compressive strains. Under uniaxial loading, the ratio of the compressive strength and the tensile strength is given by $\sigma_{fc}/\sigma_{ft} = 1/(\nu\sqrt{2})$ (Brekelmans et al., 1992). For $\nu = 0.2$ this ratio is approximately 3.5, which is still considerably lower than experimentally obtained values for concrete.

A third equivalent strain definition, first proposed in a strain based format by de Vree et al. (1995), is the modified von Mises definition. This definition originates from plasticity models for polymers, where it has been formulated in terms of stresses. It is obtained by adding the first invariant of the stress tensor to the standard von Mises flow criterion (Williams, 1973). The stress based form of the modified von Mises definition can be rewritten in terms of strains using Hooke's law, resulting in:

$$\tilde{\varepsilon} = \frac{k-1}{2k(1-2\nu)} I_1 + \frac{1}{2k} \sqrt{\frac{(k-1)^2}{(1-2\nu)^2} I_1^2 - \frac{12k}{(1+\nu)^2} J_2}, \quad (2.17)$$

with I_1 and J_2 the first invariant of the strain tensor and the second invariant of the deviatoric strain tensor, respectively, given by

$$I_1 = \varepsilon_{kk}, \quad J_2 = \frac{1}{6} I_1^2 - \frac{1}{2} \varepsilon_{ij} \varepsilon_{ij}. \quad (2.18)$$

The parameter k governs the sensitivity in compression relative to that in tension. The definition of the equivalent strain is such that a compressive uniaxial stress of magnitude $k\sigma$ has the same effect on damage growth as a tensile stress σ . The parameter k is therefore usually set equal to the ratio of the compressive and tensile strength: $k = \sigma_{fc}/\sigma_{ft}$. Two-dimensional graphical representations of the modified von Mises definition for $k = 1$ and $k = 10$ are given in Figure 2.5(c).

2.4 High-cycle fatigue damage

Engineering components are often submitted to cyclic or fluctuating loads. Fracture under these circumstances is usually the result of fatigue: the repetitive character of the loading causes an accumulation of microstructural damage, which culminates in the formation and growth of cracks. Fatigue fracture occurs at stress amplitudes which are well below the static fracture strength or even below the static yield limit of the material. When plastic strains

remain small, the process is referred to as high-cycle fatigue. The fatigue life is typically of the order of 10^5 - 10^6 cycles in high-cycle fatigue.

Elasticity based damage models of high-cycle fatigue assume a decrease of the elastic stiffness as the damage grows. This loss of stiffness can indeed be measured in some materials. Figure 2.6 shows the decrease of the effective elastic modulus, \tilde{E} , as typically measured in metals under constant stress amplitude loading (see for instance Chaboche, 1988; Lemaitre, 1996). The number of loading cycles N has been normalised by dividing it by the fatigue life N_f and the effective elastic modulus \tilde{E} has been divided by Young's modulus of the virgin material, E . The diagram shows a relatively slow loss of stiffness during a large part of the fatigue life, followed by an abrupt loss of the remaining stiffness. Other measurement techniques confirm this strongly progressive growth of damage (Marom, 1970; Ping, 1984).

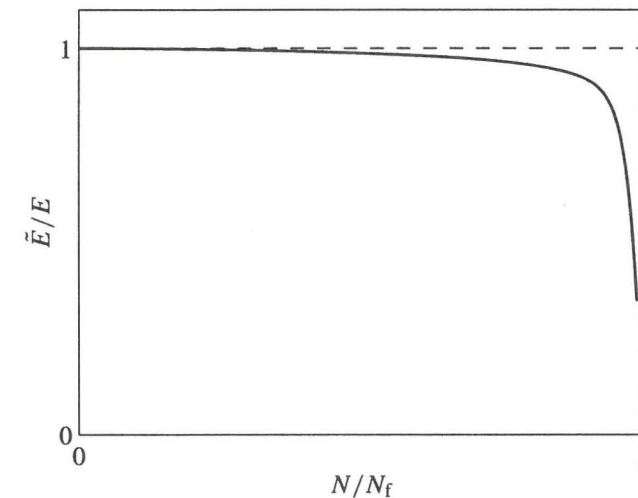


Figure 2.6: Elastic stiffness decrease in high-cycle fatigue.

The fact that stress cycles of a constant amplitude result in damage growth means that the role of the loading surface in the fatigue damage model must be different from that in the quasi-brittle model. If the Kuhn-Tucker relations were also used for fatigue, there would only be damage growth in the first loading cycle, followed by an elastic response in all subsequent cycles. Following Paas et al. (1993) the elastic domain is therefore kept fixed in the fatigue model by setting $\kappa = \kappa_0$. The strain is allowed to exceed the loading surface, so that $f > 0$ (cf. overstress viscoplasticity models). The loading surface can now be related to the fatigue limit: if the strain remains within the loading surface everywhere in a component, there will be no damage development and the component has an infinite fatigue life. For materials which do not exhibit a fatigue limit, the threshold parameter κ_0 can be set to zero. In addition to the condition $f \geq 0$, it is assumed that the damage variable can only increase for continued loading, i.e., for $\dot{f} \geq 0$, and that it remains constant during unloading (Paas, 1990; Paas et al.,

1993). The rate of damage growth can then be written as

$$\dot{D} = \begin{cases} g(D, \tilde{\varepsilon}) \dot{\tilde{\varepsilon}} & \text{if } f \geq 0 \text{ and } \dot{f} \geq 0 \text{ and } D < 1, \\ 0 & \text{else.} \end{cases} \quad (2.19)$$

When dealing with loading histories composed of well defined, discrete cycles, an evolution law in terms of the number of cycles and their amplitudes is often considered more practical in the literature. The number of cycles, N , is then regarded as a continuous, time-like variable and the growth of damage, which occurs during discrete time intervals within a cycle, is spread to a continuous evolution over the entire cycle. Such a cycle based formulation can be obtained from (2.19) by integration over one loading cycle and approximating the growth of damage within this cycle, resulting in a relation of the form (Lemaitre and Chaboche, 1990; Paas, 1990; Paas et al., 1993; Peerlings, 1997)

$$\frac{\partial D}{\partial N} = G(D, \varepsilon_a), \quad (2.20)$$

with ε_a the amplitude of the equivalent strain cycle.

Fatigue damage growth relations are often formulated directly in a cycle based format, but traditionally in terms of stresses rather than strains (e.g., Lemaitre and Plumtree, 1979; Hua and Socie, 1984; Chaboche, 1988; Chaboche and Lesne, 1988). Notice, however, that such a stress based evolution can always be rewritten in a strain format by substitution of the stress-strain relations (2.1). In this thesis (2.19) will be regarded as the primary definition. This relation does not require that the loading history consists of well defined loading cycles. As a result, variable amplitude loading, overloads, etc. can be dealt with in a natural fashion, although the load interactions and retardation effects associated to these irregular loadings can be described only to a limited degree by the elasticity based damage model (Peerlings, 1996, 1997). It will be shown in Chapter 5 that efficient numerical analyses of constant amplitude loading are nevertheless possible using definition (2.19) if the appropriate numerical techniques are used.

For the evolution function $g(D, \tilde{\varepsilon})$ an expression which is slightly different from that of Paas (1990) is used here:

$$g(D, \tilde{\varepsilon}) = C e^{\alpha D} \tilde{\varepsilon}^\beta, \quad (2.21)$$

with C , α and β material parameters. This form has the advantage that it does not become zero for $D = 1$. It can therefore also be used with an initial damage equal to zero, in contrast to the relation proposed by Paas (1990).

The growth of damage and the fatigue life can be solved in closed form for the situation of uniaxial, fully reversed loading with a constant strain amplitude ε_a . It is furthermore assumed for simplicity that the equivalent strain equals the axial strain amplitude ε_a at both extremes of the strain cycles (i.e., in tension and compression) and that there is no fatigue limit ($\kappa_0 = 0$). After substitution of (2.21), relation (2.19) can then be integrated over N cycles, yielding (Peerlings, 1997):

$$D = -\frac{1}{\alpha} \ln \left(1 - \frac{2\alpha C}{\beta + 1} \varepsilon_a^{\beta+1} N \right). \quad (2.22)$$

The fatigue life N_f is obtained as a function of the strain amplitude from (2.22) by setting $D = 1$ and solving for N , resulting in

$$N_f = \frac{\beta + 1}{2\alpha C} (1 - e^{-\alpha}) \varepsilon_a^{-(\beta+1)}. \quad (2.23)$$

This equation can also be written as

$$\varepsilon_a = \left(\frac{\beta + 1}{\alpha C} (1 - e^{-\alpha}) \right)^{\frac{1}{\beta+1}} (2N_f)^{-\frac{1}{\beta+1}}, \quad (2.24)$$

which is of the same form as the high-cycle part of the classical strain based approach to fatigue (Manson and Hirschberg, 1964), or Basquin's (1910) law,

$$\varepsilon_a = \frac{\sigma'_f}{E} (2N_f)^b, \quad (2.25)$$

with the fatigue strength coefficient σ'_f and fatigue strength exponent b given by

$$\sigma'_f = E \left(\frac{\beta + 1}{\alpha C} (1 - e^{-\alpha}) \right)^{\frac{1}{\beta+1}}, \quad b = \frac{-1}{\beta + 1}. \quad (2.26)$$

Using (2.23), relation (2.22) can be rewritten in terms of the relative number of cycles N/N_f :

$$D = -\frac{1}{\alpha} \ln \left(1 - (1 - e^{-\alpha}) \frac{N}{N_f} \right). \quad (2.27)$$

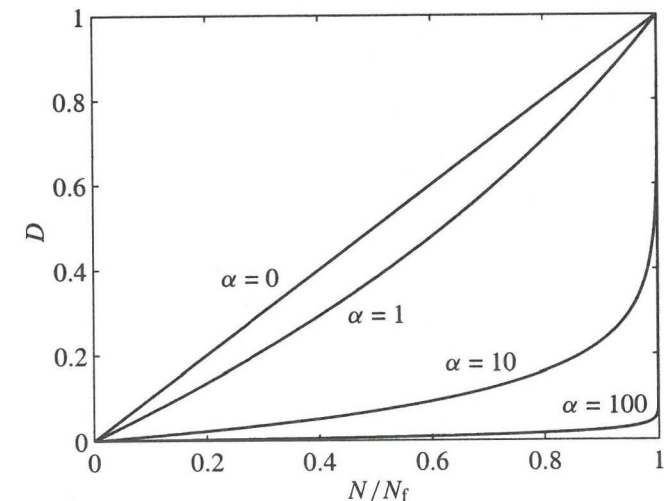


Figure 2.7: Damage variable as a function of the relative number of cycles.

This relation has been plotted in Figure 2.7 for several values of the parameter α . The effect of variation of this parameter is quite clear: a higher value of α results in an initially slower accumulation of damage, but a higher growth rate towards the end of the fatigue life. Since α is the only parameter in equation (2.27), it can be determined from experiments by fitting the growth of damage during the fatigue life (cf. Figure 2.7). The other two parameters of the evolution law, C and β , can then be solved from relations (2.26) for the fatigue strength coefficient and exponent, the values of which are available for many materials in fatigue handbooks. Notice, however, that this procedure requires that the strain amplitude in the critical cross-section is kept constant.

Since high-cycle fatigue damage is usually the result of plastic flow at the microscale, it seems natural to use the von Mises strain as equivalent strain measure in fatigue. The definition of $\bar{\varepsilon}$ then reads

$$\bar{\varepsilon} = \frac{1}{1+\nu} \sqrt{-3J_2}, \quad (2.28)$$

where the factor $1/(1+\nu)$ scales the equivalent strain such that it equals the axial strain in the uniaxial stress case. Notice that the modified von Mises definition (2.17) reduces to (2.28) for $k = 1$. A graphical representation of (2.28) is therefore given by the curve associated to $k = 1$ in Figure 2.5(c).

Chapter 3

Localisation and mesh sensitivity

Finite element simulations using continuum damage models are known to be susceptible to so-called mesh sensitivity: when the finite element discretisation is refined, the numerical solution does not converge to a physically meaningful solution of the problem (e.g., Saanouni et al., 1989; Murakami and Liu, 1995; de Vree et al., 1995). This behaviour is not unique for damage models, but also occurs in softening plasticity and other continuous representations of material degeneration (Pietruszczak and Mróz, 1981; Bažant et al., 1984; de Borst and Mühlhaus, 1991; Needleman and Tvergaard, 1994). Neither is it necessarily related to the finite element method, since other numerical solution methods also show irregularities under similar circumstances. Indeed, mesh sensitivity is not caused by numerical artifacts or inadequate solution algorithms, but it is the numerical consequence of shortcomings of the underlying mathematical modelling. In the academic case of uniform material properties and stresses, the equilibrium problem has an infinite number of solutions and the problem is therefore ill-posed. In practical problems, which are always inhomogeneous, the growth of damage tends to localise in the smallest possible volume, that is, in a surface. Consequently, no work is needed to complete the fracture process, even if the specific energy dissipation is positive. The conditions under which such pathologically localised solutions can develop in elasticity based damage are examined in Section 3.1. The discussion is then particularised to quasi-brittle fracture and fatigue in Sections 3.2 and 3.3, respectively. Section 3.4 gives a brief account of measures which can be taken to avoid the problems associated to localisation.

3.1 Localisation of deformation and damage

The fundamental difficulties associated to damage localisation are best demonstrated in a one-dimensional setting. A uniform bar is considered (Figure 3.1), which is supported at one end and loaded by a prescribed displacement $U(t)$ at the other end. The axial strain ε in the bar is assumed to be positive at all times; the equivalent strain $\bar{\varepsilon}$ can then be set equal to ε . The one-dimensional stress-strain relation

$$\sigma = (1 - D)E\varepsilon \quad (3.1)$$

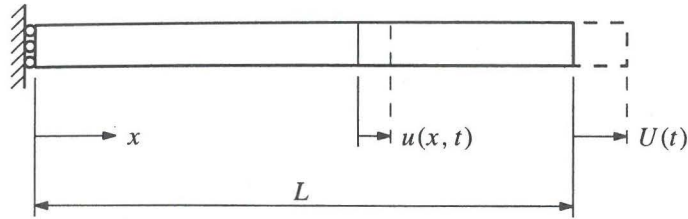


Figure 3.1: One-dimensional bar problem.

(cf. (2.1)) renders the equilibrium equation for the bar nonlinear in terms of the deformation. However, the problem can be linearised by considering the associated rate problem

$$\frac{\partial \dot{\sigma}}{\partial x} = 0 \quad (3.2)$$

and assuming damage growth everywhere in the bar. Notice that this linearisation is equivalent with the classical assumption of a linear comparison solid (Hill, 1958). Differentiation of (3.1) with respect to time, followed by substitution of the general growth law (2.8) gives the stress rate as

$$\dot{\sigma} = \bar{E} \dot{\varepsilon}, \quad (3.3)$$

where the tangential stiffness \bar{E} is defined as

$$\bar{E}(D, \varepsilon) = (1 - D)E - g(D, \varepsilon)E\varepsilon. \quad (3.4)$$

For $\bar{E} > 0$ the stress increases for an increasing strain (hardening), for $\bar{E} = 0$ the stress is stationary, and for $\bar{E} < 0$ it decreases (softening). Substitution of (3.3) and the kinematical relation $\dot{\varepsilon} = \partial v / \partial x$, with $v(x, t)$ the axial velocity in the bar, into (3.2) results in a linear differential equation in terms of v :

$$\bar{E}(D, \varepsilon) \frac{\partial^2 v}{\partial x^2} + \frac{\partial \bar{E}}{\partial x} \frac{\partial v}{\partial x} = 0, \quad (3.5)$$

with

$$\frac{\partial \bar{E}}{\partial x} = - \left(g(D, \varepsilon) + \varepsilon \frac{\partial g}{\partial \varepsilon} \right) E \frac{\partial \varepsilon}{\partial x} - \left(1 + \varepsilon \frac{\partial g}{\partial D} \right) E \frac{\partial D}{\partial x}. \quad (3.6)$$

If a reference solution with homogeneous strain and damage ε_0, D_0 is now assumed, the second term in (3.5) vanishes and the coefficient of the second derivative of v is constant:

$$\bar{E}(D_0, \varepsilon_0) \frac{\partial^2 v}{\partial x^2} = 0. \quad (3.7)$$

An obvious solution of this problem is the linear velocity field $v(x) = Vx/L$, where $V = dU/dt$ is the velocity imposed on the right end of the bar. This solution, for which the strain rate and the damage rate remain homogeneous, is the only possible solution as long as $\bar{E} > 0$. However, it can be seen directly from equation (3.7) that other solutions are possible when $\bar{E} = 0$. The stress rate is then insensitive to variations of the strain rate and the differential equation (3.7) degenerates to an identity. Each twice differentiable velocity field which satisfies the boundary conditions is a solution of the boundary value problem, which is therefore ill-posed. In addition to these classical, strong solutions, an infinite number of weak solutions of the problem exist. A weak or generalised solution satisfies the differential equation in a distribution sense and can therefore have discontinuities in its first and second-order derivatives or even in the solution itself, see for instance Courant and Hilbert (1953) for a precise definition.

In the inhomogeneous situation where the limit point $\bar{E} = 0$ is first reached in only one cross-section of the bar, say at $x = x_c$, a discontinuous velocity field is the only possible solution of the linear rate problem. Since the stress cannot be constant for increasing strain in the remaining part of the bar, where $\bar{E} > 0$, the strain rate $\dot{\varepsilon} = \partial v / \partial x$ must be zero for $x \neq x_c$. In order still to satisfy the boundary conditions, the velocity field must then have a jump at the critical cross-section $x = x_c$. This jump in the velocity field means that $\dot{\varepsilon}$ is singular and thus that \dot{D} is singular. For continued loading the damage variable therefore immediately reaches its critical value $D = 1$ at $x = x_c$ and the stress becomes zero. The only way for the rest of the bar to follow this stress drop is to unload elastically. Thus, the deformation and growth of damage are localised in the critical cross-section, which immediately turns into a crack. This crack divides the bar in two stress-free bodies, the separation of which (i.e., the crack opening) is equal to the rigid body movement U that is imposed on the right body.

In the general, three-dimensional case similar difficulties arise when the traction rate vector acting on an arbitrary surface is insensitive to a velocity gradient across the surface (Rice, 1976). In order to further define this situation, consider a surface S given by $\varphi(\mathbf{x}) = 0$, with $|\nabla\varphi| = (\sum_{i=1}^3 (\partial\varphi/\partial x_i)^2)^{1/2} \neq 0$. New independent variables ξ_m ($m = 1, 2, 3$) are introduced, with $\xi_3 = \varphi$ (i.e., normal to S) and ξ_1, ξ_2 interior variables on S , see Figure 3.2 for a schematic representation. The transformation from the coordinates x_i to the new coordinates ξ_m is given by the derivatives $\partial\xi_m/\partial x_i = \xi_{mi}$; in particular, $\partial\xi_3/\partial x_i = \partial\varphi/\partial x_i = \varphi_i$. The unit normal $\mathbf{n} = [n_1, n_2, n_3]^T$ to S is then given by

$$n_i = \frac{1}{|\nabla\varphi|} \frac{\partial\varphi}{\partial x_i} = \frac{\varphi_i}{|\nabla\varphi|}. \quad (3.8)$$

Differentiation of the stress-strain relation (2.1) gives for the stress rate

$$\dot{\sigma}_{ij} = \bar{C}_{ijkl} \dot{\varepsilon}_{kl}, \quad (3.9)$$

where the tangential stiffness tensor \bar{C}_{ijkl} is defined by

$$\bar{C}_{ijkl} = (1 - D)C_{ijkl} - g(D, \bar{\varepsilon})C_{ijmn}\varepsilon_{mn} \frac{\partial \bar{\varepsilon}}{\partial \varepsilon_{kl}}. \quad (3.10)$$

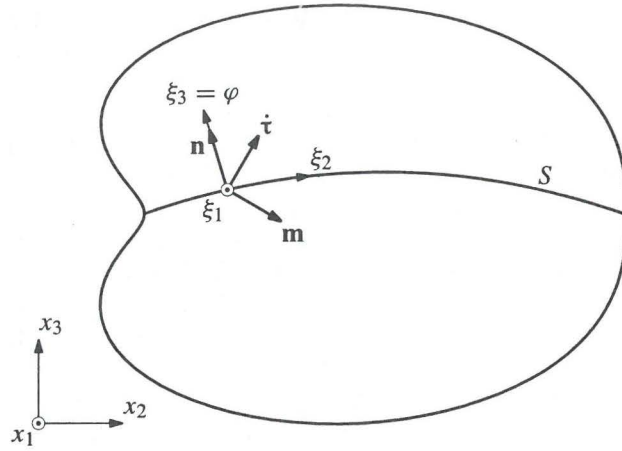


Figure 3.2: Definition of surface coordinates ξ_m .

The tensor \bar{C}_{ijkl} satisfies the left symmetry $\bar{C}_{ijkl} = \bar{C}_{jikl}$ as a consequence of the symmetry of the stress rate tensor $\dot{\sigma}_{ij}$. Because of the symmetry of the strain rate $\dot{\epsilon}_{kl}$ it can also be assumed to satisfy the right symmetry $\bar{C}_{ijkl} = \bar{C}_{ijlk}$ without loss of generality. Using (3.9), the traction rates $\dot{\tau}_j$ acting on S can be written as

$$\dot{\tau}_j = n_i \dot{\sigma}_{ij} = n_i \bar{C}_{ijkl} \frac{\partial v_k}{\partial x_l}. \quad (3.11)$$

Rewritten in terms of derivatives with respect to the new independent variables ξ_m this relation reads

$$\dot{\tau}_j = n_i \bar{C}_{ijkl} \frac{\partial v_k}{\partial \xi_m} \xi_{ml}, \quad (3.12)$$

or, separating the derivative normal to S and using (3.8),

$$\dot{\tau}_j = n_i \bar{C}_{ijkl} n_l \frac{\partial v_k}{\partial n} + \sum_{m=1}^2 n_i \bar{C}_{ijkl} \xi_{ml} \frac{\partial v_k}{\partial \xi_m}, \quad (3.13)$$

where $\partial/\partial n = n_i \partial/\partial x_i = |\nabla\phi| \partial/\partial\phi$ denotes differentiation in the direction of the surface normal \mathbf{n} .

If the second-order tensor $n_i \bar{C}_{ijkl} n_l$, which is sometimes referred to as acoustic tensor, is now singular, i.e.,

$$\det(n_i \bar{C}_{ijkl} n_l) = 0, \quad (3.14)$$

the traction rate does not depend on the velocity derivative $\partial v_k/\partial n = m_k$, with \mathbf{m} the right eigenvector associated to the vanishing eigenvalue of $n_i \bar{C}_{ijkl} n_l$. This means that the normal derivative of the velocity component $v_k m_k$ need not be defined in order to satisfy rate

equilibrium, i.e., $v_k m_k$ may be discontinuous across S . Notice that, in contrast to the one-dimensional case, the stationarity of $\dot{\tau}_j$ with respect to the velocity derivative $m_k \partial v_k/\partial n$ does not automatically imply that $\dot{\tau}_j = 0$, i.e., that the traction vector itself is stationary.

If relation (3.14) holds in each point of the surface S , then S is a characteristic surface of the rate equilibrium equations

$$\bar{C}_{ijkl} \frac{\partial^2 v_k}{\partial x_i \partial x_l} + \frac{\partial \bar{C}_{ijkl}}{\partial x_i} \frac{\partial v_k}{\partial x_l} = 0. \quad (3.15)$$

It can be shown that (weak) solutions of linear partial differential equations with smooth coefficients can have discontinuities or discontinuous derivatives only across characteristic surfaces (Courant and Hilbert, 1953). No characteristic surface can be constructed through a point if the characteristic form $\det(n_i \bar{C}_{ijkl} n_l)$ has no real roots in this point. The set of equilibrium equations is then called elliptic and solutions cannot have jumps or derivative jumps in this point.

Boundary value problems are normally associated to partial differential equations which are elliptic in the entire domain. Indeed, the rate equilibrium equations can easily be shown to be elliptic for linear elastic behaviour. In this case the characteristic determinant reads $\det(n_i C_{ijkl} n_l)$, which, after substitution of the elastic constants (2.3) and some algebra, can be written as

$$\det(n_i C_{ijkl} n_l) = \mu^2 (\lambda + 2\mu). \quad (3.16)$$

It can be seen directly that the characteristic determinant is positive for all \mathbf{n} , so that no characteristic surfaces exist and the elastic rate equilibrium equations are elliptic.

Under the influence of damage growth, the ellipticity of the rate equilibrium equations may be lost at a certain stage and consequently discontinuities may arise. Conditions for the loss of ellipticity are difficult to obtain in closed form for general, three-dimensional deformations. Such conditions have been derived by Oliver and Pulido (1998) for plane-stress and plane-strain and a damage model which is somewhat different from that considered here. The loss of ellipticity is illustrated here by the relatively simple case of a triaxial deformation state $\epsilon_{ij} = \epsilon \delta_{ij}$. A closed form expression can then be derived if the normalised energy release rate as defined in (2.15) is used as equivalent strain (cf. Benallal et al., 1989). Substitution of $\epsilon_{ij} = \epsilon \delta_{ij}$ into (2.15) gives the equivalent strain as a function of ϵ :

$$\bar{\epsilon} = 3\sqrt{\frac{K}{E}} \epsilon, \quad (3.17)$$

where the compression modulus K is defined as

$$K = \lambda + \frac{2}{3}\mu = \frac{E}{3(1-2\nu)}. \quad (3.18)$$

For the normalised energy release rate definition of the equivalent strain the tangential moduli (3.10) can be written as

$$\bar{C}_{ijkl} = (1-D)C_{ijkl} - \frac{g(D, \bar{\epsilon})}{E\bar{\epsilon}} C_{ijmn} \epsilon_{mn} \epsilon_{pq} C_{pqkl}, \quad (3.19)$$

or, after substitution of the elastic moduli, the assumed triaxial strain state and relation (3.17),

$$\bar{C}_{ijkl} = (1 - D) \left(\lambda \delta_{ij} \delta_{kl} + \mu (\delta_{ik} \delta_{jl} + \delta_{il} \delta_{jk}) \right) - 3 \varepsilon g(D, \bar{\varepsilon}) K \sqrt{\frac{K}{E}} \delta_{ij} \delta_{kl}. \quad (3.20)$$

This expression can also be written as

$$\bar{C}_{ijkl} = \bar{\lambda} \delta_{ij} \delta_{kl} + \bar{\mu} (\delta_{ik} \delta_{jl} + \delta_{il} \delta_{jk}), \quad (3.21)$$

with $\bar{\lambda}$ and $\bar{\mu}$ defined by

$$\bar{\lambda} = (1 - D) \lambda - 3 \varepsilon g(D, \bar{\varepsilon}) K \sqrt{\frac{K}{E}}, \quad \bar{\mu} = (1 - D) \mu. \quad (3.22)$$

Expression (3.21) is of the same form as expression (2.3) for the elastic moduli. The characteristic determinant can therefore be written down immediately as (cf. (3.16))

$$\det(n_i \bar{C}_{ijkl} n_l) = \bar{\mu}^2 (\bar{\lambda} + 2\bar{\mu}). \quad (3.23)$$

Thus, the characteristic determinant is equal to zero if $\bar{\mu} = 0$ or $\bar{\lambda} + 2\bar{\mu} = 0$. The first solution implies that $D = 1$, i.e., that the material is completely damaged. In this situation one cannot speak of loss of ellipticity because the equilibrium equations are no longer defined. The second solution results in a meaningful condition for the loss of ellipticity before crack initiation:

$$\frac{\varepsilon g(D, \bar{\varepsilon})}{1 - D} = \frac{\lambda + 2\mu}{3K \sqrt{K/E}}. \quad (3.24)$$

When the ellipticity of the partial differential equations is lost in homogeneous problems, the situation becomes similar to the one-dimensional problem. This is the case which is usually considered in localisation studies (e.g., Rudnicki and Rice, 1975; Rice, 1976; Ottosen and Runesson, 1991). Indeed, equation (3.14) is identical to the classical condition for localisation resulting from these analyses. The same criterion also follows from the analysis of acceleration waves in the limit of a vanishing wave velocity (Hill, 1962; Pijaudier-Cabot and Benallal, 1993). For homogeneous damage and homogeneous strains the coefficients of the second-order derivatives in the partial differential system (3.15) are constant, whereas the first-order terms vanish because of $\partial \bar{C}_{ijkl} / \partial x_i = 0$. Loss of ellipticity occurs simultaneously in the entire domain, resulting in a family of parallel, flat characteristic surfaces $\varphi(\mathbf{x}) = C$. Arbitrary velocity fields $v_k = w(\varphi) m_k$, with $w(\varphi)$ zero at those parts of the boundary where kinematic boundary conditions exist, can now be added to the homogeneous solution, such that the resulting velocity field still satisfies the differential equations and boundary conditions. Thus, the boundary value problem has an infinite number of solutions and the problem ceases to be well-posed. If the derivative of $w(\varphi)$ has a finite number of discontinuities, the classical localisation bands of finite width (weak discontinuities) are retrieved (Rudnicki and Rice, 1975; Rice, 1976). Similarly, the case where the function $w(\varphi)$ itself contains jumps corresponds to so-called strong discontinuities, i.e., localisation in a surface (Ottosen and Runesson, 1991; Simo et al., 1993; Oliver, 1996).

In inhomogeneous problems the ellipticity of the differential equations is usually first lost at only one point of the domain. When the velocity field becomes discontinuous at this point, the strain rate is singular. Similar to the one-dimensional inhomogeneous case, this strain rate singularity results in a singular damage growth rate. For continued deformation all stiffness is therefore immediately lost at this point and a crack is initiated. The equilibrium equations locally degenerate and, as discussed in Chapter 2, an internal boundary must be introduced. But the singularity of the damage growth rate also means that the most critical point in front of the crack tip will fail instantaneously, i.e., that the crack starts to propagate. Since the material adjacent to the crack must unload elastically in order to follow the resulting stress drop, the width of the crack remains zero. This implies that the strain and damage growth rate at the crack tip remain singular as the crack grows and consequently that the crack grows at an infinite rate, since each new critical point in front of the momentary crack tip fails immediately. No work is needed in this instantaneous fracture process, since it involves damage growth in a vanishing volume. Thus, the development of a displacement (velocity) jump at some point in the material domain leads to instantaneous, perfectly brittle fracture.

3.2 Quasi-brittle fracture

It has been shown in Chapter 2 that the damage model for quasi-brittle fracture must show a rapid growth of damage immediately after reaching the elastic limit in order to realistically describe the softening behaviour observed in experiments (Figure 2.4). As a consequence of this rapid initial damage growth, loss of ellipticity occurs immediately after reaching the damage threshold in quasi-brittle damage models. It has further been shown in the previous section that loss of ellipticity in one point of the domain may result in immediate, complete fracture without energy dissipation. It can therefore be concluded that the quasi-brittle damage model predicts perfectly brittle fracture right after the elastic limit has been reached somewhere in the component. The gradual loss of stiffness in the post-peak regime, which the model was supposed to describe, cannot be observed at the structural level because the strain softening comes only into play in a vanishing volume.

Finite element solutions try to follow the nonphysical behaviour of the actual solution, but are limited in doing so by their finite spatial resolution. Standard finite element methods deliver weak solutions of boundary value problems, but in a Galerkin sense rather than a distribution sense. For the second-order partial differential equations of the equilibrium problem this means that the displacement field must be C_0 -continuous, i.e., the displacements are continuous and piecewise continuously differentiable. The displacement jumps and singular strains of the actual solution can therefore only be approximated by high, but finite displacement gradients in the finite element solution. As a consequence, a finite volume is involved in the damage process, and thus a positive amount of energy is dissipated in the fracture process. Also, because the damage growth rate at the tip of the damage band remains finite, the crack propagates at a finite velocity.

When the spatial discretisation grid is refined, however, the finite element approximation becomes more accurate in the sense that the displacement gradients which describe the discontinuities become stronger. Consequently, the predicted fracture energy becomes smaller

and the crack propagates faster. In the limit of vanishingly small elements, the actual solution is retrieved, i.e., zero fracture energy and an infinite crack growth rate. This convergence of the finite element approximation to the actual, nonphysical solution of the problem is the origin of the apparent mesh sensitivity of damage models and other continuous descriptions of fracture.

An example is given in Figure 3.3, which shows the load-displacement curves obtained from two-dimensional finite element analyses of crack growth in a compact tension specimen made of a composite material. The problem and modelling will be described in detail in Chapter 6. Four different finite element meshes have been used, with an increasingly finer discretisation in the region which is affected by damage. In the coarsest mesh square elements with an edge length of $h = 2$ mm were used; this length was successively halved in the finer meshes. Figure 3.3 shows that each level of further refinement results in a lower predicted fracture strength and in a more brittle post-peak response.

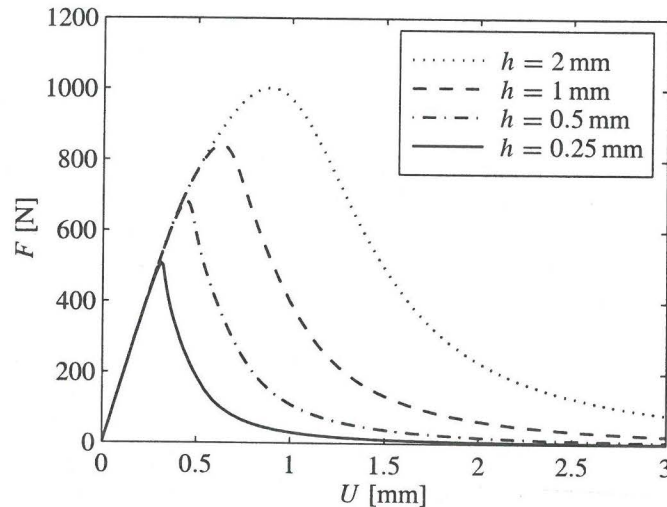


Figure 3.3: Predicted load-displacement response of a compact tension specimen modelled with elements of 2, 1, 0.5 and 0.25 mm.

Apart from the dependence of the fracture energy and crack growth rate on the mesh fineness, the finite element description of displacement discontinuities by strong gradients also introduces preferential directions for the propagation of damage. As a consequence, crack patterns predicted by numerical damage analyses tend to be aligned with the finite element grid (e.g., Sluys, 1992; Jirásek, 1998).

3.3 Fatigue

In contrast to the quasi-brittle damage model, the initial damage growth in the fatigue model is slow and therefore has little effect on stresses and strains (cf. Figure 2.6). Consequently, the rate equilibrium equations remain elliptic until near the end of the fatigue life, when the growth of damage becomes faster. Even if the ellipticity of the governing equations is lost at this stage and a crack is immediately initiated, this has a limited effect on the predicted number of cycles needed to initiate the crack (i.e., the initiation life).

It can be shown that there can be no loss of ellipticity at all for the cycle based growth law (2.20). If f denotes the frequency of the loading cycles, the rate of damage growth is given by (2.20) as

$$\dot{D} = fG(D, \varepsilon_a). \quad (3.25)$$

Using this relation, the stress rate $\dot{\sigma}_{ij}$ can be written as

$$\dot{\sigma}_{ij} = (1 - D)C_{ijkl}\dot{\varepsilon}_{kl} - fG(D, \varepsilon_a)C_{ijkl}\varepsilon_{kl}, \quad (3.26)$$

where ε_{kl} must be interpreted as the strain state for which $\bar{\varepsilon} = \varepsilon_a$. Likewise, σ_{ij} represents the stress envelope rather than the stress variations within the loading cycles. Notice that the second term in (3.26), which represents the effect of damage growth on the stress rate, does not depend on the strain rate. As a consequence, this term appears as a source term rather than a differential coefficient when (3.26) is substituted into the rate equilibrium equations $\partial\dot{\sigma}_{ij}/\partial x_i = 0$:

$$(1 - D)C_{ijkl}\frac{\partial^2 v_k}{\partial x_i \partial x_l} = fG(D, \varepsilon_a)C_{ijkl}\frac{\partial \varepsilon_{kl}}{\partial x_i} + f\left(\frac{\partial G}{\partial D}\frac{\partial D}{\partial x_i} + \frac{\partial G}{\partial \varepsilon_a}\frac{\partial \varepsilon_a}{\partial x_i}\right)C_{ijkl}\varepsilon_{kl}. \quad (3.27)$$

Ellipticity is lost when the characteristic determinant associated to this set of equations becomes zero, i.e., when

$$\det((1 - D)n_i C_{ijkl} n_l) = 0, \quad (3.28)$$

or, invoking (3.16), when

$$(1 - D)^3 \mu^2 (\lambda + 2\mu) = 0. \quad (3.29)$$

This equation cannot be satisfied when $D < 1$, and the rate equilibrium equations thus remain elliptic until a crack is initiated. Apparently, the transition from the rate form (2.8) to the cycle based form (2.20) removes the possibility of loss of ellipticity. As a result, displacements remain continuously differentiable and a stable growth of damage is obtained in a finite volume (see Peerlings, 1997, for an example).

Even if loss of ellipticity does not occur, the initiation of a crack (when $D = 1$ at a certain point) still introduces a singularity in the problem. Indeed, a singularity may already be present in the initial problem as a result of the geometry. Since the crack faces must be stress-free, the strain at the crack tip becomes singular for continued loading. As a consequence of

this singularity of the strain, or of the strain amplitude in a cycle approach, the damage growth rate is infinite. This in turn means that the crack will immediately traverse the remaining cross-section of the component (cf. the discussion at the end of Section 3.1). Thus, the model predicts instantaneous, perfectly brittle fracture, instead of the small amount of crack growth per cycle which is observed in experiments.

Similar to quasi-brittle damage, finite element solutions are limited by their spatial resolution in capturing the singularity at the crack tip. Consequently, finite element simulations show a finite crack growth rate, which increases as the spatial discretisation is refined. An example of this apparent mesh sensitivity is given in Figure 3.4. The diagram shows the steady-state fatigue crack growth rate predicted by a finite element analysis versus the size of the elements which were used in this analysis. The problem geometry, loading conditions and modelling for which these results have been obtained will be detailed in Chapter 6. The dependence of the crack growth per cycle, da/dN , on the element size h is quite strong in this example: a decrease of the element size by roughly one decade leads to an increase of the crack growth rate by almost three decades.

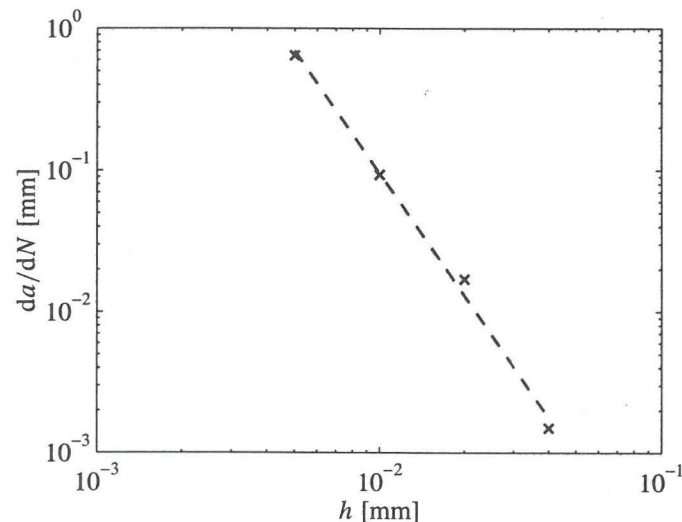


Figure 3.4: Predicted fatigue crack growth rate versus element size.

A similar trend has been observed in dynamic ductile fracture by Needleman and Tvergaard (1998) and in creep crack growth problems by Saanouni et al. (1989) and Liu et al. (1994). However, only the latter authors seem to have made a connection with singularities at the crack tip. It is further noted that the sensitivity of predicted crack paths to the orientation of the discretisation may be even larger in fatigue (and creep) problems than in quasi-brittle damage because the strongly progressive damage growth of these models renders them more sensitive to initial conditions and numerical errors.

3.4 Regularisation methods

From the previous sections it has become clear that merely improving numerical solution schemes cannot eliminate the problems associated to localisation and mesh sensitivity. Even if the convergence to the actual solution is improved, the fact remains that this solution does not show the intended behaviour and may not even make sense from a physical point of view. Nevertheless, some authors have proposed to adapt the parameters of the damage growth relation to the spatial discretisation in such a way that a constant global response (e.g., fracture energy) is obtained for different element sizes (Pietruszczak and Mróz, 1981; Simo, 1989; Brekelmans and de Vree, 1995). Damage growth remains limited to a band of elements in this so-called fracture energy approach, and the width of the predicted damage zone thus still depends on the element size. Furthermore, the direction of crack growth is still sensitive to the orientation of the finite element mesh. Nevertheless, this approach may be practical in some situations when used carefully.

A second, related strategy introduces enhanced finite element interpolations to describe the damage zone as a band of fixed width (weak discontinuity) or a surface (strong discontinuity) (Ortiz et al., 1987; Larsson and Runesson, 1993; Oliver, 1996; Sluys and Berends, 1998). For some particular cases the weak discontinuity approach can be shown to yield finite element formulations which are identical to those resulting from the fracture energy approach (Berends, 1996; Sluys, 1998) and may thus inherit some of its disadvantages. Indeed, finite element analyses using weak discontinuities may be sensitive to the mesh orientation (Sluys, 1997). When a strong discontinuity is used to model the damage zone, the constitutive relations must be reformulated in terms of relative displacements instead of strains in order to obtain a finite fracture energy. These models are therefore closely related to the cohesive zone and fictitious crack approaches of nonlinear fracture mechanics (Dugdale, 1960; Barenblatt, 1962; Hillerborg et al., 1976).

On the other hand, a number of methods have been developed which aim at avoiding the pathological localisation of deformation and damage growth (or plastic flow) by improving the continuum model. The preceding discussion has shown that it is not sufficient for these so-called regularisation methods to preserve the ellipticity of the rate equilibrium problem, since loss of ellipticity only acts as the initiator of instantaneous fracture. In order to realistically describe the growth of cracks the regularisation must also remove the damage growth rate singularity at the crack tip. The different approaches are discussed here only briefly; see for instance Pijaudier-Cabot et al. (1988), Sluys (1992) or de Borst et al. (1993) for detailed discussions and comparisons.

Viscous or time-dependent terms in the constitutive model may prevent the loss of ellipticity of the original, time-independent solids. Under transient loading conditions a natural approach is therefore to include the inherent rate sensitivity of many materials in the constitutive description (Needleman, 1988; Sluys and de Borst, 1994).

Cosserat continua introduce micro-rotations as degrees of freedom, in addition to the conventional displacements. Gradients of these rotations give rise to micro-couples, which appear in the moment of momentum equations. The interaction between these rotational balances and the conventional, translational balances prevents the concentration of deformations

in a surface. However, a mode-II component is needed in the deformation field in order to activate this mechanism. As a consequence, pathological localisation may still occur in problems which are dominated by mode-I loading (Mühlhaus and Vardoulakis, 1987; de Borst and Mühlhaus, 1991; Sluys, 1992).

Nonlocal models abandon the principle of local action satisfied by conventional continuum models. Weighted volume averages of certain state variables appear in the continuum model, thus introducing direct spatial interactions. The nonlocality has a smoothing effect on the deformation and on the damage, thus precluding localisation in a surface (Bažant et al., 1984; Pijaudier-Cabot and Bažant, 1987; Tvergaard and Needleman, 1995; de Vree et al., 1995).

Gradient-enhanced models or higher-order continua use higher-order deformation gradients or gradients of internal variables to create spatial interactions. Similar to the nonlocal models, discontinuities are smoothed by these models so that strains remain finite (Aifantis, 1984; Coleman and Hodgdon, 1985; Lasry and Belytschko, 1988; Mühlhaus and Aifantis, 1991; de Borst et al., 1995).

The nonlocal and gradient approaches, which are closely related, seem to be the most generally applicable. The potential of these methods in describing crack growth problems is therefore examined in detail in the next chapter.

Chapter 4

Nonlocal and gradient-enhanced damage

Damage in engineering materials is highly inhomogeneous and localised. Microcracks are initiated at stress concentrations and their subsequent growth affects a volume which is usually small compared to the entire structural component. Since the development of damage is governed by microstructural changes and interactions, the scale of the microstructure plays an important role in setting the size of the damaged region. For instance, the intragranular slip processes which are responsible for metal fatigue are strongly influenced by the grain boundaries. As a consequence, the grain size has an important effect on the extent of fatigue damage (Hertzberg, 1989; Suresh, 1991). Similarly, cracks in concrete and fibre reinforced polymers are bridged by aggregates and fibres, respectively, which renders the fracture process sensitive to the size and distribution of these microstructural elements. Indeed, the dependence of the width of damaged zones on the length of fibres in short fibre reinforced polymers has been established experimentally by Geers et al. (1998a, 1999a).

However, the scale of the microstructure is not included in the classical damage models as discussed in the previous chapters. The volume that is affected by damage is therefore not properly defined by these models. As a consequence of this indefiniteness the growth of damage localises in a surface, thus bringing about the physically unrealistic behaviour demonstrated in the previous chapter. In order to limit the localisation of damage to the scale of the microstructure, terms must be added to the constitutive modelling which describe the influence of the microstructure on the damage process. A conceptually simple way to do so is by introducing nonlocality into the constitutive relations. This approach is explained in Section 4.1. The nonlocality can also take the form of higher-order deformation gradients in the constitutive relations. Section 4.2 shows how gradient-enhanced models can be derived as approximations of the nonlocal theory. Special attention is given to the treatment of boundaries in both approaches (Section 4.3). The effect of the nonlocality on the initiation and propagation of cracks is shown in Sections 4.4 and 4.5, respectively. The salient properties of both approaches are briefly reviewed, finally, in Section 4.6.

4.1 Nonlocal damage mechanics

In Chapter 2 damage variables have been introduced as field variables which describe microstructural defects in a continuum sense. This implies that the damage variables vary smoothly at the scale of the microstructure, or at least that they do not vary strongly within microstructural elements (e.g., grains). In the previous chapter it has been shown, however, that in the standard model damage tends to localise in a vanishing volume, i.e., in a volume which is much smaller than that of the microstructural elements. This strongly discontinuous damage distribution conflicts with the supposed smoothness of the damage variable. The nonphysical behaviour of the model is a direct consequence of this inconsistency.

The necessary piecewise smoothness of the damage field can be ensured by defining the damage variable explicitly at the level of the microstructural elements. The growth of the damage variable associated to an element then depends on the average deformation in the element. In terms of the elasticity based damage model the above reasoning means that the growth of damage in a point \mathbf{x} is no longer governed by the local equivalent strain $\tilde{\epsilon}(\mathbf{x})$, but by the average of $\tilde{\epsilon}$ on the volume $\Omega_e(\mathbf{x})$ occupied by the microstructural element at \mathbf{x} :

$$\bar{\epsilon}(\mathbf{x}) = \frac{1}{\Omega_e(\mathbf{x})} \int_{\Omega_e(\mathbf{x})} \tilde{\epsilon}(\mathbf{y}) d\Omega. \quad (4.1)$$

where \mathbf{y} denotes the position of the infinitesimal volume $d\Omega$. The loading function (2.7) and the damage evolution law (2.8) must then be replaced by

$$f(\bar{\epsilon}, \kappa) = \bar{\epsilon} - \kappa \quad (4.2)$$

and

$$\dot{D} = g(D, \bar{\epsilon}) \dot{\bar{\epsilon}}. \quad (4.3)$$

The dependence of the value of $\bar{\epsilon}$ in \mathbf{x} on the strain state in a finite volume $\Omega_e(\mathbf{x})$ implies that the constitutive model does no longer satisfy the principle of local action. The model has become nonlocal, i.e., stresses in a point \mathbf{x} depend on the deformation not only in \mathbf{x} itself, but also in its vicinity. Accordingly, the averaged strain $\bar{\epsilon}$ is often referred to as nonlocal equivalent strain. Physically, this nonlocality represents long-range interactions and heterogeneities at the microscale, which can no longer be neglected when the scale of fluctuations of the constitutive variables approaches that of the microstructure (Beran and McCoy, 1970; Eringen and Edelen, 1972; Bažant, 1991).

Definition (4.1) of the nonlocal equivalent strain corresponds with the cell averaging of Hall and Hayhurst (1991). It is meaningful when the microstructure is known in detail, for instance because the material consists of a regular stacking of well defined microstructural elements. When the microstructure is not periodic, however, such as in polycrystalline materials, concrete, etc., taking into account the full detail of the material structure becomes unpractical. The cell average can then be replaced by a moving average on a volume which corresponds to the average size of the microstructural elements, for instance to the average

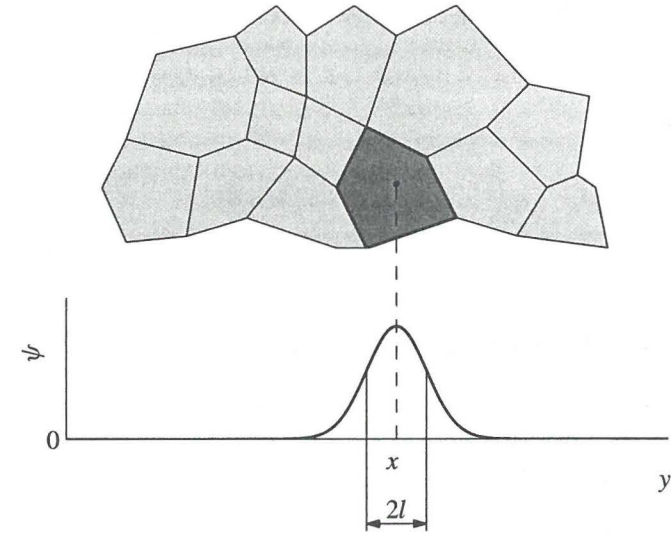


Figure 4.1: Weighted averaging for an irregular microstructure.

grain size. Furthermore, since the averaging volume is no longer explicitly related to the material structure, and to account for variations in the grain size, it seems appropriate to use a smooth weight function rather than the piecewise uniform weighting which has been implicitly assumed in (4.1), see Figure 4.1. The nonlocal equivalent strain $\bar{\epsilon}$ is then defined by (Pijaudier-Cabot and Bažant, 1987)

$$\bar{\epsilon}(\mathbf{x}) = \frac{1}{\Psi(\mathbf{x})} \int_{\tilde{\Omega}} \psi(\mathbf{y}; \mathbf{x}) \tilde{\epsilon}(\mathbf{y}) d\Omega, \quad (4.4)$$

with $\psi(\mathbf{y}; \mathbf{x})$ the weight function. The factor $1/\Psi(\mathbf{x})$, with $\Psi(\mathbf{x})$ defined by

$$\Psi(\mathbf{x}) = \int_{\tilde{\Omega}} \psi(\mathbf{y}; \mathbf{x}) d\Omega, \quad (4.5)$$

scales $\bar{\epsilon}$ such that it equals $\tilde{\epsilon}$ for homogeneous strain states. Notice that the integration in (4.4) and (4.5) is limited to the domain $\tilde{\Omega} = \Omega \setminus \Omega_c$ where $D < 1$, because $\tilde{\epsilon}$ is not uniquely defined on Ω_c (see also the next section).

The weight function $\psi(\mathbf{y}; \mathbf{x})$ is assumed to be homogeneous and isotropic, i.e., it depends only on the distance $\rho = |\mathbf{x} - \mathbf{y}|$ between the points \mathbf{y} and \mathbf{x} : $\psi(\mathbf{y}; \mathbf{x}) = \psi(\rho)$. Several functions $\psi(\rho)$ have been considered in the literature, of which the Gaussian function seems to have become the most popular (see Figure 4.1):

$$\psi(\rho) = \frac{1}{(2\pi)^{3/2} l^3} \exp\left[-\frac{\rho^2}{2l^2}\right]. \quad (4.6)$$

The factor $(2\pi)^{-3/2}l^{-3}$ in this expression normalises the weight function on \mathbb{R}^3 such that

$$\int_{\mathbb{R}^3} \psi(\rho) d\Omega = 1. \quad (4.7)$$

The length parameter l determines the volume which contributes significantly to the nonlocal equivalent strain and must therefore be related to the scale of the microstructure. Notice that the local continuum is retrieved when $l \rightarrow 0$, since $\bar{\varepsilon}$ then becomes equal to $\tilde{\varepsilon}$.

4.2 Gradient formulations

For sufficiently smooth $\tilde{\varepsilon}$ -fields, the integral relation (4.4) can be rewritten in terms of gradients of $\tilde{\varepsilon}$ by expanding $\tilde{\varepsilon}(\mathbf{y})$ into a Taylor series (Bažant et al., 1984; Lasry and Belytschko, 1988; Peerlings et al., 1995, 1996a):

$$\begin{aligned} \bar{\varepsilon}(\mathbf{y}) = & \tilde{\varepsilon}(\mathbf{x}) + \frac{\partial \tilde{\varepsilon}}{\partial x_i} (y_i - x_i) + \frac{1}{2!} \frac{\partial^2 \tilde{\varepsilon}}{\partial x_i \partial x_j} (y_i - x_i)(y_j - x_j) \\ & + \frac{1}{3!} \frac{\partial^3 \tilde{\varepsilon}}{\partial x_i \partial x_j \partial x_k} (y_i - x_i)(y_j - x_j)(y_k - x_k) \\ & + \frac{1}{4!} \frac{\partial^4 \tilde{\varepsilon}}{\partial x_i \partial x_j \partial x_k \partial x_l} (y_i - x_i)(y_j - x_j)(y_k - x_k)(y_l - x_l) + \dots \end{aligned} \quad (4.8)$$

Substitution of this relation into (4.4) yields after some calculus

$$\bar{\varepsilon}(\mathbf{x}) = \tilde{\varepsilon}(\mathbf{x}) + c_i \frac{\partial^2 \tilde{\varepsilon}}{\partial x_i^2} + c_{ij} \frac{\partial^4 \tilde{\varepsilon}}{\partial x_i^2 \partial x_j^2} + \dots \quad (4.9)$$

where the coefficients c_i and c_{ij} are given by

$$\begin{aligned} c_i &= \frac{1}{2! \Psi} \int_{\tilde{\Omega}} \psi(\rho) (y_i - x_i)^2 d\Omega, \\ c_{ij} &= \frac{1}{4! \Psi} \int_{\tilde{\Omega}} \psi(\rho) (y_i - x_i)^2 (y_j - x_j)^2 d\Omega. \end{aligned} \quad (4.10)$$

Odd derivatives vanish in (4.9) as a result of the isotropy of the weight function and the coefficients c_i (with $i = 1, 2, 3$) are all equal, so that the index i can be dropped. It should be noted that this is true only when the support of the weight function ψ lies entirely in the domain $\tilde{\Omega}$, i.e., if \mathbf{x} is sufficiently far from the boundary $\tilde{\Gamma}$ of $\tilde{\Omega}$. For the Gaussian function (4.6) this condition can only be met when $\tilde{\Omega}$ equals \mathbb{R}^3 . However, the relevance of

the equation (4.9) lies not so much in its strict equivalence with (4.4), but in the fact that it provides the possibility to approximate the integral relation (4.4) by the differential relation

$$\bar{\varepsilon} = \tilde{\varepsilon} + c \nabla^2 \tilde{\varepsilon}, \quad (4.11)$$

where the Laplacian operator ∇^2 is defined by $\nabla^2 = \sum_i \partial^2 / \partial x_i^2$. Equation (4.11) is obtained by neglecting terms of order four and higher in (4.9). The dependence on the coordinates \mathbf{x} has been dropped for brevity. If the nonlocal equivalent strain defined by (4.11) is used in the loading function (4.2) and growth law (4.3), a gradient-enhanced damage model is obtained. The internal length scale of the nonlocal model is preserved in the gradient coefficient c , which is of the dimension length squared. For instance, for the Gaussian weight function (4.6) on \mathbb{R}^3 (4.10)¹ gives $c = \frac{1}{2}l^2$. Substitution of (4.11) into the equilibrium equations results in a set of fourth-order partial differential equations instead of the usual second-order equations. For this reason, additional boundary conditions must be specified in order for the equilibrium problem to be well-posed, see Section 4.3.

An alternative gradient formulation can be derived from (4.9) by applying the Laplacian operator to it and multiplying by c . If the result is subtracted from (4.9), the following relation is obtained:

$$\bar{\varepsilon} - c \nabla^2 \bar{\varepsilon} = \tilde{\varepsilon} + (c_{ij} - c^2) \frac{\partial^4 \tilde{\varepsilon}}{\partial x_i^2 \partial x_j^2} + \dots \quad (4.12)$$

Again neglecting terms of order four and higher in the right-hand-side gives a second approximation of (4.4):

$$\bar{\varepsilon} - c \nabla^2 \bar{\varepsilon} = \tilde{\varepsilon}. \quad (4.13)$$

In contrast to definition (4.11), the nonlocal strain $\bar{\varepsilon}$ is not given explicitly in terms of $\tilde{\varepsilon}$ and its derivatives, but as the solution of the boundary value problem consisting of the Helmholtz equation (4.13) and appropriate boundary conditions, see Section 4.3. The resulting gradient damage formulation will therefore be referred to as implicit, while the model based on (4.11) will be referred to as explicit gradient formulation.

For simple geometries equation (4.13) can be solved analytically using Green's function associated to the boundary value problem. Green's function $G(\mathbf{x}; \mathbf{y})$ is defined as the (weak) solution of the partial differential equation (4.13) with the source term replaced by a Dirac function $\delta(\mathbf{x} - \mathbf{y})$,

$$G(\mathbf{x}; \mathbf{y}) - c \nabla^2 G(\mathbf{x}; \mathbf{y}) = \delta(\mathbf{x} - \mathbf{y}), \quad (4.14)$$

which satisfies the boundary conditions associated to (4.13). For the free-space problem (i.e., $\Omega = \mathbb{R}^3$) these boundary conditions are replaced by the requirement that $G(\mathbf{x}; \mathbf{y}) \rightarrow 0$ as $|\mathbf{x}| \rightarrow \infty$. The corresponding free-space Green's function is given by (Zauderer, 1989):

$$G(\mathbf{x}; \mathbf{y}) = \frac{1}{4\pi c \rho} \exp \left[-\frac{\rho}{\sqrt{c}} \right], \quad (4.15)$$

where $\rho = |\mathbf{x} - \mathbf{y}|$. The right-hand-side of the original equation (4.13) is now considered as a superposition of Dirac functions:

$$\tilde{\varepsilon}(\mathbf{x}) = \int_{\Omega} \tilde{\varepsilon}(\mathbf{y}) \delta(\mathbf{x} - \mathbf{y}) \, d\Omega. \quad (4.16)$$

The solution of this problem is then obtained by the same superposition of Green's functions:

$$\bar{\varepsilon}(\mathbf{x}) = \int_{\Omega} \tilde{\varepsilon}(\mathbf{y}) G(\mathbf{x}; \mathbf{y}) \, d\Omega. \quad (4.17)$$

Since Green's function is symmetric in its arguments, i.e., $G(\mathbf{x}; \mathbf{y}) = G(\mathbf{y}; \mathbf{x})$, this relation can also be written as

$$\bar{\varepsilon}(\mathbf{x}) = \int_{\Omega} G(\mathbf{y}; \mathbf{x}) \tilde{\varepsilon}(\mathbf{y}) \, d\Omega, \quad (4.18)$$

which is of exactly the same form as equation (4.4) for the nonlocal model. This means that the gradient damage model based on the differential equation (4.13) can be considered as a special case of the class of nonlocal models, in which the weight function $\psi(\mathbf{y}; \mathbf{x})$ is defined as Green's function $G(\mathbf{y}; \mathbf{x})$. For the free-space problem this weight function has been plotted as a function of ρ in Figure 4.2. A value of $\sqrt{c} = 1$ mm has been used for the internal length scale. The Gaussian weight function (4.6), with the corresponding internal length $l = \sqrt{2c} = \sqrt{2}$ mm, is also shown for comparison. Notice that

$$\int_{\mathbb{R}^3} G(\mathbf{y}; \mathbf{x}) \, d\Omega = 1, \quad (4.19)$$

so that both weight functions are normalised. The most striking difference between the two functions is that Green's function is singular at $\rho = 0$, while the Gaussian weight function remains finite. However, since the volume associated to small ρ is relatively small, this singularity probably has a limited effect on the overall response of the implicit formulation. Green's function assigns more weight to points at a smaller distance ρ compared to the Gaussian function. The 'average' interaction distance is therefore smaller for the implicit gradient model than for the nonlocal model.

Relation (4.18) shows that the gradient model according to (4.13) is truly nonlocal in the sense that variations of the local equivalent strain in a point \mathbf{y} always affect the nonlocal equivalent strain $\bar{\varepsilon}$ in \mathbf{x} . This is not true for the explicit approximation (4.11), since variations of $\tilde{\varepsilon}(\mathbf{y})$ at some distance from \mathbf{x} may have no effect on $\tilde{\varepsilon}(\mathbf{x})$ and $\nabla^2 \tilde{\varepsilon}(\mathbf{x})$, and thus on $\bar{\varepsilon}(\mathbf{x})$. For a sufficiently smooth $\tilde{\varepsilon}$ -field, (4.18) can be written in the differential format (4.9). The coefficients of the higher-order derivatives, which then depend on Green's function, will not generally vanish. Thus, although terms with higher-order derivatives of $\tilde{\varepsilon}$ were neglected in

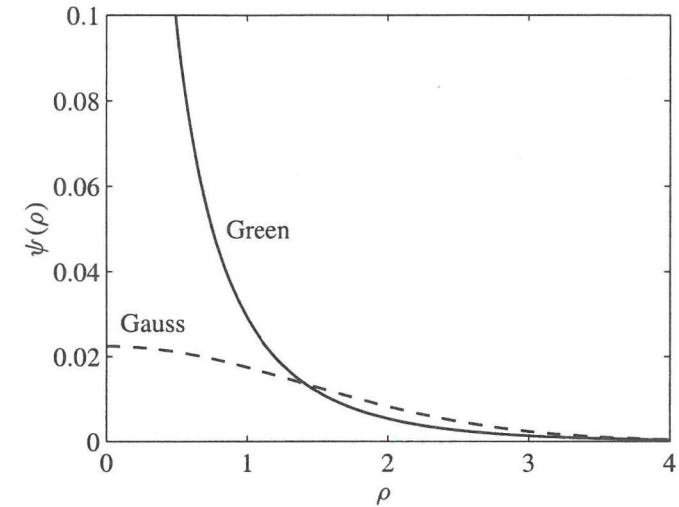


Figure 4.2: Comparison of Green's function (4.15) and Gaussian weight function (4.6).

constructing (4.13), they are still implicitly present in the derivative of $\bar{\varepsilon}$ in (4.13). This is in contrast to the explicit gradient approximation (4.11), in which the higher-order terms have been entirely neglected. It will be shown in the remainder that these subtle differences between the two gradient approximations have an important effect on the localisation behaviour of the resulting gradient damage models.

It is noted that gradient models need not necessarily be considered as approximations of the corresponding nonlocal theory. Some authors have directly included gradient terms on a thermodynamical or phenomenological basis. Assuming that the power of internal forces depends on the gradient of the damage variable, Frémond and Nedjar (1995) have arrived at a second-order partial differential equation of the same type as the implicit relation (4.13), but in terms of the damage variable. A similar formulation has been derived by Pijaudier-Cabot and Burlion (1996) from a void growth model. Phenomenological considerations have led to the gradient damage formulations of Comi and Driemeier (1997); Comi (1998) and de Borst et al. (1996).

4.3 Boundary conditions

The need for additional boundary conditions in the gradient damage formulations has already been touched upon briefly in the previous section. The treatment of boundaries may have an important effect on the behaviour of the models, particularly in terms of crack growth. The subject is therefore discussed here in detail for the two gradient formulations and for the nonlocal model.

The situation is perhaps the clearest in the implicit gradient model, based on equation (4.13). This approach defines an additional, second-order partial differential equation in terms of the nonlocal strain $\bar{\epsilon}$. A unique solution requires that the value of $\bar{\epsilon}$, its normal derivative, or a linear combination of these quantities is specified on the boundary Γ . Fixing $\bar{\epsilon}$ itself seems to be difficult to motivate on physical grounds. The natural boundary condition

$$\frac{\partial \bar{\epsilon}}{\partial n} \equiv n_i \frac{\partial \bar{\epsilon}}{\partial x_i} = 0, \quad (4.20)$$

with \mathbf{n} the unit normal to Γ , is therefore adopted here. With this boundary condition $\bar{\epsilon}$ equals $\bar{\epsilon}$ for homogeneous deformations and the gradient approximation is thus consistent with the nonlocal relation (4.4) in this respect.

In the presence of cracks, equation (4.13) is defined only on the domain $\tilde{\Omega}$ where the damage variable has not yet become critical. This is not only natural, since the equilibrium problem is defined only on $\tilde{\Omega}$, but also necessary because the right-hand-side $\bar{\epsilon}$ is not uniquely defined in the cracked region as a result of the indefiniteness of the displacement field (see Chapter 2). The boundary condition (4.20) associated to (4.13) must therefore be defined on the boundary $\tilde{\Gamma}$ of $\tilde{\Omega}$, i.e., not only at the boundary of the problem domain, but also at the internal boundary which represents the crack.

The explicit gradient approach according to (4.11) does not introduce an additional differential equation, but renders the stresses dependent on second-order derivatives of the equivalent strain. Since these second-order derivatives of $\bar{\epsilon}$ are related to third-order derivatives of the displacements and since equilibrium involves one more differentiation, fourth-order displacement derivatives enter the equilibrium equations. However, these fourth-order terms become active only in the process zone, i.e., in the region where damage grows. In the remaining part of the body the equilibrium equations are still of order two, except, obviously, in the completely damaged region Ω_c , where the equilibrium equations are meaningless. A similar situation thus arises as in the gradient plasticity model of de Borst and Mühlhaus (1992). Additional conditions must be provided at the internal boundary between the process zone and the remaining material, or, where the process zone touches the boundary $\tilde{\Gamma}$ of the equilibrium problem, at this external boundary. At the internal boundary these conditions are provided by continuity requirements (cf. de Borst and Mühlhaus, 1992). At the external boundary, however, they must be explicitly defined in terms of higher-order normal derivatives of the displacements.

The treatment of boundaries in the nonlocal model seems to be the most natural. The normalisation of $\bar{\epsilon}$ by Ψ ensures that $\bar{\epsilon}$ does not become unrealistically small when part of the support of the weight function lies outside the problem domain. This normalisation can therefore be considered as the nonlocal counterpart of the additional boundary conditions in the gradient models. It has already been stipulated in Section 4.1 that the cracked region Ω_c must not be included in the integral which defines $\bar{\epsilon}$. Accordingly, the normalisation by Ψ must also be applied at the internal boundary which represents the crack and it must be re-evaluated as the crack grows. The necessity of this identical treatment of internal and external boundaries does not seem to have been recognised in the literature. If the – nonphysical – strains in the crack are included in the integration, however, the nonlocal equivalent strains at

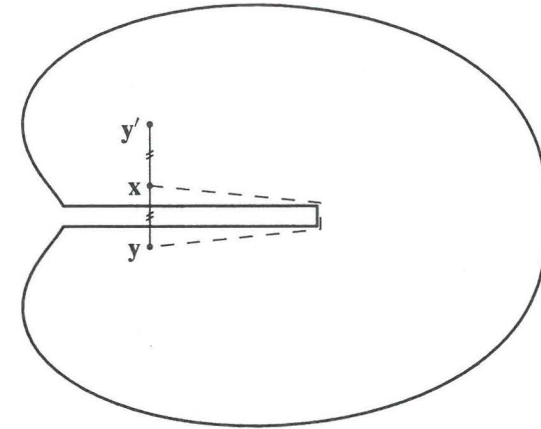


Figure 4.3: Nonlocality at a sharp notch.

both faces of the crack increase as the crack opening increases. As a consequence, the damage variable continues to grow at the crack faces and the width of the crack thus continues to increase along the entire crack surface, until it finally occupies the entire domain. The implicit gradient formulation exhibits the same behaviour if the crack is not correctly separated from the remaining material by defining the boundary condition (4.20) at the internal boundary (Geers, 1997).

For strongly concave geometries the spatial interactions modelled by the standard nonlocal approach become questionable. Consider for instance the sharp notch of Figure 4.3. In the standard nonlocal model the influence of the strain in a point \mathbf{y} across the notch has the same effect on the nonlocal strain in \mathbf{x} as that in a point \mathbf{y}' at the same distance, but on the same side of the notch. This example may seem academic, since the domain of influence around \mathbf{x} , which is related to the intrinsic length scale l , will often be small compared with the thickness of the notch. However, the same situation arises at cracks, which have a thickness which is of the same order as l or even smaller. The problem can be avoided by reformulating the weight function in (4.4) in terms of the smallest distance within the domain $\tilde{\Omega}$ (i.e., the dashed line in Figure 4.3). This is done in a natural way in the gradient models, in which direct interactions between the faces of the notch are impossible.

4.4 Crack initiation

It has been shown in Chapter 3 that the classical, local damage model predicts the immediate initiation of a crack when the displacement field becomes discontinuous. This is particularly undesirable in quasi-brittle damage modelling, where discontinuities may arise right after reaching the elastic limit and stable damage growth thus becomes impossible. A necessary condition for the existence of displacement discontinuities is the loss of ellipticity of the rate equilibrium equations. The introduction of nonlocality – either in an integral or in a

differential format – can prevent the loss of ellipticity. This can be easily shown for the implicit gradient formulation. For the three regularised models the stress rate can be written as

$$\dot{\sigma}_{ij} = (1 - D)C_{ijkl} \frac{\partial v_k}{\partial x_l} - g(D, \bar{\varepsilon})C_{ijkl}\varepsilon_{kl}\dot{\bar{\varepsilon}}. \quad (4.21)$$

Substitution of this relation into the rate equilibrium equations yields

$$(1 - D)C_{ijkl} \frac{\partial^2 v_k}{\partial x_i \partial x_l} - \frac{\partial D}{\partial x_i} C_{ijkl} \frac{\partial v_k}{\partial x_l} - g(D, \bar{\varepsilon})C_{ijkl}\varepsilon_{kl} \frac{\partial \dot{\bar{\varepsilon}}}{\partial x_i} - C_{ijkl} \left(g(D, \bar{\varepsilon}) \frac{\partial \varepsilon_{kl}}{\partial x_i} + \varepsilon_{kl} \frac{\partial g}{\partial D} \frac{\partial D}{\partial x_i} + \varepsilon_{kl} \frac{\partial g}{\partial \bar{\varepsilon}} \frac{\partial \bar{\varepsilon}}{\partial x_i} \right) \dot{\bar{\varepsilon}} = 0 \quad (4.22)$$

for $j = 1, 2, 3$. After differentiation with respect to time, relation (4.13) for the implicit gradient formulation can be rewritten as

$$c \sum_{i=1}^3 \frac{\partial^2 \dot{\bar{\varepsilon}}}{\partial x_i^2} + \frac{\partial \bar{\varepsilon}}{\partial \varepsilon_{kl}} \frac{\partial v_k}{\partial x_l} - \dot{\bar{\varepsilon}} = 0. \quad (4.23)$$

Together, equations (4.22) and (4.23) form a system of four second-order partial differential equations in terms of the variables $\mathbf{v}^* = [v_1, v_2, v_3, \dot{\bar{\varepsilon}}]^T$. The classification of this system depends on the principal part of the differential equations, i.e., on the second-order terms. If the coefficients of these second-order derivatives $\partial^2 v_k^* / \partial x_i \partial x_l$ are defined as C_{ijkl}^* ($i, l = 1, 2, 3$ and $j, k = 1, 2, 3, 4$), with

$$\begin{aligned} C_{ijkl}^* &= (1 - D)C_{ijkl} & \text{for } j, k = 1, 2, 3, \\ C_{ijkl}^* &= 0 & \text{for } j = 1, 2, 3, k = 4 \text{ and } j = 4, k = 1, 2, 3, \\ C_{ijkl}^* &= c\delta_{il} & \text{for } j, k = 4, \end{aligned} \quad (4.24)$$

the characteristic determinant associated to the system is given by $\det(n_i C_{ijkl}^* n_l)$. Using (4.24) this determinant can be elaborated as

$$\det(n_i C_{ijkl}^* n_l) = c \det(n_i (1 - D) C_{ijkl} n_l). \quad (4.25)$$

Comparison with (3.28) shows that

$$\det(n_i C_{ijkl}^* n_l) = c(1 - D)^3 \mu^2 (\lambda + 2\mu). \quad (4.26)$$

This expression is positive for all $D < 1$ and the partial differential system is therefore elliptic throughout the initiation phase.

As a result of the fact that the rate equilibrium equations remain elliptic, the deformation and damage cannot concentrate in a surface. Instead, finite deformation bands are formed,

with a width which depends on the internal length scale provided by the nonlocal or gradient terms. This is best demonstrated for the one-dimensional problem of Section 3.1. In the one-dimensional case with a homogeneous reference state ε_0, D_0 , the rate equilibrium equations (4.22) reduce to

$$(1 - D_0)E \frac{\partial^2 v}{\partial x^2} - g(D_0, \varepsilon_0)E\varepsilon_0 \frac{\partial \dot{\bar{\varepsilon}}}{\partial x} = 0, \quad (4.27)$$

where use has been made of the fact that the nonlocal strain $\bar{\varepsilon}_0$ equals ε_0 for homogeneous deformations.

For the explicit gradient model the nonlocal strain rate $\dot{\bar{\varepsilon}}$ can be written in terms of the velocity by differentiation of the one-dimensional equivalent of (4.11) with respect to time and substitution of $\dot{\bar{\varepsilon}} = \dot{\varepsilon} = \partial v / \partial x$:

$$\dot{\bar{\varepsilon}} = \frac{\partial v}{\partial x} + c \frac{\partial^3 v}{\partial x^3}. \quad (4.28)$$

Using this relation, (4.27) can be rewritten as the fourth-order differential equation

$$\bar{E}(D_0, \varepsilon_0) \frac{\partial^2 v}{\partial x^2} - cg(D_0, \varepsilon_0)E\varepsilon_0 \frac{\partial^4 v}{\partial x^4} = 0, \quad (4.29)$$

where \bar{E} denotes the tangential stiffness of the local model as defined by (3.4). In contrast to the corresponding equation (3.7) for the conventional, local model, the left-hand-side in equation (4.29) does not vanish when \bar{E} becomes zero. The remaining, fourth-order term does not allow for strong or weak discontinuities in the velocity field. Although bifurcation into an inhomogeneous solution is still possible, the deformation and damage growth can no longer localise in a surface and the strain and damage growth rate thus remain finite.

Inhomogeneous terms in the velocity field satisfying (4.29) must be harmonic, i.e., of the form

$$v(x) = \hat{v}e^{ikx}, \quad (4.30)$$

with \hat{v} the complex amplitude and k the wave number. Substitution of this expression into (4.29) gives

$$-k^2 \left(\bar{E}(D_0, \varepsilon_0) + k^2 cg(D_0, \varepsilon_0)E\varepsilon_0 \right) \hat{v}e^{ikx} = 0. \quad (4.31)$$

For a positive tangent \bar{E} this equation has only the trivial solutions $\hat{v} = 0$ and $k = 0$. This means that the response remains homogeneous in the hardening regime. When $\bar{E} \leq 0$, however, a nontrivial solution exists, given by

$$k = \sqrt{\frac{1}{c} \left(1 - \frac{1 - D_0}{\varepsilon_0 g(D_0, \varepsilon_0)} \right)}. \quad (4.32)$$

Thus, the inhomogeneous velocity field has a wave length $\lambda = 2\pi/k$ with k according to (4.32). This wave length depends on the reference state ε_0, D_0 and it is a linear function of

the length scale \sqrt{c} of the gradient enhancement. Discontinuous solutions, for which $\lambda = 0$, cannot exist for positive c .

In the implicit gradient formulation the nonlocal strain is defined by (4.13). Differentiation of this relation with respect to time gives for the one-dimensional case (cf. (4.23))

$$c \frac{\partial^2 \dot{\varepsilon}}{\partial x^2} + \frac{\partial v}{\partial x} - \dot{\varepsilon} = 0. \quad (4.33)$$

Substitution of (4.30) and

$$\dot{\varepsilon}(x) = \hat{\varepsilon} e^{ikx} \quad (4.34)$$

into relations (4.27) and (4.33) gives the set of equations

$$k^2(1 - D_0) \hat{v} + ik\varepsilon_0 g(D_0, \varepsilon_0) \hat{\varepsilon} = 0, \quad (4.35)$$

$$-ik \hat{v} + (1 + k^2 c) \hat{\varepsilon} = 0. \quad (4.36)$$

For a nontrivial solution the coefficient determinant of these equations must be zero, i.e.,

$$k^2 \left((1 + k^2 c)(1 - D_0) - \varepsilon_0 g(D_0, \varepsilon_0) \right) = 0, \quad (4.37)$$

which gives the nontrivial wave number

$$k = \sqrt{\frac{1}{c} \left(\frac{\varepsilon_0 g(D_0, \varepsilon_0)}{1 - D_0} - 1 \right)}. \quad (4.38)$$

Again, the inhomogeneous velocity field has a finite wave length and discontinuous solutions are impossible.

For the nonlocal model a similar analysis can be carried out if it is assumed that the bar has an infinite length (cf. the dynamic analysis of Pijaudier-Cabot and Benallal (1993) and Huerta and Pijaudier-Cabot (1994)). If it is furthermore assumed that the weight function ψ has been normalised such that the scaling factor $\Psi = 1$, the nonlocal strain rate can be written as (cf. (4.4))

$$\dot{\varepsilon}(x) = \int_{-\infty}^{\infty} \psi(|y - x|) \frac{\partial v}{\partial x} dy, \quad (4.39)$$

or, using $y' = y - x$,

$$\dot{\varepsilon}(x) = \int_{-\infty}^{\infty} \psi(|y'|) \frac{\partial v}{\partial x} dy', \quad (4.40)$$

where the velocity derivative must be evaluated at $y = x + y'$. Substitution of relations (4.40) and (4.30) into (4.27) results in

$$k^2 E(1 - D_0 - \varepsilon_0 g(D_0, \varepsilon_0) \hat{\Psi}(k)) \hat{v} e^{ikx} = 0, \quad (4.41)$$

with $\hat{\Psi}(k)$ the Fourier transform of the weight function ψ . Nontrivial solutions must satisfy

$$\hat{\Psi}(k) = \frac{1 - D_0}{\varepsilon_0 g(D_0, \varepsilon_0)}. \quad (4.42)$$

For the one-dimensional case the Gaussian weight function (4.6) is defined as

$$\psi(\rho) = \frac{1}{\sqrt{2\pi}l} \exp\left[-\frac{\rho^2}{2l^2}\right]. \quad (4.43)$$

It can be verified that the scaling factor Ψ is indeed equal to one for this definition. The Fourier transform of (4.43) reads

$$\hat{\Psi}(k) = \exp\left[\frac{1}{2}k^2 l^2\right], \quad (4.44)$$

so that for the Gaussian weight function equation (4.42) can be rewritten as

$$k = \frac{1}{l} \sqrt{2 \ln\left(\frac{1 - D_0}{\varepsilon_0 g(D_0, \varepsilon_0)}\right)}. \quad (4.45)$$

The wave lengths λ associated to the wave numbers given by (4.32), (4.38) and (4.45) have been plotted versus the reference strain ε_0 in Figure 4.4. The linear softening law (2.11) has been used in this figure, with parameters $\kappa_0 = 0.0001$ and $\kappa_c = 0.0125$. The gradient parameter has been set to $c = 1 \text{ mm}^2$. For the nonlocal model, the corresponding internal length $l = \sqrt{2c} = \sqrt{2} \text{ mm}$ has been used. The diagram shows a qualitative agreement between the three localisation limiters. The wave length of the inhomogeneous solution decreases as ε_0 increases for all three models. Quantitatively, the differences between the three curves become more apparent for higher strain levels. This is due to the fact that the higher-order terms which have been neglected in the gradient approximations become more important as the wave length of the velocity field decreases.

In the nonlocal and implicit gradient models λ approaches zero as ε_0 goes to κ_c . These models thus show a gradual transition from a damaged zone into a line crack. In the explicit gradient formulation the wave length remains finite. A dynamic analysis of the three models has shown that the behaviour of the explicit gradient formulation in terms of wave propagation is also fundamentally different from that of the other two models and even doubtful from a physical viewpoint (Peerlings et al., 1996b, 1998c). The rigorous neglect of higher-order terms in the explicit formulation apparently renders the approximation too crude to follow the behaviour of the nonlocal model. It has been shown in Section 4.2 that higher-order terms are still present in the implicit gradient formulation. Accordingly, the response of this formulation shows a better agreement with the nonlocal model. The fact that λ is smaller for the implicit gradient model is consistent with the observation in Section 4.2 that the average interaction distance is smaller in the implicit model than in the nonlocal model.

Although the analysis of harmonic solutions of the rate problem (4.27) provides much insight in the localisation behaviour of the three regularised damage models and the relation between the regularisation methods, it is unrealistic in a number of respects. The assumption

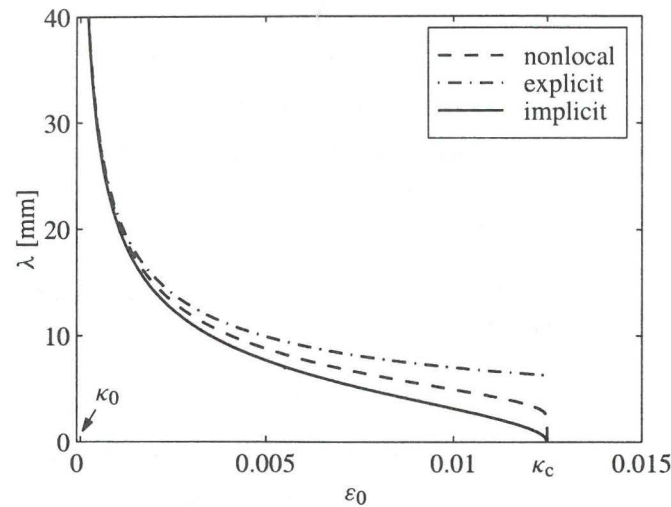
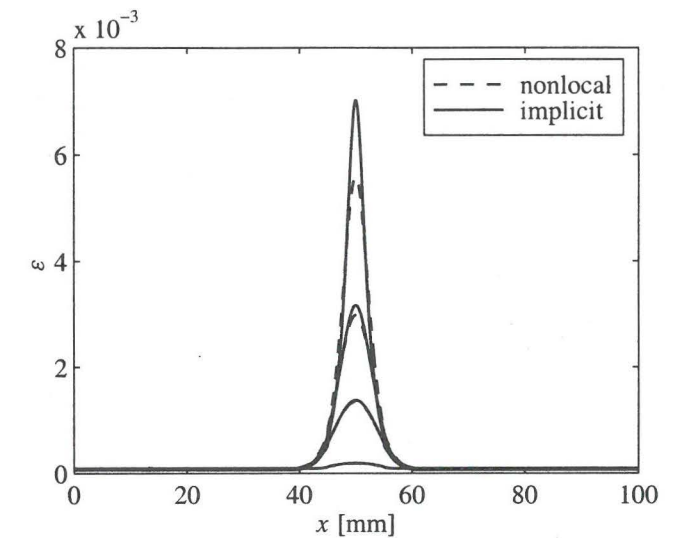


Figure 4.4: Wave length of inhomogeneous response in the gradient and nonlocal models.

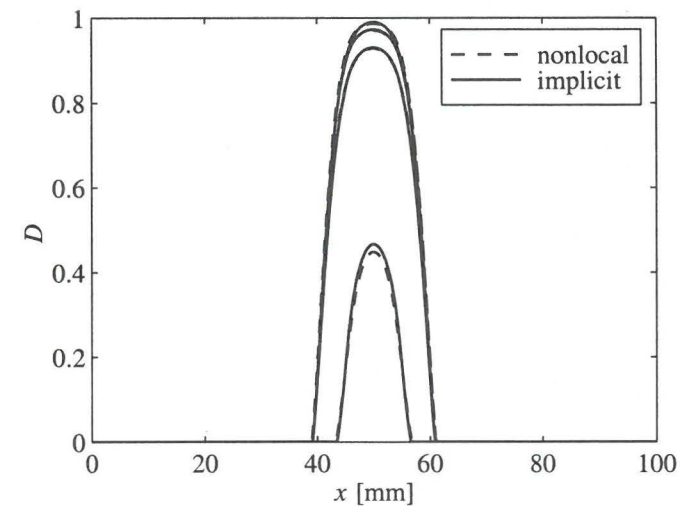
of a perfectly homogeneous configuration is seldom justified in practice. Even if the initial problem is homogeneous, the strain and damage will not generally be homogeneous in the softening stage. But the most important limitation is probably that the analysis is valid only for the linear comparison solid. By considering the rate equilibrium equation (4.27) it has been tacitly assumed that relation (4.3) holds everywhere in the bar. This means that the damage variable decreases in regions where $\dot{\epsilon} < 0$, whereas it would remain constant in the real, nonlinear solid.

Analytical solutions of the nonlinear equilibrium problem are difficult to obtain, even in the one-dimensional case. A semi-analytical solution has been derived by Peerlings et al. (1996a) for the damage equivalent of perfect plasticity, i.e., a damage growth law which results in a constant stress level. For the linear softening law the one-dimensional nonlinear bar problem (3.1) has been solved numerically using the nonlocal model and the implicit gradient model (Peerlings et al., 1996a,b). The same parameter set has been used as in the linear analysis. Furthermore, a value of $E = 20$ GPa has been used for Young's modulus. The length of the bar has been set to $L = 100$ mm and the cross-section has been reduced by 10% in the centre of the bar in order to trigger a localised response.

Figure 4.5 shows the development of the strain and the damage along the bar for the two enhanced models. For relatively small deformations, the strain distributions of the nonlocal and the gradient-dependent model match almost perfectly. At a certain stage the deformation and damage growth start to localise in an ever smaller region. For the gradient model this localisation is slightly stronger than for the nonlocal model. This trend is consistent with the linear analysis, which predicts a decreasing wave length for increasing deformation and a smaller wave length for the (implicit) gradient formulation than for the nonlocal model.



(a)



(b)

Figure 4.5: Comparison of the development of (a) strain and (b) damage in the nonlocal and implicit gradient formulations.

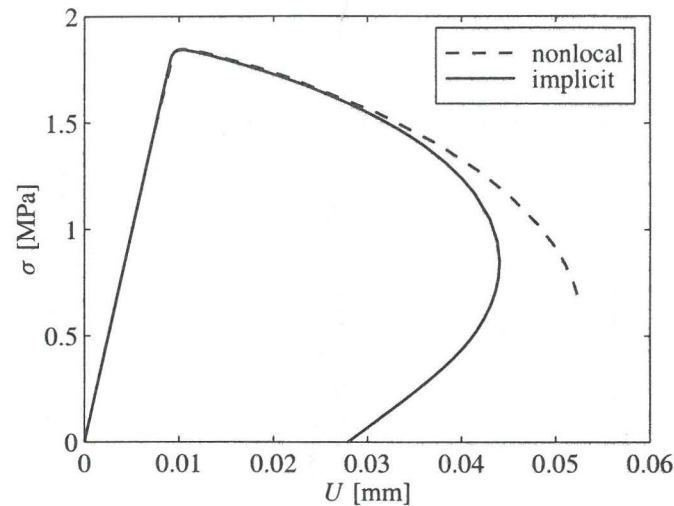


Figure 4.6: Comparison of the stress-displacement responses of the nonlocal and implicit gradient formulations.

The stress in the bar has been plotted versus the displacement of its right end, U , in Figure 4.6 for the two models. Although the linear softening law has been used, the softening branches of these load-displacement curves are nonlinear as a result of the progressive localisation of deformation. The strongly localised deformations at the end of the process result in snap-back behaviour. The responses of the two models agree quite well in a qualitative sense. The predicted tensile strengths are practically equal, but the gradient-enhanced formulation exhibits a somewhat more brittle post-peak behaviour than the nonlocal model as a result of the slightly more localised damage growth (Figure 4.5).

The influence of the internal length scale on the final damage distribution and the load-displacement response is shown for the implicit gradient formulation in Figure 4.7. Apart from the reference value of $\sqrt{c} = 1$ mm, results are shown for $\sqrt{c} = 0.5$ and 2 mm. Figure 4.7(a) clearly shows that a larger value of the internal length scale results in a more widespread development of damage. As a consequence, the load-displacement response becomes less brittle (Figure 4.7(b)).

4.5 Crack growth

It has been shown in the previous section that the introduction of nonlocality in the elasticity based damage model precludes the development of displacement discontinuities and the associated strain singularities for noncritical damage values, i.e., for $D < 1$. As a result, the premature initiation of cracks which is observed in the local damage model is no longer possible. However, when the damage variable is critical somewhere in the component, and

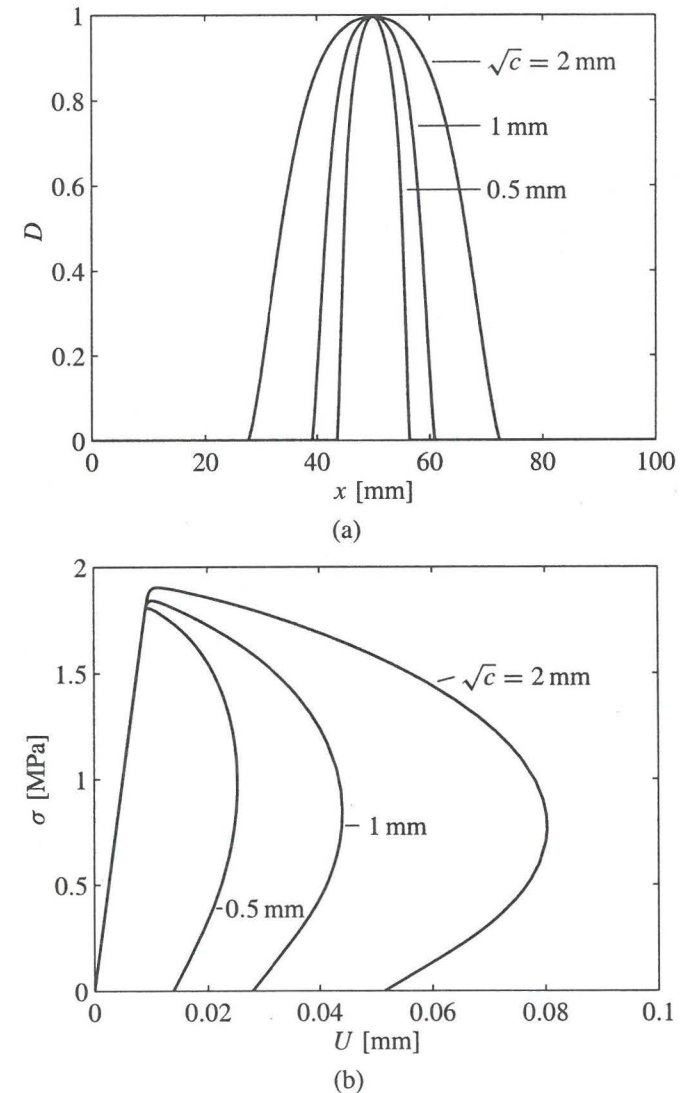


Figure 4.7: (a) Damage and (b) stress response of the implicit gradient formulation for $\sqrt{c} = 0.5, 1$ and 2 mm.

a crack has thus been initiated, a strain singularity may be unavoidable at the crack tip. It is important that the damage growth rate still remains finite, because the crack growth would otherwise be instantaneous (see Section 3.1). Since the damage growth rate depends on the nonlocal equivalent strain $\bar{\varepsilon}$ in the nonlocal and gradient formulations, this implies that $\bar{\varepsilon}$ must remain finite at the crack tip in order to have a finite crack growth rate.

Analytical expressions for the nonlocal strain can be obtained for a linear elastic crack in an infinite medium. One should realise that this situation is not representative for crack growth in a damaging material, since the development of damage in front of the crack may have an important effect on the strain singularity at the crack tip. Indeed, for a mode-III problem Liu and Murakami (1998) have shown that the degree of singularity of the asymptotic strain field is larger for an assumed damage field than in the elastic case. For the cylindrical damage distribution considered by these authors the strain singularity varies from the elastic $r^{-1/2}$ singularity for no damage to a r^{-1} singularity for widespread damage. The present analysis, which assumes the $r^{-1/2}$ singularity predicted by linear fracture mechanics, can therefore only give an indication of the real crack growth behaviour. It is also relevant for situations where a singularity is a priori present as a consequence of the problem geometry, e.g., at sharp notches. The conventional, local damage theory then predicts immediate, complete fracture for each positive loading level. In order to avoid this nonphysical behaviour, $\bar{\varepsilon}$ must also remain finite for such geometrical singularities.

A two-dimensional, plane-stress configuration is considered here, see Figure 4.8. Cartesian coordinates x_1, x_2 and polar coordinates r, ϑ will be used as convenient; the origin of both coordinate systems coincides with the crack tip. The crack is assumed to be loaded in mode-I. The nontrivial asymptotic strains at the crack tip can be derived from the displacement field given by linear elastic fracture mechanics (e.g., Kanninen and Popelar, 1985) as

$$\begin{aligned}\varepsilon_{11} &= \frac{K_I}{E\sqrt{2\pi r}} \cos \frac{1}{2}\vartheta \left(1 - \nu - (1 + \nu) \sin \frac{1}{2}\vartheta \sin \frac{3}{2}\vartheta\right), \\ \varepsilon_{22} &= \frac{K_I}{E\sqrt{2\pi r}} \cos \frac{1}{2}\vartheta \left(1 - \nu + (1 + \nu) \sin \frac{1}{2}\vartheta \sin \frac{3}{2}\vartheta\right), \\ \varepsilon_{12} &= \frac{K_I}{E\sqrt{2\pi r}} (1 + \nu) \cos \frac{1}{2}\vartheta \sin \frac{1}{2}\vartheta \cos \frac{3}{2}\vartheta, \\ \varepsilon_{33} &= -\frac{2\nu K_I}{E\sqrt{2\pi r}} \cos \frac{1}{2}\vartheta,\end{aligned}\tag{4.46}$$

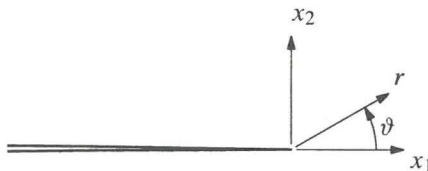


Figure 4.8: Linear elastic crack problem.

with K_I the stress intensity factor. The von Mises equivalent strain (2.28) is used here. Substitution of relations (4.46) in (2.28) and some algebra then give the equivalent strain as

$$\bar{\varepsilon} = \frac{K_I}{2E\sqrt{2\pi r}} \sqrt{(1 - \cos \vartheta)(5 - 3 \cos \vartheta)}.\tag{4.47}$$

For the nonlocal damage model, the nonlocal strain equivalent strain at the crack tip, $\bar{\varepsilon}(\mathbf{0})$, is given by

$$\bar{\varepsilon}(\mathbf{0}) = \int_{\Omega} \psi(r) \bar{\varepsilon}(r, \vartheta) d\Omega,\tag{4.48}$$

where Ω is defined as $\{\mathbf{x} \in \mathbb{R}^2 | r > 0, -\pi < \vartheta < \pi\}$ and it has been assumed that $\Psi = 1$. Substitution of the normalised Gaussian weight function in \mathbb{R}^2 ,

$$\psi(\rho) = \frac{1}{2\pi l^2} \exp\left[-\frac{\rho^2}{2l^2}\right],\tag{4.49}$$

and the equivalent strain according to (4.47) into this relation results in

$$\bar{\varepsilon}(\mathbf{0}) = \frac{K_I}{4\pi E l^2} \int_0^{\infty} \sqrt{r} \exp\left[-\frac{r^2}{2l^2}\right] dr \int_{-\pi}^{\pi} \sqrt{(1 - \cos \vartheta)(5 - 3 \cos \vartheta)} d\vartheta.\tag{4.50}$$

The first integral in this expression can be rewritten as

$$\int_0^{\infty} \sqrt{r} \exp\left[-\frac{r^2}{2l^2}\right] dr = \frac{l^{3/2}}{\sqrt{2}} \Gamma\left(\frac{3}{4}\right),\tag{4.51}$$

where $\Gamma(\alpha)$ denotes the gamma function

$$\Gamma(\alpha) = \int_0^{\infty} e^{-t} t^{\alpha-1} dt.\tag{4.52}$$

The second integral in (4.50) yields after some manipulation

$$\int_{-\pi}^{\pi} \sqrt{(1 - \cos \vartheta)(5 - 3 \cos \vartheta)} d\vartheta = 8 + \frac{4}{\sqrt{3}} \operatorname{arctanh}\left(\frac{1}{2}\sqrt{3}\right).\tag{4.53}$$

Substitution of these two results into (4.50) finally results in

$$\bar{\varepsilon}(\mathbf{0}) = \frac{\sqrt[4]{2} K_I \Gamma\left(\frac{3}{4}\right)}{\pi^{3/2} E \sqrt{l}} \left(1 + \frac{1}{2\sqrt{3}} \operatorname{arctanh}\left(\frac{1}{2}\sqrt{3}\right)\right).\tag{4.54}$$

This expression is indeed finite for $l > 0$, so that the damage growth rate at the crack tip remains finite in the nonlocal model.

For the implicit gradient formulation, the partial differential equation (4.13) must be solved to obtain $\bar{\varepsilon}$. Because of the symmetry of the problem with respect to the x_1 -axis, the equation need only be solved for the half-plane $\Omega^+ : x_2 > 0$. A Neumann boundary condition $\partial\bar{\varepsilon}/\partial x_2 = 0$ must then be applied at $x_2 = 0$. For $x_1 \leq 0$ this condition represents the free boundary of the crack surface and for $x_1 > 0$ it follows from the symmetry of the problem. The boundary value problem is solved using Green's function. The free-space Green's function for the Helmholtz equation (4.13) in \mathbb{R}^2 reads (Zauderer, 1989):

$$G(\mathbf{x}; \mathbf{y}) = \frac{1}{2\pi c} K_0\left(\frac{\rho}{\sqrt{c}}\right), \quad (4.55)$$

with $\rho = |\mathbf{x} - \mathbf{y}|$ and $K_0(z)$ the modified zero-order Bessel function of the second kind. It can easily be verified that Green's function for the half-space problem with the homogeneous Neumann boundary condition is then given by

$$\tilde{G}(\mathbf{x}; \mathbf{y}) = G(\mathbf{x}; \mathbf{y}) + G(\mathbf{x}; \mathbf{y}'), \quad (4.56)$$

with $\mathbf{x}, \mathbf{y} \in \Omega^+$ and $\mathbf{y}' = [y_1, -y_2]^T$ the mirror point of \mathbf{y} in the line $x_2 = 0$. The solution of the half-space problem can now be written as

$$\bar{\varepsilon}(\mathbf{x}) = \int_{\Omega^+} \bar{\varepsilon}(\mathbf{y}) \tilde{G}(\mathbf{x}; \mathbf{y}) d\Omega, \quad (4.57)$$

or, using (4.56) and the symmetry $\bar{\varepsilon}(\mathbf{y}') = \bar{\varepsilon}(\mathbf{y})$ of the equivalent strain, as

$$\bar{\varepsilon}(\mathbf{x}) = \int_{\Omega} \bar{\varepsilon}(\mathbf{y}) G(\mathbf{x}; \mathbf{y}) d\Omega. \quad (4.58)$$

In the limit $x_i \rightarrow 0$ the nonlocal strain approaches

$$\bar{\varepsilon}(\mathbf{0}) = \int_{\Omega} \bar{\varepsilon}(\mathbf{y}) G(\mathbf{0}; \mathbf{y}) d\Omega, \quad (4.59)$$

which, using (4.47) and (4.55), can be written as

$$\bar{\varepsilon}(\mathbf{0}) = \frac{K_I}{4\sqrt{2}\pi^{3/2}Ec} \int_0^\infty \sqrt{r} K_0\left(\frac{r}{\sqrt{c}}\right) dr \int_{-\pi}^\pi \sqrt{(1 - \cos \vartheta)(5 - 3 \cos \vartheta)} d\vartheta. \quad (4.60)$$

The second integral in the right-hand-side is identical with that in (4.50) and is thus given by (4.53). The first integral can be written as (Gradshteyn and Ryzhik, 1994)

$$\int_0^\infty \sqrt{r} K_0\left(\frac{r}{\sqrt{c}}\right) dr = \frac{1}{\sqrt{2}} c^{3/4} \Gamma^2\left(\frac{3}{4}\right). \quad (4.61)$$

Combination of these results yields

$$\bar{\varepsilon}(\mathbf{0}) = \frac{K_I \Gamma^2\left(\frac{3}{4}\right)}{\pi^{3/2} E \sqrt{c}} \left(1 + \frac{1}{2\sqrt{3}} \operatorname{arctanh}\left(\frac{1}{2}\sqrt{3}\right)\right), \quad (4.62)$$

which is again finite. This result can be compared with expression (4.54) for the nonlocal model by setting $c = \frac{1}{2}l^2$. The two expressions then differ exactly by a factor $\Gamma\left(\frac{3}{4}\right) \approx 1.23$, i.e., the nonlocal equivalent strain is approximately 23% higher in the implicit gradient model than in the nonlocal model.

The nonlocal equivalent strain (4.11) according to the explicit gradient model follows by differentiation of (4.47). It can be seen directly that the $r^{-1/2}$ singularity of $\bar{\varepsilon}$ then results in a $r^{-5/2}$ singularity of $\bar{\varepsilon}$, which means that the $\bar{\varepsilon}$ -field has a stronger singularity than the local strain field. Indeed, $\bar{\varepsilon}$ may become singular at the crack tip even if the local strain is nonsingular. This result seems to indicate that the explicit gradient model cannot realistically describe crack growth.

The above analysis of a crack problem is relevant for quasi-brittle as well as for fatigue fracture, since the local models of both phenomena predict perfectly brittle fracture. An interesting difference exists, however, in the shape of the crack that results in the enhanced quasi-brittle and fatigue models. In the quasi-brittle model the crack is still a line, or, in the three-dimensional case, a surface. This follows from the fact that the nonlocal equivalent strain will always have its maximum at the crack tip. When the point with the highest damage value in front of the crack tip becomes critical, and the crack tip thus propagates, the nonlocal strain decreases in points adjacent to the previous crack tip, which are now at the crack face. Since the damage variable can only increase when $\bar{\varepsilon} = \kappa$ and since κ has been set by the value of $\bar{\varepsilon}$ at the crack tip, the damage ceases to grow in these points, so that the width of the propagated crack remains zero.

The situation in the fatigue model is different as a consequence of the loading surface being fixed ($\kappa = \kappa_0$). Even if the nonlocal strain amplitude decreases at the faces of the propagating crack, it may still be well above the damage threshold κ . In each subsequent loading cycle the damage therefore still grows by a certain amount, so that points adjacent to the crack can also become critical and the width of the crack locally increases. This process continues until the nonlocal strain amplitude has become smaller than the threshold value κ . The width of the crack thus depends on – among other parameters – the threshold value κ and the internal length scale of the material. Since this length scale, which follows either from the weight function (in the integral model) or the gradient parameter (in the gradient formulations), will generally be small, the width of the fatigue crack will also be small.

The zero crack thickness predicted by the quasi-brittle model corresponds to the classical notion of a line crack. However, the finite crack width of the fatigue model seems equally defensible if the microstructural origin of the nonlocality is taken into account. The crack can then be considered as a band of 'cracked' microstructural elements (grains). Indeed, this notion is consistent with the fact that the width of the crack depends on the internal length scale, which represents the microstructure of the material. Although these different perceptions may give rise to some theoretical debate, the practical consequences are probably limited since the positive crack width in fatigue problems will usually be small compared to the size of the component.

4.6 Discussion

The two types of gradient enhancement have been shown to result in quite different responses in crack initiation and particularly in crack growth. The implicit method shows a good qualitative agreement with the nonlocal model. Quantitatively, the differences between the implicit and nonlocal approaches are limited, given the large degree of uncertainty in most practical problems. The behaviour of the explicit model, on the other hand, is entirely different and may even be nonphysical in some aspects. This difference between the two gradient formulations is quite remarkable since both methods introduce the same degree of approximation with respect to the nonlocal model. However, two fundamental differences exist between the two approaches, which must be held responsible for their different behaviour.

Firstly, gradient terms of orders higher than two have been rigorously neglected in the explicit model, whereas these terms have been partially preserved in the implicit formulation. As a result, spatial interactions span the entire domain in the implicit model, similarly to the nonlocal model. The explicit formulation is local in a mathematical sense, because the nonlocal strain in a point depends only on the local strain and its gradients in that same point. Spatial interactions are therefore limited to the immediate neighbourhood in this model.

Secondly, the explicit gradient formulation imposes stronger continuity requirements on the displacements than the implicit and nonlocal approaches, since it introduces fourth-order displacement derivatives in the equilibrium equations. These requirements may be difficult to meet in the strongly localised or singular deformation fields considered here and may therefore have an important effect on the predicted response.

The results obtained in the previous two sections give reason to doubt the applicability of the explicit gradient model to fracture problems. The two remaining approaches, i.e., the nonlocal and implicit gradient formulations, are largely equivalent. The quantitative differences can be accounted for by using different parameters for the two models. In the rare situation where well defined spatial interactions exist in a material, the nonlocal approach may be preferred, because it models the nonlocality in a more transparent way. On the other hand, the treatment of – external and internal – boundaries seems to be better defined in the gradient approach. In most practical cases, neither of these arguments is decisive and the choice between the two regularisation methods is therefore largely a matter of convenience. An advantage of the gradient approach in this respect is that the set of partial differential equations which describes the damage problem can be cast in the form of a standard nonlinear equilibrium problem with four instead of three dependent variables, cf. equations (4.22) and (4.23). As a result, the implementation of the method in standard nonlinear finite element codes may be less complicated than for the nonlocal model, which does not fit into a standard, local finite element framework. This is the reason why the following chapters will concentrate on the gradient formulation. Reference is made to Saanouni et al. (1989); Pijaudier-Cabot and Huerta (1991); Huerta and Pijaudier-Cabot (1994) for details of the numerical implementation and numerical results of nonlocal damage models.

Chapter 5

Finite element implementation

Analytical solutions of the equations which govern damage and fracture problems are difficult to obtain even for simple geometries and loading conditions. Practical problems, with complex geometries and nonuniform loading, invariably require a numerical approach. The success of numerical analyses using nonlocal or gradient damage models in realistically describing damage processes depends critically on the numerical methods which are used. If the numerical implementation is not consistent with the continuum model, the enhanced localisation properties of the nonlocal and gradient formulations may be completely lost and the predicted behaviour may even become physically unrealistic. This has been found to be true particularly in crack growth problems, where the numerical treatment of the completely damaged zone (crack) may have an important effect on the predicted crack growth if the discretisation is not consistent with the underlying initial-boundary value problem. For this reason the numerical implementation of the implicit gradient damage formulation is discussed here in detail.

The partial differential equations of the equilibrium problem are first discretised in space by a finite element interpolation. The time discretisation of the problem follows by dividing the loading history in a finite number of time increments and integrating the growth of damage within these increments. The resulting set of nonlinear algebraic equations is solved in each increment by an iterative process. These three steps are discussed in Sections 5.1, 5.2 and 5.3, respectively. It is assumed in these sections that the damage is noncritical everywhere in the body, i.e., that no crack has been initiated yet. The extension to crack growth is discussed in Section 5.4.

5.1 Spatial discretisation

The equilibrium problem for the implicit gradient damage formulation consists of the standard equilibrium equations (2.5) combined with the partial differential equation (4.13) for the nonlocal equivalent strain. These equations must be supplemented by the standard kinematic and dynamic boundary conditions and the additional boundary condition (4.20). Both partial differential equations are first cast in a weighted residuals weak form, which is subsequently discretised using a Galerkin approach.

The weak form of the equilibrium equations follows in a standard fashion by multiplication by test functions ζ_j , integration on the domain Ω and use of the divergence theorem:

$$\int_{\Omega} \frac{\partial \zeta_j}{\partial x_i} \sigma_{ij} d\Omega = \int_{\Gamma} \zeta_j \tau_j d\Gamma, \quad (5.1)$$

where $j = 1, 2, 3$ and $\tau_j = n_i \sigma_{ij}$ denote the boundary tractions at Γ . Equations (5.1) must be satisfied for all admissible test functions ζ_j . For equation (4.13) multiplication by the test function $\bar{\zeta}$, integration and application of the divergence theorem result in the weak form

$$\int_{\Omega} \left(c \frac{\partial \bar{\zeta}}{\partial x_i} \frac{\partial \bar{\varepsilon}}{\partial x_i} + \bar{\zeta} (\bar{\varepsilon} - \tilde{\varepsilon}) \right) d\Omega = \int_{\Gamma} \bar{\zeta} n_i \frac{\partial \bar{\varepsilon}}{\partial x_i} d\Gamma, \quad (5.2)$$

and consequently, using the boundary condition (4.20),

$$\int_{\Omega} \left(c \frac{\partial \bar{\zeta}}{\partial x_i} \frac{\partial \bar{\varepsilon}}{\partial x_i} + \bar{\zeta} (\bar{\varepsilon} - \tilde{\varepsilon}) \right) d\Omega = 0. \quad (5.3)$$

Standard, C_0 -continuous finite element interpolations are now introduced for the displacement vector and the nonlocal equivalent strain:

$$\mathbf{u} = \mathbf{N} \mathbf{a}, \quad (5.4)$$

$$\bar{\varepsilon} = \bar{\mathbf{N}} \mathbf{e}, \quad (5.5)$$

where the column matrices \mathbf{a} and \mathbf{e} contain the nodal values of the displacement components and the nonlocal equivalent strain. Following a Galerkin approach, the interpolations \mathbf{N} and $\bar{\mathbf{N}}$ are also used for the respective test functions ζ_j and $\bar{\zeta}$. Differentiation of (5.4) gives the strain components, gathered in the column $\boldsymbol{\varepsilon} = [\varepsilon_{11}, \varepsilon_{22}, \varepsilon_{33}, 2\varepsilon_{12}, 2\varepsilon_{23}, 2\varepsilon_{31}]^T$, as

$$\boldsymbol{\varepsilon} = \mathbf{B} \mathbf{a}. \quad (5.6)$$

Because of the symmetry of the stress tensor the same mapping can be used for the derivatives of the test functions ζ_j . Likewise, the derivatives $\nabla_i \bar{\varepsilon} = \partial \bar{\varepsilon} / \partial x_i$ ($i = 1, 2, 3$) are given by

$$\nabla \bar{\varepsilon} = \bar{\mathbf{B}} \mathbf{e}. \quad (5.7)$$

The derivatives of $\bar{\zeta}$ again follow from the same interpolation.

Substitution of the interpolations (5.4)-(5.7) into (5.1) and taking into account that the resulting equations must be satisfied for all admissible test functions results in the discrete force balance

$$\mathbf{f}_{ai} = \mathbf{f}_{ae}, \quad (5.8)$$

where the internal and external nodal forces \mathbf{f}_{ai} and \mathbf{f}_{ae} are given by

$$\mathbf{f}_{ai} = \int_{\Omega} \mathbf{B}^T \boldsymbol{\sigma} d\Omega, \quad (5.9)$$

$$\mathbf{f}_{ae} = \int_{\Gamma} \mathbf{N}^T \boldsymbol{\tau} d\Gamma. \quad (5.10)$$

The stress column $\boldsymbol{\sigma}$ in (5.9) is defined as $\boldsymbol{\sigma} = [\sigma_{11}, \sigma_{22}, \sigma_{33}, \sigma_{12}, \sigma_{23}, \sigma_{31}]^T$ and the traction column $\boldsymbol{\tau}$ in (5.10) as $\boldsymbol{\tau} = [\tau_1, \tau_2, \tau_3]^T$. Similarly, discretisation of equation (5.3) yields

$$\mathbf{K}_{ee} \mathbf{e} - \mathbf{f}_e = \mathbf{0}, \quad (5.11)$$

with the matrix \mathbf{K}_{ee} and the vector \mathbf{f}_e given by

$$\mathbf{K}_{ee} = \int_{\Omega} (c \bar{\mathbf{B}}^T \bar{\mathbf{B}} + \bar{\mathbf{N}}^T \bar{\mathbf{N}}) d\Omega, \quad (5.12)$$

$$\mathbf{f}_e = \int_{\Omega} \bar{\mathbf{N}}^T \tilde{\varepsilon} d\Omega. \quad (5.13)$$

The interpolation functions in \mathbf{N} and $\bar{\mathbf{N}}$ can be defined independently and need not be of the same order. Indeed, it has been found that using interpolation polynomials of the same order may result in stress oscillations. The origin of these oscillations is illustrated in Figure 5.1 for a one-dimensional problem with piecewise linear interpolations of u and $\bar{\varepsilon}$. The linearity of the displacements within each element results in the local strain ε being piecewise constant (Figure 5.1(a)). Since the damage variable depends on the nonlocal equivalent strain, which is piecewise linear, D is continuous and nearly linear within the elements for sufficiently small elements (Figure 5.1(b)). The combination of the constant local strain and varying damage in the stress-strain relation (3.1) leads to a stress distribution as shown in Figure 5.1(c). The stress gradient within the elements is set by the damage gradient and the strain; the oscillations are therefore observed particularly in regions with high gradients of the damage variable and high strains. Refining the discretisation does not lead to a decrease of the stress gradients. Indeed, it may even result in an increase because high damage and displacement gradients can be described more accurately with a finer mesh. Similar incompatibilities of higher-order polynomials have been observed to cause similar, but less pronounced stress oscillations.

Although the stress field of Figure 5.1(c) is a perfectly valid solution of the weak equilibrium problem, the stress oscillations may lead to serious misinterpretations and should therefore be avoided. An obvious way to do so is by using quadratic instead of linear polynomials for the displacements, so that the strain field is no longer constant and agrees with the linear nonlocal equivalent strain. Particularly when combined with a reduced Gauss integration for the equilibrium equations and a full Gauss integration for equation (5.11), this discretisation has been found to be effective and efficient. A second possibility is to retain

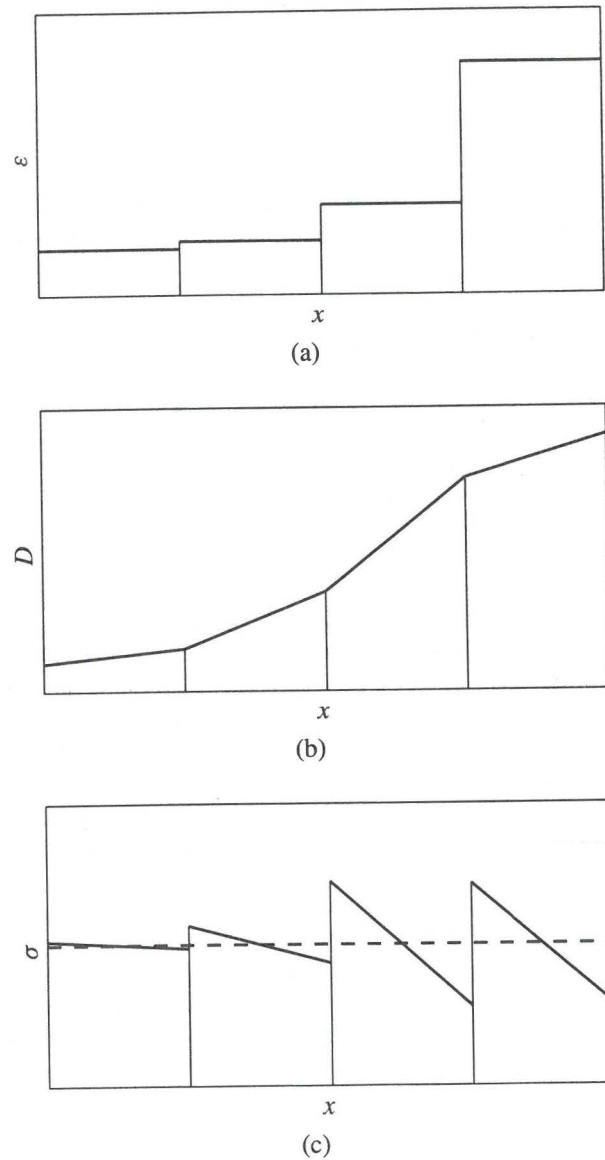


Figure 5.1: Stress oscillations caused by a linear-linear finite element interpolation.

the linear interpolations of the displacements and nonlocal equivalent strain, but to define the damage variable as uniform in each element. The strain and damage are then both piecewise constant, so that the stress is also piecewise constant. This approach is preferred in crack growth problems, see Section 5.4.

5.2 Temporal discretisation

The time discretisation of the equilibrium problem follows by dividing the loading history into a finite number of time intervals and requiring the discrete balances (5.8) and (5.11) to be satisfied only at the end of each interval. Assuming the complete deformation and damage state to be known at time t , the problem then reduces to finding the displacements and nonlocal strains which satisfy (5.8) and (5.11) at the end of a time increment Δt , i.e.,

$$\mathbf{f}_{\text{ai}}^{t+\Delta t} = \mathbf{f}_{\text{ae}}^{t+\Delta t}, \quad (5.14)$$

$$\mathbf{K}_{\text{ee}} \mathbf{e}^{t+\Delta t} - \mathbf{f}_{\text{e}}^{t+\Delta t} = \mathbf{0}. \quad (5.15)$$

Both left-hand-side terms in (5.15) can be written directly in terms of the unknowns $\mathbf{a}^{t+\Delta t}$ and $\mathbf{e}^{t+\Delta t}$. The internal nodal force vector $\mathbf{f}_{\text{ai}}^{t+\Delta t}$ in (5.14) depends on the stresses, which are given by

$$\boldsymbol{\sigma}^{t+\Delta t} = (1 - D^{t+\Delta t}) \mathbf{C} \boldsymbol{\varepsilon}^{t+\Delta t}, \quad (5.16)$$

with \mathbf{C} containing the elastic constants. The strains $\boldsymbol{\varepsilon}^{t+\Delta t}$ can also be directly related to $\mathbf{a}^{t+\Delta t}$, but the damage variable $D^{t+\Delta t}$ cannot generally be written in terms of $\mathbf{a}^{t+\Delta t}$ and $\boldsymbol{\varepsilon}^{t+\Delta t}$ since it depends on the growth of damage during the interval $(t, t + \Delta t)$. To obtain $D^{t+\Delta t}$ the damage growth rate must be integrated from t to $t + \Delta t$. In the quasi-brittle damage model, this integration can be carried out analytically (see Section 2.3), resulting in a direct relation between the damage variable $D^{t+\Delta t}$ and the value of the threshold variable κ at $t + \Delta t$, which in turn depends on $\boldsymbol{\varepsilon}^{t+\Delta t}$ for an incrementally uniform process.

In the fatigue model the damage rate cannot be integrated analytically and an approximation must therefore be used. The damage variable at $t + \Delta t$ can formally be written as

$$D(t + \Delta t) = D(t) + \int_t^{t+\Delta t} \dot{D}(\tau) d\tau. \quad (5.17)$$

The integral in the right-hand-side of this expression is now approximated by the one-step linear integration rule

$$\int_t^{t+\Delta t} \dot{D}(\tau) d\tau \approx ((1 - \vartheta) \dot{D}^t + \vartheta \dot{D}^{t+\Delta t}) \Delta t, \quad (5.18)$$

with the parameter ϑ satisfying $0 \leq \vartheta \leq 1$. For $\vartheta = 0$ this rule reduces to the explicit Euler rule. The damage rate in the interval $(t, t + \Delta t)$ is then approximated by its value at t .

Similarly, \dot{D} is approximated by $\dot{D}^{t+\Delta t}$ in the implicit Euler scheme, which is obtained by setting $\vartheta = 1$. Both these integration rules are of order 1, i.e., the truncation error is approximately proportional to Δt^2 . For $\vartheta = 0.5$, (5.18) equals the trapezoidal rule, which is of order 2 (order Δt^3 truncation error). If it is assumed that the damage variable increases during the entire interval $(t, t + \Delta t)$, which means for the fatigue model that $f^t \geq 0$ and $\Delta f \equiv f^{t+\Delta t} - f^t \geq 0$, the damage rate \dot{D} is given by the evolution law (4.3). Using (5.18) and assuming that $\bar{\varepsilon}$ is constant within the increment then results in the discrete approximation of (5.17)

$$D^{t+\Delta t} = D^t + ((1 - \vartheta)g(D^t, \bar{\varepsilon}^t) + \vartheta g(D^{t+\Delta t}, \bar{\varepsilon}^{t+\Delta t})) \Delta \bar{\varepsilon}. \quad (5.19)$$

If $\vartheta \neq 0$, (5.19) is a nonlinear algebraic equation for $D^{t+\Delta t}$. This equation must be solved iteratively, for instance by a Newton-Raphson scheme.

As an alternative to solving the nonlinear equation (5.19), the damage variable at $t + \Delta t$ can first be estimated with the explicit Euler rule ($\vartheta = 0$). This estimate is then substituted in the right-hand-side of (5.19):

$$D^P = D^t + g(D^t, \bar{\varepsilon}^t) \Delta \bar{\varepsilon}, \quad (5.20)$$

$$D^{t+\Delta t} = D^t + ((1 - \vartheta)g(D^t, \bar{\varepsilon}^t) + \vartheta g(D^P, \bar{\varepsilon}^{t+\Delta t})) \Delta \bar{\varepsilon}. \quad (5.21)$$

This is a so-called predictor-corrector scheme; (5.20) is called the predictor step and (5.21) the corrector step. For $\vartheta = 0.5$ equations (5.20), (5.21) are known as the improved Euler scheme or Heun's method. It can be shown that the accuracy of this scheme is of the same order as the implicit trapezoidal rule, i.e., the truncation error is of the order Δt^3 (see for instance Kreyszig, 1993). For other values of ϑ , the integration is also of the same order as that of the implicit rule (5.19). The price that is paid to avoid solving a nonlinear equation consists of more stringent stability requirements. The predictor-corrector scheme is only conditionally stable, whereas the implicit scheme (5.19) is unconditionally stable for $\vartheta \geq 0.5$. However, numerical stability is not an issue in the fatigue model because the growth of damage is usually strongly progressive.

Relations (5.19) and (5.20), (5.21) must be modified slightly if the conditions for damage growth are not satisfied during the entire interval $(t, t + \Delta t)$. If the conditions $f^{t+\Delta t} \geq 0$ and $\Delta f \geq 0$ are satisfied, but the deformation state at the beginning of the increment does not give rise to damage growth ($f^t < 0$), evolution law (4.3) is not valid on the linear elastic part of the increment. The value of the nonlocal equivalent strain at t , $\bar{\varepsilon}^t$, must then be replaced by κ_0 and the nonlocal equivalent strain increment $\Delta \bar{\varepsilon}$ by $\bar{\varepsilon}^{t+\Delta t} - \kappa_0$ to account for the fact that the damage variable starts to grow from the moment that $\bar{\varepsilon} = \kappa_0$. Furthermore, if the damage value at the end of the increment $D^{t+\Delta t}$ as computed using (5.19) or (5.21) is greater than one, it must be set to $D^{t+\Delta t} = 1$ and kept constant in subsequent increments. The damage variable must be set to $D^{t+\Delta t} = D^t$ if there is no damage growth because $f^{t+\Delta t} < 0$ or $\Delta f \leq 0$.

The discrete approximation (5.18), on which the implicit and explicit integration schemes are based, is accurate when the damage rate varies slowly within the time increment. Under cyclic loading conditions this implies that each loading cycle must be interpolated with a

number, say $O(10)$, of increments. The total number of increments needed to simulate the entire fatigue fracture process would then be of the order of ten times the fatigue life. For low-cycle fatigue analyses, where the fatigue life is typically between 10 and 1000 cycles, this may still be acceptable. But high-cycle fatigue simulations, involving fatigue lives of 10^5 cycles and more, would become impractical. For such analyses there is a need for an approximate integration which allows to span a large number of cycles within each time increment. The loss of resolution which is inevitable in such a procedure is acceptable since it is usually not the precise, small growth of damage within each loading cycle which is relevant, but rather the more substantial changes in the damage field resulting from larger numbers of cycles.

The evolution of $\bar{\varepsilon}$ during an interval $(t, t + \Delta t)$ which comprises a number of loading cycles is shown schematically in Figure 5.2. It has been assumed in this figure that the loading is proportional and fully reversed. Furthermore, the equivalent strain has been assumed to be equally sensitive to tensile and compressive strains. The nonlocal equivalent strain is then identical in the tensile and compressive parts of the cycles for constant damage. This assumption, which is satisfied by the von Mises equivalent strain (2.28), and the assumption of fully reversed loading are not essential and are only made here for simplicity, see Peerlings (1997) for a more general development. The extension to nonproportional loading is less trivial, because the maximum of the nonlocal equivalent strain then cannot be linked directly to the loading cycle. Each loading cycle results in two maxima of $\bar{\varepsilon}$ in the diagram of Figure 5.2, one corresponding to the tensile part of the cycle and one to the compressive part. Both these maxima, which are denoted by $\bar{\varepsilon}_{a1}$ and $\bar{\varepsilon}_{a2}$, follow the envelope $\bar{\varepsilon}_a$.

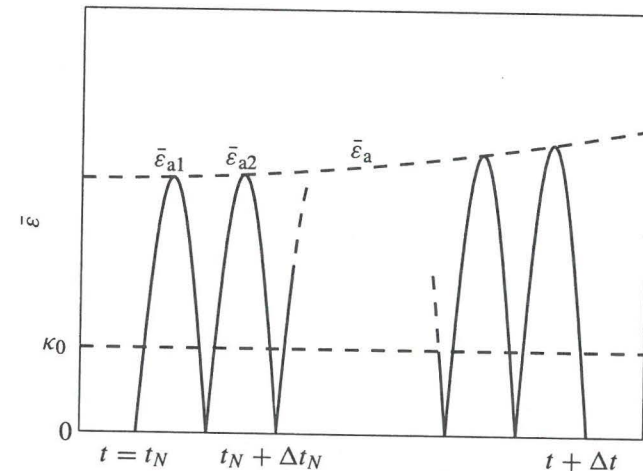


Figure 5.2: Nonlocal equivalent strain cycles.

The integration of the damage rate according to (5.17) still holds for the situation of Figure 5.2. However, the difficulty is that the integral in the right-hand-side of (5.17) can no longer be directly approximated by (5.18) because $\bar{\varepsilon}$ and $\dot{\bar{\varepsilon}}$, and thus also \dot{D} , fluctuate strongly within the increment. Instead of directly using an integration rule, the integral is

formally written as a sum of integrals on the cycles within the increment Δt :

$$D^{t+\Delta t} = D^t + \sum_{n=N}^{N+\Delta N} \int_{t_n}^{t_n+\Delta t_n} \dot{D} \, d\tau, \quad (5.22)$$

where t_n and $t_n + \Delta t_n$ correspond to the beginning and end of cycle n , respectively, and N and $N + \Delta N$ correspond to t and $t + \Delta t$. Taking into account that damage growth is possible only if $\bar{\varepsilon} \geq \kappa_0$ and $\dot{f} \equiv \dot{\bar{\varepsilon}} \geq 0$ and using evolution law (4.3), relation (5.22) can be rewritten as

$$D^{N+\Delta N} = D^N + \sum_{n=N}^{N+\Delta N} \left(\int_{\kappa_0}^{\bar{\varepsilon}_{a1}} g(D, \bar{\varepsilon}) \, d\bar{\varepsilon} + \int_{\kappa_0}^{\bar{\varepsilon}_{a2}} g(D, \bar{\varepsilon}) \, d\bar{\varepsilon} \right), \quad (5.23)$$

where it has been assumed that $\bar{\varepsilon}_a \geq \kappa_0$. Obviously, cycles in which $\bar{\varepsilon}_a < \kappa_0$ do not contribute to the growth of damage. In contrast to $\bar{\varepsilon}$ and \dot{D} , the amplitudes $\bar{\varepsilon}_{a1}$ and $\bar{\varepsilon}_{a2}$ as well as the damage variable D can be assumed to vary slowly within the increment. Thus, similar to the integration rule used for the rate type evolution law, the sum over the cycle numbers in (5.23) can be approximated by a weighted average of the integrals evaluated at the beginning and end of the increment multiplied by the number of cycles in the increment, ΔN :

$$D^{N+\Delta N} = D^N + ((1 - \vartheta)G(D^N, \bar{\varepsilon}_a^N) + \vartheta G(D^{N+\Delta N}, \bar{\varepsilon}_a^{N+\Delta N})) \Delta N, \quad (5.24)$$

with $G(D, \bar{\varepsilon}_a)$ defined by

$$G(D, \bar{\varepsilon}_a) = 2 \int_{\kappa_0}^{\bar{\varepsilon}_a} g(D, \bar{\varepsilon}) \, d\bar{\varepsilon}, \quad (5.25)$$

while $G(D, \bar{\varepsilon}_a) = 0$ if $\bar{\varepsilon}_a < \kappa_0$ or if $D = 1$. The integral in (5.25) must be evaluated for fixed D and can often be determined analytically. For instance, for the evolution function (2.21), with $\bar{\varepsilon}$ replaced by $\bar{\varepsilon}$, (5.25) can be elaborated as

$$G(D, \bar{\varepsilon}_a) = \frac{2C}{\beta + 1} e^{\alpha D} (\bar{\varepsilon}_a^\beta - \kappa_0^\beta). \quad (5.26)$$

Interestingly, exactly the same expression for $D^{N+\Delta N}$ is obtained by applying the linear, one-step integration rule to the nonlocal equivalent of the cycle based evolution of damage, (2.20) (Peerlings, 1997). The 'jump-in-cycles'-procedure which has been derived by Lemaitre and Doghri (1994) on the basis of this approach can be retrieved from (5.24) by setting $\vartheta = 0$. When $\vartheta \neq 0$, relation (5.24) is a nonlinear equation in terms of the damage variable $D^{N+\Delta N}$. It can either be solved iteratively, or approximated by replacing $D^{N+\Delta N}$ in the right-hand-side by a predictor value. In the latter case the integration scheme reads (cf. (5.20), (5.21)):

$$D^p = D^N + G(D^N, \bar{\varepsilon}_a^N) \Delta N, \quad (5.27)$$

$$D^{N+\Delta N} = D^N + ((1 - \vartheta)G(D^N, \bar{\varepsilon}_a^N) + \vartheta G(D^p, \bar{\varepsilon}_a^{N+\Delta N})) \Delta N. \quad (5.28)$$

Since the incremental damage growth is given by (5.24) or (5.27), (5.28) in terms of the nonlocal equivalent strain envelope $\bar{\varepsilon}_a$, the equilibrium problem must be solved for this envelope at $t + \Delta t$. This means that the unknowns $\mathbf{a}^{t+\Delta t}$, $\mathbf{e}^{t+\Delta t}$ and the external nodal forces in equations (5.14), (5.15) must be interpreted as the momentary amplitudes of the displacements, nonlocal strains and nodal forces, rather than the actual values of these variables at $t + \Delta t$ (which would be zero in Figure 5.2). The nonlocal equivalent strain $\bar{\varepsilon}$ equals $\bar{\varepsilon}_a$ in this interpretation, so that the index a can be dropped in the sequel.

The increment size ΔN in (5.24) and (5.27), (5.28) can be selected arbitrarily, with smaller increments resulting in a more accurate integration of the damage growth and thus in a more accurate solution. A straightforward approach is to use the same increment size for the entire loading history. Yet, considering for instance the damage growth curves for $\alpha = 10$ and 100 in Figure 2.7, it is obvious that the size needed to describe the fast growth near the end of the fatigue life with sufficient accuracy is much smaller than that needed for the slow initial growth of damage. A more sophisticated distribution of increment sizes is therefore called for, with relatively large steps in the first stages of damage growth and smaller steps near failure. This concept can be formalised by considering the error that is made in computing the damage growth. Two types of errors can be distinguished in the numerical integration of damage growth: truncation error and inherited error. Truncation error is the error made in each increment as a result of the approximations involved in the time discretisation. For instance the error made in (5.18) is of the order Δt^3 for the trapezoidal rule ($\vartheta = 0.5$). Inherited error is the error which is propagated from the previous increments. For a converging family of solutions this propagation tends to be damped, but for diverging solution families the inherited error increases as the solution progresses. Realistic fatigue damage growth laws lead to highly divergent growth curves. For this reason inherited error is believed to be critical in the present situation. The step size will therefore be related to the inherited error, in contrast to Paas (1990), who has proposed a step size algorithm based on the truncation error.

Substitution of $G(D^{N+\Delta N}, \bar{\varepsilon}_a^{N+\Delta N}) = G(D^N, \bar{\varepsilon}_a^N) + O(\Delta N)$ in relation (5.24) gives the damage variable at the end of the increment ΔN as

$$D^{N+\Delta N} = D^N + G(D^N, \bar{\varepsilon}_a^N) \Delta N + O(\Delta N^2). \quad (5.29)$$

Now suppose that the computed value of the damage variable at N , denoted as \tilde{D}^N , contains a small error δ : $\tilde{D}^N = D^N + \delta$. Using this initial value, expression (5.29) gives the damage variable at the end of the increment as

$$\tilde{D}^{N+\Delta N} = D^N + \delta + G(D^N + \delta, \bar{\varepsilon}_a^N) \Delta N + O(\Delta N^2). \quad (5.30)$$

Linearising this result with respect to δ gives a first-order approximation of the inherited error at $N + \Delta N$ due to the error δ at N :

$$\tilde{D}^{N+\Delta N} - D^{N+\Delta N} \approx \left(1 + \frac{\partial G}{\partial D} \Delta N \right) \delta. \quad (5.31)$$

This relation indeed shows that the inherited error is smaller than its source δ if the direction field associated with the growth of damage is convergent, i.e., if $\partial G / \partial D < 0$. If $\partial G / \partial D > 0$,

on the other hand, the error is amplified. Since this amplification is repeated in each following increment, the inherited error will increase exponentially. Additionally, a truncation error is made in each increment, which is again propagated exponentially, etc. Relation (5.31) is used to control the error propagation by choosing the increment size ΔN such that the second term in the amplification factor equals a predefined constant η :

$$\Delta N = \frac{\eta}{\partial G / \partial D}. \quad (5.32)$$

In order to prevent excessively small or large cycle increments, additional lower and upper bounds can be imposed upon ΔN .

Figure 5.3 shows the effect of using relation (5.32) to determine the increment size in numerical analyses (Peerlings, 1997). The diagram shows the growth of damage in a one-dimensional, uniform bar under constant strain amplitude cycling. Since the nonlocal equivalent strain equals the local strain in this situation, the growth of damage is given in closed form by (2.22). This analytical solution is shown for comparison in Figure 5.3; it predicts failure after $6.6 \cdot 10^5$ cycles. In the numerical analyses the cycle based integration (5.27), (5.28) has been used, with $\vartheta = 0.5$. Two values have been used for the error control parameter η : $\eta = 0.5$ and 0.1 . Each marker in the diagram represents one increment of the numerical analyses. The adaptive step size algorithm indeed selects relatively large increments early in the fatigue life and reduces the step size as the damage growth becomes steeper. With the value $\eta = 0.5$ a reasonable approximation is already obtained using 16 increments. Notice that this analysis would require $O(10^7)$ increments with the standard, direct integration of

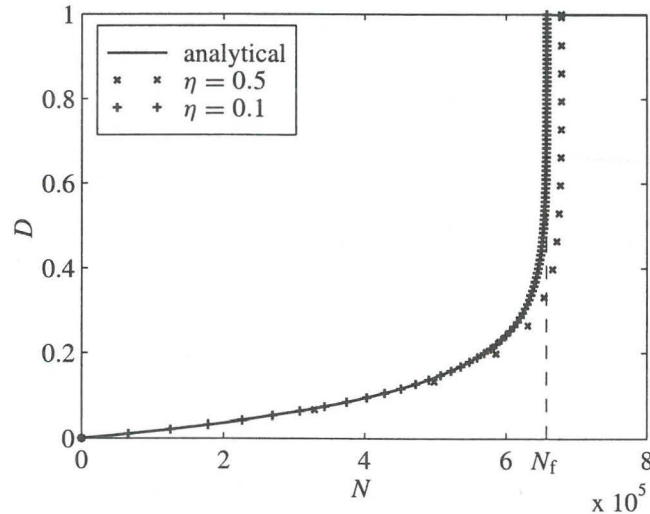


Figure 5.3: Influence of adaptive step size control parameter η on the predicted damage growth.

damage growth. The value $\eta = 0.1$ results in smaller increments than $\eta = 0.5$ during the entire loading and in a more accurate prediction of the growth of damage and the fatigue life.

5.3 Iterative procedure

Using the appropriate analytical or numerical integration to determine the damage $D^{t+\Delta t}$, the discrete equations (5.14), (5.15) have been written entirely in terms of the unknowns $\mathbf{a}^{t+\Delta t}$, $\mathbf{e}^{t+\Delta t}$ in the previous section. The dependence of $\mathbf{f}_{ai}^{t+\Delta t}$ and $\mathbf{f}_e^{t+\Delta t}$ on these variables is nonlinear, so that the set of equations cannot be solved directly. Instead, a Newton-Raphson procedure is used. This means that a new approximation of the solution is obtained in each iteration by linearising the system of equations around the approximate solution obtained in the previous iteration and solving the resulting linear system. This sequence is repeated until it has converged to a sufficiently accurate solution. The convergence of this process is quadratic if the linearisation is consistent.

Relations (5.14) and (5.15) can be rewritten for iteration $i + 1$ as

$$\delta \mathbf{f}_{ai} = \mathbf{f}_{ae} - \mathbf{f}_{ai}^i, \quad (5.33)$$

$$\mathbf{K}_{ee} \delta \mathbf{e} - \delta \mathbf{f}_e = \mathbf{f}_e^i - \mathbf{K}_{ee} \mathbf{e}^i, \quad (5.34)$$

where the superscript $t + \Delta t$ has been dropped for brevity and \mathbf{f}_{ai} and \mathbf{f}_e have been written as the sum of their value in the previous iteration \mathbf{f}_{ai}^i , \mathbf{f}_e^i and iterative corrections $\delta \mathbf{f}_{ai}$, $\delta \mathbf{f}_e$. The column \mathbf{f}_e depends on the local equivalent strain $\tilde{\epsilon}$; its variation can therefore be linearised using

$$\delta \tilde{\epsilon} = \mathbf{s}^T \mathbf{B} \delta \mathbf{a}, \quad (5.35)$$

where

$$\mathbf{s} = \left. \frac{\partial \tilde{\epsilon}}{\partial \mathbf{e}} \right|_{\mathbf{e}=\mathbf{e}^i}. \quad (5.36)$$

Similarly, the change of the internal nodal forces, $\delta \mathbf{f}_{ai}$, is linearised by

$$\delta \boldsymbol{\sigma} = (1 - D^i) \mathbf{C} \mathbf{B} \delta \mathbf{a} - \delta D \mathbf{C} \mathbf{B} \mathbf{a}^i. \quad (5.37)$$

The second right-hand-side term in this equation vanishes when the conditions for damage growth are not satisfied. In the quasi-brittle model this is the case when $\tilde{\epsilon}^i < \kappa^t$ or $D^i = 1$. If iteration i predicts damage growth, δD is linearised in the quasi-brittle model as

$$\delta D = q \tilde{\mathbf{N}} \delta \mathbf{e}, \quad (5.38)$$

with q defined by

$$q = \left. \frac{dD}{d\kappa} \right|_{\kappa=\kappa^i}. \quad (5.39)$$

For the fatigue model the linearisation of δD depends on the type of integration which is used. If the damage growth relation is integrated directly in its rate form using (5.19), the conditions for damage growth read $f^i \geq 0$, $\Delta f^i \geq 0$ and $D^i < 1$. If these conditions are satisfied, linearisation of (5.19) results in

$$\delta D = ((1 - \vartheta)g(D^i, \bar{\varepsilon}^i) + \vartheta g(D^i, \bar{\varepsilon}^i)) \delta \bar{\varepsilon} + \vartheta \frac{\partial g}{\partial D} \delta D \Delta \bar{\varepsilon}^i + \vartheta \frac{\partial g}{\partial \bar{\varepsilon}} \delta \bar{\varepsilon} \Delta \bar{\varepsilon}^i, \quad (5.40)$$

where the derivatives $\partial g / \partial D$ and $\partial g / \partial \bar{\varepsilon}$ are evaluated for iteration i . Notice that this linearisation is consistent since indirect variations, through the evolution function $g(D, \bar{\varepsilon})$, have also been taken into account by the second and third right-hand-side term. Relation (5.40) can be written in the form (5.38) by defining q as

$$q = \frac{(1 - \vartheta)g(D^i, \bar{\varepsilon}^i) + \vartheta g(D^i, \bar{\varepsilon}^i) + \vartheta \frac{\partial g}{\partial \bar{\varepsilon}} \Delta \bar{\varepsilon}^i}{1 - \vartheta \frac{\partial g}{\partial D} \Delta \bar{\varepsilon}^i}. \quad (5.41)$$

The corresponding expression for the predictor-corrector scheme (5.20), (5.21) is obtained by setting the denominator equal to one in (5.41) and evaluating the second and third term in the numerator for $D = D^p$ instead of $D = D^i$. In the implicit as well as the explicit scheme $\bar{\varepsilon}^i$ and $\Delta \bar{\varepsilon}^i$ must be replaced by κ_0 and $\bar{\varepsilon}^i - \kappa_0$ in (5.41) if part of the nonlocal equivalent strain increment lies within the loading surface, i.e., if $f^i < 0$ (see Section 5.2). In the cycle based integration according to (5.24) q can be derived along the same lines, resulting in

$$q = \frac{\vartheta \frac{\partial G}{\partial \bar{\varepsilon}} \Delta N}{1 - \vartheta \frac{\partial G}{\partial D} \Delta N}, \quad (5.42)$$

where the index a of $\bar{\varepsilon}_a$ has been dropped. The predictor-corrector expression for q is again obtained by setting the denominator to one and evaluating $\partial G / \partial \bar{\varepsilon}$ for $D = D^p$.

Using (5.35), (5.37), (5.38) and the appropriate expression for q , the set of equations (5.33), (5.34) can be written as one linear system

$$\begin{bmatrix} \mathbf{K}_{aa} & \mathbf{K}_{ac} \\ \mathbf{K}_{ca} & \mathbf{K}_{cc} \end{bmatrix} \begin{bmatrix} \delta \mathbf{a} \\ \delta \mathbf{e} \end{bmatrix} = \begin{bmatrix} \mathbf{f}_{ac} - \mathbf{f}_{ai}^i \\ \mathbf{f}_c^i - \mathbf{K}_{cc} \mathbf{e}^i \end{bmatrix}, \quad (5.43)$$

with

$$\mathbf{K}_{aa} = \int_{\Omega} \mathbf{B}^T (1 - D^i) \mathbf{C} \mathbf{B} \, d\Omega, \quad (5.44)$$

$$\mathbf{K}_{ac} = - \int_{\Omega} \mathbf{B}^T \mathbf{C} \bar{\varepsilon}^i q \bar{\mathbf{N}} \, d\Omega, \quad (5.45)$$

$$\mathbf{K}_{ca} = - \int_{\Omega} \bar{\mathbf{N}}^T \mathbf{s}^T \mathbf{B} \, d\Omega. \quad (5.46)$$

Solving this system gives improved approximations $\mathbf{a}^{i+1} = \mathbf{a}^i + \delta \mathbf{a}$ and $\mathbf{e}^{i+1} = \mathbf{e}^i + \delta \mathbf{e}$ of $\mathbf{a}^{t+\Delta t}$ and $\mathbf{e}^{t+\Delta t}$. The field variables which correspond to this new approximation are computed and the terms of equations (5.14), (5.15) are updated. If the residual on these equations exceeds a predefined convergence tolerance, the procedure is repeated until the residual has become smaller than this tolerance. If the Newton-Raphson process does not converge, it is restarted with a smaller increment size.

5.4 Crack growth

A crack is represented by a region of completely damaged material, Ω_c , in continuum damage models. It has been argued in Chapter 2 that this cracked region should not be a part of the equilibrium problem because the equilibrium equations are not meaningful in it. Accordingly, the equilibrium equations and the additional partial differential equation (4.13) of the gradient approach are defined only on the domain $\tilde{\Omega} = \Omega \setminus \Omega_c$ and boundary conditions must be provided at the boundary $\tilde{\Gamma}$ of $\tilde{\Omega}$. For the finite element formulation this means that the weak forms (5.1), (5.3) and the finite element interpolations of the displacements and nonlocal equivalent strain must be limited to the noncritical domain $\tilde{\Omega}$. The difficulty is, however, that this effective domain may change as the numerical simulation progresses. Under the influence of damage growth the crack propagates and the remaining domain $\tilde{\Omega}$ thus shrinks. Consequently, the problem domain must be redefined in the numerical analysis for each increment of crack growth and a new finite element discretisation must be defined.

In order to avoid the reformulation of the finite element problem after each time step, numerical damage analyses are often defined on the original domain Ω even if this domain contains a crack. The material in the crack is given a small residual stiffness, for instance by limiting the damage variable to a value which is slightly smaller than one, in order to avoid the discrete equilibrium equations becoming singular. It is then argued that the stresses which are still transferred by the crack influence equilibrium only marginally if the residual stiffness is sufficiently small. This may indeed be true in local damage models, in which the large – nonphysical – strains in the crack do not influence the surrounding material. But if this approach is followed for nonlocal and gradient damage models, the nonlocal equivalent strain maps the large strains in the cracked region onto the surrounding material in which the damage variable is not (yet) critical. This does not only result in faster growth of damage in front of the crack and consequently in higher predicted crack growth rates, but also in damage growth at the faces of the crack, thus causing the thickness of the crack to increase, see Section 4.3.

In truly nonlocal damage models it may be sufficient to limit the averaging volume in (4.4) to $\tilde{\Omega}$ in order to remove the influence of the strains in Ω_c on the remaining material. For the implicit gradient model considered here, Geers (1997) has proposed to eliminate the interaction between crack and surrounding material by using a variable length scale. However, since the difficulties originate in the numerical implementation rather than the underlying continuum model, it seems more natural to improve the numerical description of the problem instead of adding complexity to the continuum model. A rigorous and elegant approach would be to track the movement of the internal boundary which represents the crack contour

and to adapt the finite element discretisation to the new crack front after each increment. The remeshing can be used at the same time to adapt the element size to local variations of the solution, so that the accuracy is optimal. A disadvantage is that constitutive variables must be mapped from the old mesh onto the new mesh, which inevitably introduces interpolation errors. Instead, a rather crude remeshing method is used here: completely damaged elements are removed from an otherwise fixed finite element mesh. The crack contour always follows the (initial) grid lines in this approach, which means that a fine discretisation is needed in a relatively large region. When the damage variable is critical at the end of an increment in a certain element, this element is removed from the finite element mesh. Nodes and degrees of freedom which are not connected to other elements are also removed and the set of equations (5.8), (5.11) is resized accordingly. The increment which led to the critical damage is then recomputed starting from the converged state in the previous increment, in which the element was not yet cracked, so that the growth of damage in other elements is consistent with the momentary configuration.

It has been found that partly cracked elements, i.e., elements in which the damage variable has become critical in only a part of the element, have a negative influence on the mesh objectivity of the analysis. Deformations in the cracked part of the element, which should theoretically be excluded from the boundary value problem, may become unrealistically large. These large strains lead to an increase of the nonlocal equivalent strain and consequently to an overprediction of the damage growth. This effect decreases when the discretisation is refined and the crack contour is thus described more accurately. But the convergence upon mesh refinement has been found to be significantly better if partially cracked elements are avoided by using elements with constant damage. As an additional advantage, the convergence of the Newton-Raphson process is better with these elements because nearly singular elements are largely avoided. A critical value of the damage variable is used which is slightly smaller than one (typically 0.999999) to avoid numerical singularities, but this does not influence the growth of damage since the increment in which it is reached is discarded after removing the element.

Chapter 6

Applications

The behaviour of the gradient-enhanced damage formulations for quasi-brittle and fatigue fracture is demonstrated in this chapter by numerical analyses of these fracture processes. The simulations have been carried out using the finite element implementation discussed in the previous chapter. The quasi-brittle model has been applied to concrete (Section 6.1) and to a short glass-fibre reinforced composite (Section 6.2). Two problems have been considered in the concrete fracture analyses: a direct tension experiment taken from Hordijk (1991) and a single-edge notched beam under an anti-symmetric four-point loading (Schlangen, 1993). The numerical difficulties in describing crack growth have been avoided in these analyses by using a damage growth relation for which the damage variable will never become critical. This approach can no longer be followed for the large crack openings observed in the fibre reinforced composite. The remeshing procedure of Section 5.4 has therefore been used in these analyses. The results are compared with the experimental data given by Geers (1997). The fatigue model has been tested on a thin steel specimen with a rounded notch (Section 6.3). This problem has also been used to study the influence of the internal length scale in the gradient formulation on crack growth.

6.1 Concrete fracture

The direct tension experiments of Hordijk (1991) on lightweight concrete have been taken as a reference for the first concrete fracture problem considered here (see also Peerlings et al., 1998a; de Borst et al., 1999). In these experiments, double-edge notched specimens of different lengths were glued to loading platens and subjected to an axial, tensile load, see Figure 6.1. Following Rots and de Borst (1989), these loading conditions have been modelled by fixing the bottom of the specimen and keeping the upper edge straight by introducing the appropriate displacement constraints. A translational and a rotational spring have been fixed to the upper loading platen, representing the stiffness of the testing machine. The translational and rotational stiffnesses have been computed by Hordijk (1991) as 148 000 N/mm and 10^9 Nmm/rad respectively. The thickness of the specimens is 50 mm. Although the response observed in the experiments was essentially three-dimensional, a plane-stress situation has been assumed in the numerical analyses.

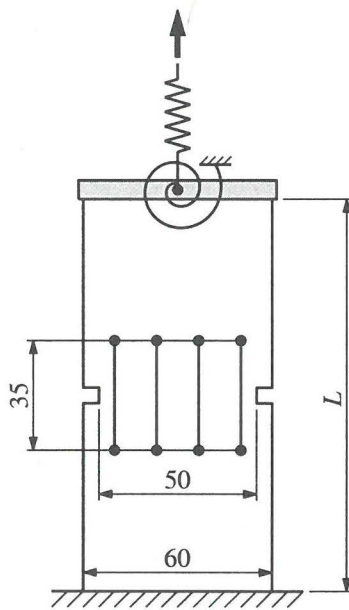


Figure 6.1: Modelling of the direct tension experiments (dimensions in mm).

Specimens of three different lengths were tested by Hordijk (1991) and have also been analysed numerically: $L = 50, 125$ and 250 mm. The tests were performed under servo control, with the average deformation in the fracture zone, δ , as the control parameter; δ was measured by four pairs of extensometers with a gauge length of 35 mm, attached as indicated in Figure 6.1. In the simulations, the servo control has been replaced by its numerical counterpart, i.e., indirect displacement control (de Borst, 1986). This procedure uses the average deformation of a 35 mm section of the specimen to control the loading force, which corresponds to the 35 mm gauge length of the extensometers in the experiments.

The elastic constants have been set to $E = 18$ GPa and $\nu = 0.2$. The exponential damage growth law (2.12) has been used, with the parameters $\kappa_0 = 2.1 \cdot 10^{-4}$, $\alpha = 0.96$ and $\beta = 350$. The damage variable never reaches its critical value $D = 1$ for this growth law, so that theoretically a crack will never be initiated and the material will never be completely separated. As a result, no remeshing is necessary in the analyses. For large deformations this assumption is physically unrealistic, but for the relatively small crack openings with considerable crack bridging observed in concrete, realistic responses can be obtained with this approach. For the equivalent strain the modified von Mises definition (2.17) has been used, with a compressive/tensile strength ratio k equal to 10. The gradient parameter c has been set to 1 mm^2 . This value is based on the fact that the largest aggregates in the material are of the order of several millimetres.

The $L = 50$ mm geometry has been used to examine the mesh sensitivity of the gradient damage model. For this purpose, the problem has been analysed with three finite element discretisations with increasingly smaller elements in the area between the notches. The three

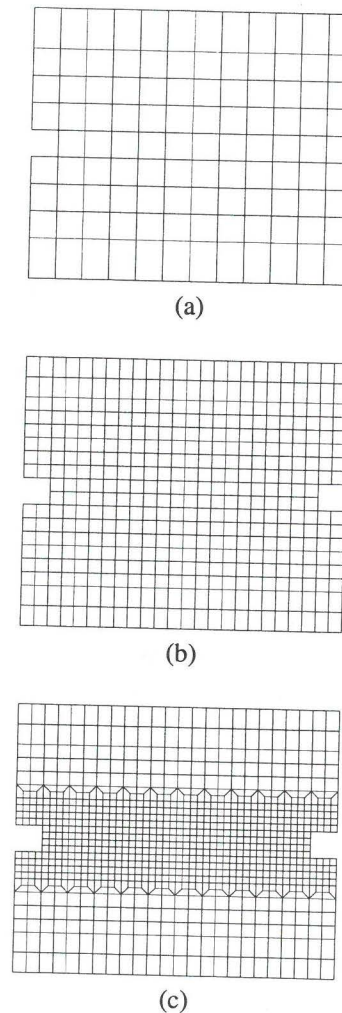


Figure 6.2: Finite element discretisations used in the mesh sensitivity study: (a) $h = 5$ mm, (b) $h = 2.5$ mm and (c) $h = 1.25$ mm.

discretisations are shown in Figure 6.2; they consist of 106, 424 and 928 elements, respectively and have square elements with edge lengths $h = 5, 2.5$ and 1.25 mm in the fracture zone. Eight-noded serendipity shape functions have been used for the displacements and four-noded, bilinear shape functions for the nonlocal equivalent strain. A 2×2 Gauss integration scheme has been applied; it has been verified that the reduced integration of the equilibrium equations does not influence the results.

The stress-deformation curves obtained with the three meshes are shown in Figure 6.3. The deformation is represented by the average relative vertical displacement of the 35 mm measuring section, δ ; the stress in Figure 6.3 is the engineering stress with respect to the

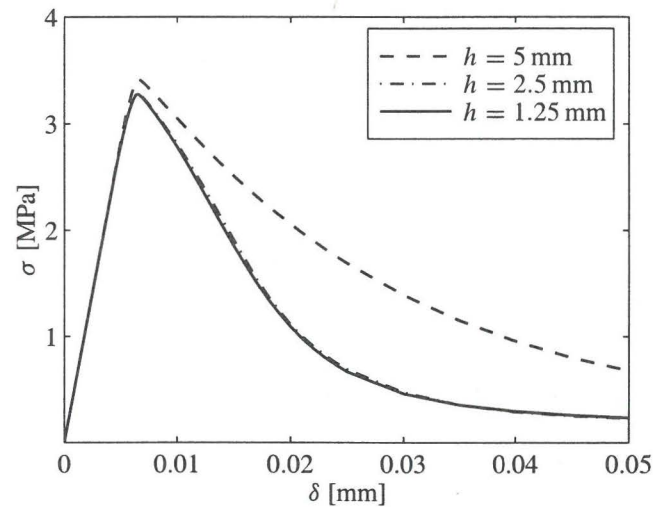


Figure 6.3: Stress-deformation curves for the three meshes.

smallest cross-section of the bar. For an increasing level of mesh refinement the curves converge to a solution with a positive, finite energy dissipation. Whereas the $h = 5$ mm mesh slightly overestimates the strength, the finer meshes give practically identical results. The discretisations used in the remainder of this section therefore have the same fineness in the process zone as the coarsest of these two meshes, i.e., $h = 2.5$ mm. Figure 6.4 shows the evolution of the damage variable as computed with the $h = 1.25$ mm mesh. The damage zones which have been formed in the hardening stage at both notches coalesce after reaching the fracture strength of the specimen. The damage then continues to grow more uniformly along the smallest cross-section. In contrast with local damage models, in which the damage would have localised in a line, the final damage band has a finite width. The damage distribution is therefore insensitive to the element size as long as the discretisation is sufficiently fine to describe the width of the band with a reasonable accuracy.

As demonstrated in Figure 6.5(a), in which the numerical responses of the three specimen sizes ($L = 50, 125$ and 250 mm) have been plotted together, the stress-deformation curves of the different specimens practically coincide. The same trend was observed in the experimental data, with the exception of the 50 mm specimen, which showed a substantially less brittle response (Hordijk, 1991). In Figure 6.5(a) the fracture strength is slightly higher for this length than for the other two lengths. This is probably due to the influence of the boundary constraints at the top and bottom of the specimen, which are much closer to the fracture zone in the small specimen than in the longer specimens. Figure 6.5(b) gives the engineering stress versus the vertical displacement of the top of the bar, U . A snap-back response is observed for the 250 mm specimen after reaching the fracture strength, that is, continued loading results in a decreasing displacement with a decreasing load. This demonstrates the necessity of the indirect displacement control procedure in the simulations. If the analyses

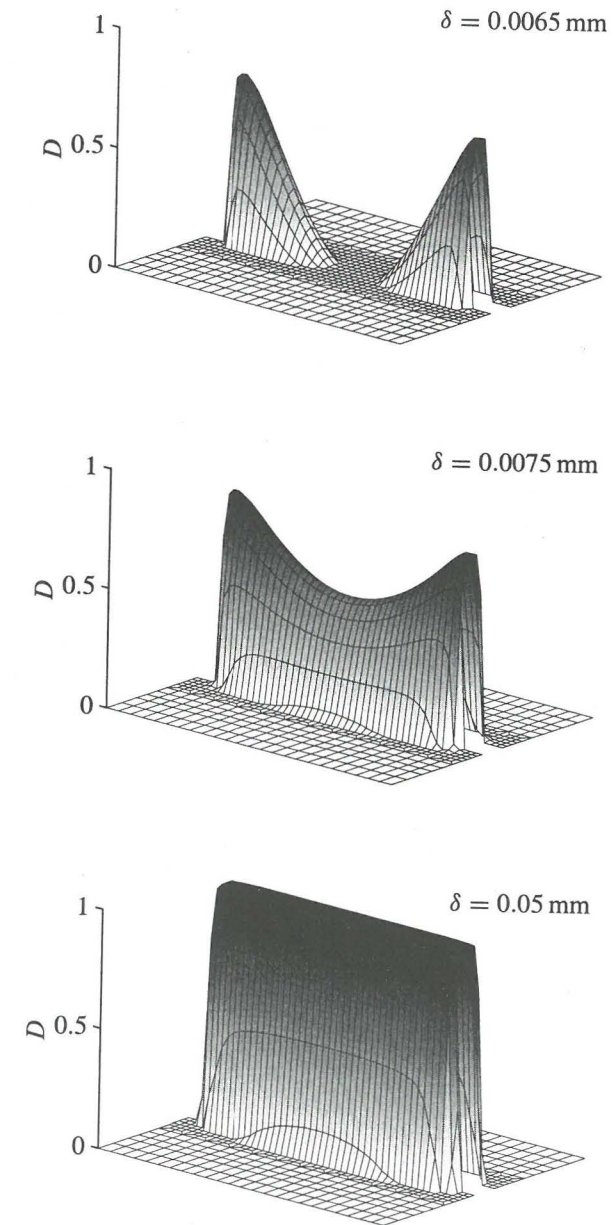
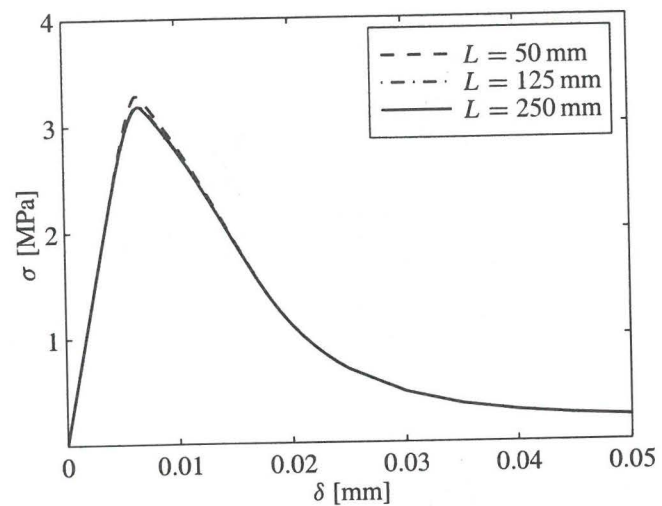
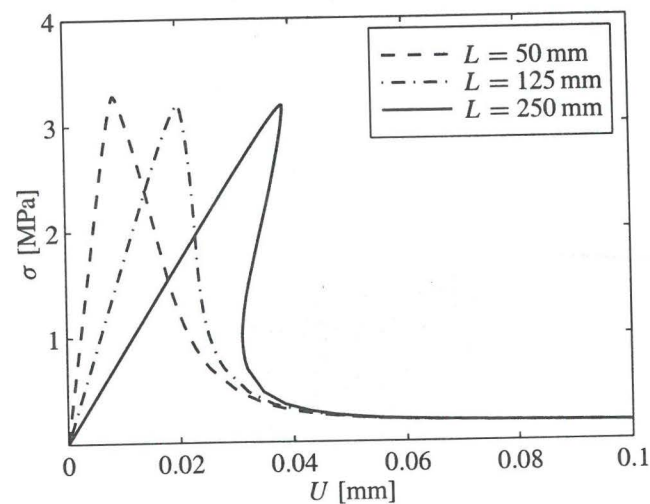


Figure 6.4: Damage evolution in the 50 mm specimen ($h = 1.25$ mm discretisation).



(a)



(b)

Figure 6.5: Computed stress versus (a) deformation of the process zone and (b) total elongation of the $L = 50$, 125 and 250 mm specimens.

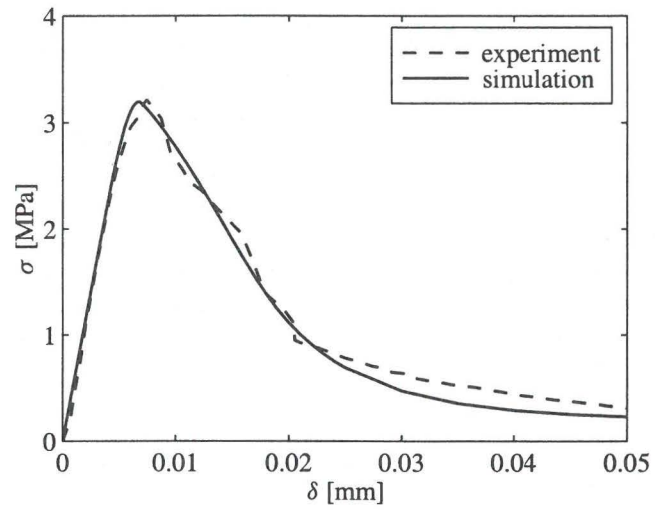
had been performed under direct displacement control or direct load control, it would have been impossible to follow the entire softening path for the longest specimen.

In Figure 6.6 the computed stress-deformation curves are compared with the experimentally obtained curves for the 125 and 250 mm specimens as given by Hordijk (1991). The 50 mm specimen has not been included in the comparison because the experimental data for this specimen do not seem to be consistent with that of the other specimens. A reasonable agreement of the numerical and experimental curves can be observed. Most striking are the two 'bumps' in the experimental curves, which are not present in the numerical curves. Numerical as well as experimental studies have demonstrated that these bumps are related to asymmetry in the response of the bar (Rots and de Borst, 1989; Hordijk, 1991). This asymmetry is triggered by the fact that the specimen geometry and its properties are not perfectly symmetric in the experiments. In the numerical idealisation, however, this symmetry theoretically exists. If the accuracy of the computations is sufficient, the damage growth and deformation are perfectly symmetric with respect to the vertical axis of the specimen, see Figures 6.4 and 6.7(a). An asymmetric response can be obtained if the symmetry of the problem is removed by the introduction of a small imperfection at one of the notches. This has been done for the 250 mm bar by reducing the damage threshold κ_0 by 1% in a $5 \times 5 \text{ mm}^2$ area in front of the left notch. With this imperfection an asymmetric response is indeed obtained, as shown in Figure 6.7(b).

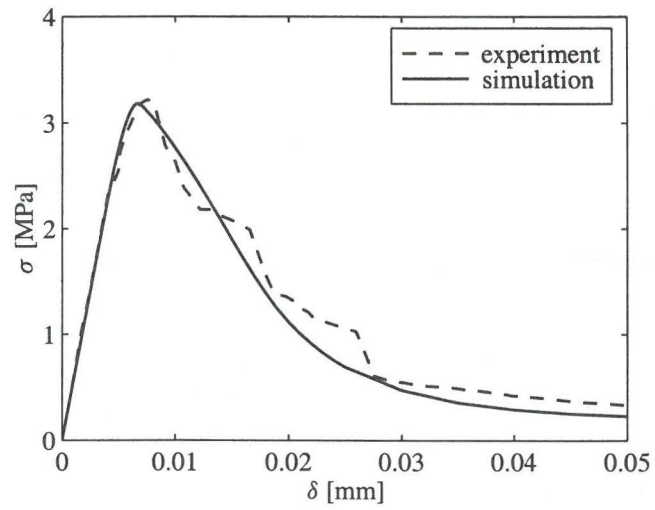
The stress-deformation responses of the symmetric and asymmetric problems are given in Figure 6.8. The curve for the specimen with an imperfection clearly shows a bump. The damage growth corresponding to this stress-displacement curve has been plotted in Figure 6.9. Initially, the growth of damage is essentially symmetric. At the peak in the stress curve, however, damage growth is arrested at one notch, while the damage zone at the other notch continues to grow. When this zone has reached the damage zone at the other notch, the response again becomes symmetric. It is in the transition from the asymmetric to the symmetric response that the bump occurs in the stress-deformation diagram. Only one bump is observed in the simulation instead of the two bumps in the experimental curves as a consequence of the fact that the simulation is two-dimensional. In the finite element idealisation the response can only be asymmetric in the model plane, whereas the experiments also showed out of plane displacements.

The second concrete fracture problem consists of a single-edge notched beam subjected to an anti-symmetric four-point loading (Figure 6.10). The geometry and loading conditions have been taken from Schlangen (1993), who analysed the problem experimentally as well as numerically with a lattice model. The thickness of the beam is 50 mm. The anti-symmetric loading results in a curved crack path in experiments, starting from the right corner of the notch and ending to the right of the lower-right support (Schlangen, 1993).

The specimen has been modelled with 1362 elements with an eight-noded quadratic displacement field and a bilinear nonlocal equivalent strain, see Figure 6.11. The elements in the fracture zone have an edge $h = 2.5 \text{ mm}$. The two supports near the centre of the beam have been modelled as (20 mm wide) rigid bodies by introducing the appropriate linear dependencies between the nodal displacements. Since the supports at the ends of the beam are not expected to have a significant effect on the response, they have been represented by a nodal



(a)



(b)

Figure 6.6: Comparison of numerical and experimental stress-deformation curves for the (a) $L = 125$ mm and (b) $L = 250$ mm specimens.

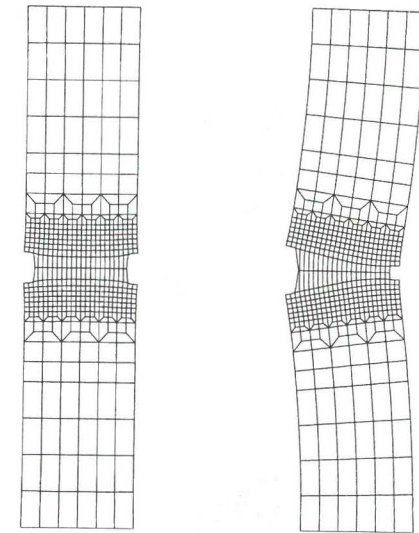


Figure 6.7: Deformation in the (a) symmetric and (b) asymmetric solutions; displacements have been scaled by a factor 750.

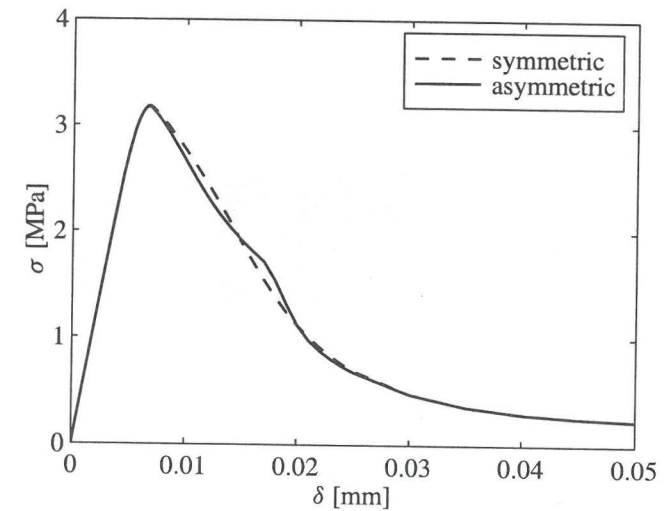


Figure 6.8: Stress-deformation curves for the symmetric and asymmetric configurations.

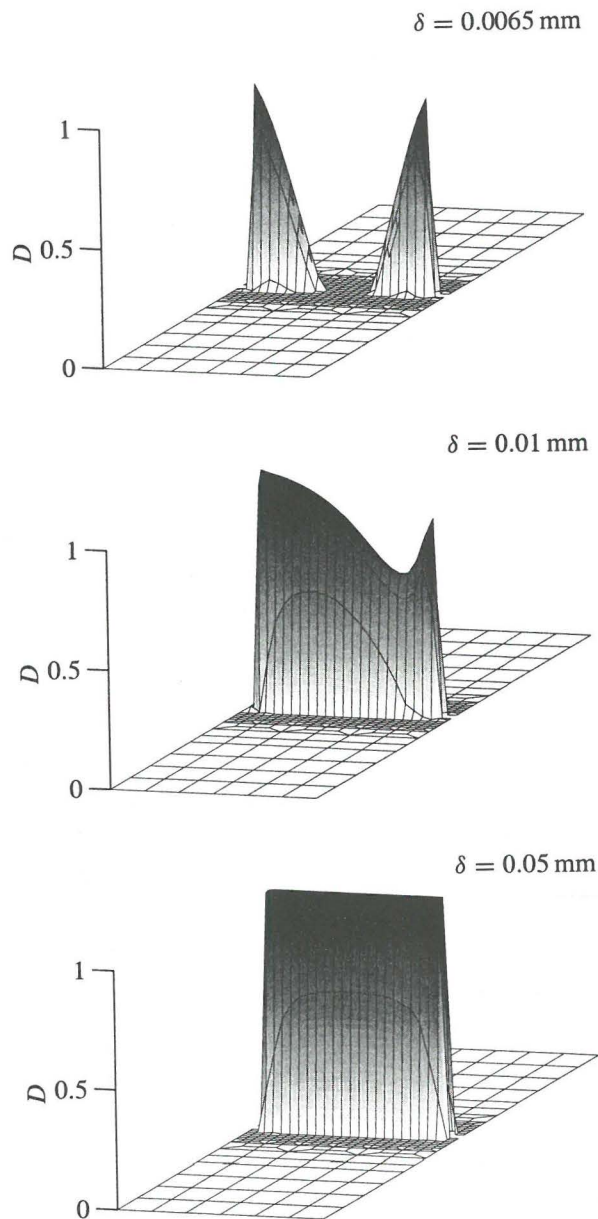


Figure 6.9: Asymmetric damage evolution in the $L = 250$ mm specimen.

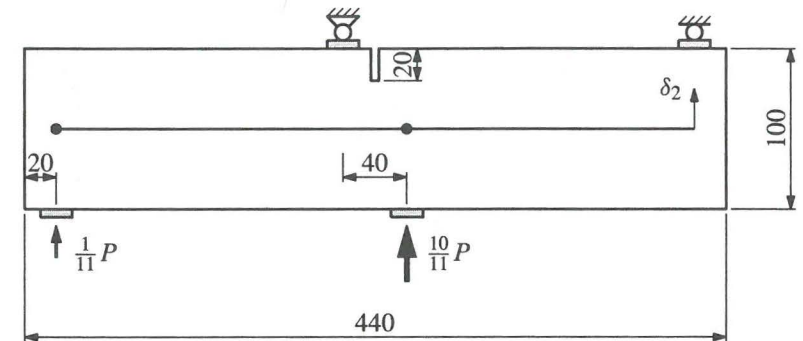


Figure 6.10: Single-edge notched beam problem (dimensions in mm).

restraint and a nodal force. A plane-stress situation has been assumed. The parameters ν , k , α and c have been taken identical to those of the direct tension analyses, i.e., $\nu = 0.2$, $k = 10$, $\alpha = 0.96$ and $c = 1 \text{ mm}^2$. In the experiments the specimens were made of normal-weight concrete, so that Young's modulus and the parameters related to the material strength must be altered. These parameters have been set to $E = 35 \text{ GPa}$, $\kappa_0 = 6.0 \cdot 10^{-5}$ and $\beta = 100$. An indirect displacement control procedure has again been used, with the deformation parameter δ_2 defined by Schlangen (1993), as input, see Figure 6.10. In the experiments the deformation δ_2 was measured as the vertical displacement of a steel bar, which was glued to the centre of the specimen near the lower supports, with respect to the upper-right support (Schlangen, 1993). Since the vertical displacement of the upper supports is zero in the finite element model, δ_2 is represented by a linear combination of the displacements of the lower supports.

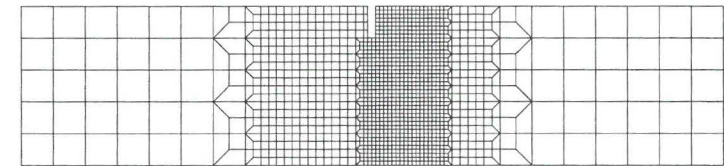


Figure 6.11: Finite element discretisation of the single-edge notched beam.

The evolution of the damage variable has been plotted in Figure 6.12. In the first stage of the fracture process, damage is initiated at the right corner of the notch and opposite to the central supports. The damage growth at the latter locations, which is due to bending of the specimen, is arrested at a certain stage. In the experiments, some cracking was indeed observed in these areas (van Mier, 1997). The damage zone at the notch continues to grow, following a curved path which ends to the right of the lower-right support. The final damage distribution is given in Figure 6.13, along with the experimentally determined crack paths in three different specimens as given by Schlangen (1993). A satisfactory agreement of the experimental and numerical paths is observed, with the cracks lying within the damage band

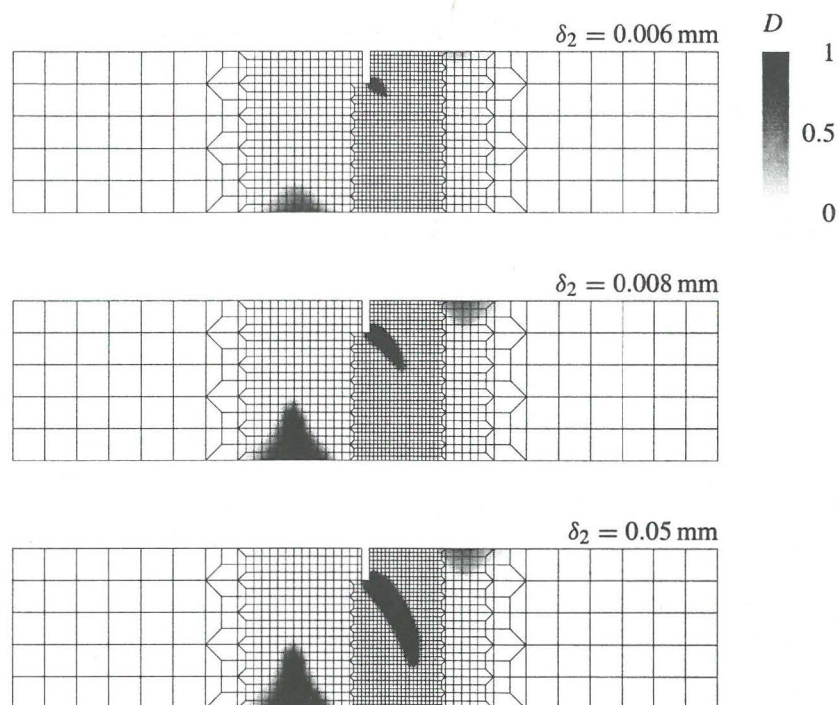


Figure 6.12: Damage evolution in the single-edge notched specimen.

obtained in the numerical analysis. It has been shown by Peerlings et al. (1998a) that the development of a curved crack in the numerical analysis depends critically on the definition of the equivalent strain. If the influence of compressive strain components on the equivalent strain is too large, as in the normalised energy release rate (2.15) and Mazars definition (2.16), failure by a straight crack or by penetration of the lower support is predicted.

The displacements at the end of the fracture process (magnified by a factor 100) are given in Figure 6.14. This figure and Figure 6.13 show that the deformation and damage are localised in a band which comprises a number of elements. The damage distribution is therefore insensitive to the element size for sufficiently fine meshes. Indeed, if the size of the elements is doubled ($h = 5$ mm), the shape and width of the damage band change only marginally (Geers et al., 1998c; de Borst et al., 1999). Furthermore, the curved crack shape shows that the direction of damage growth and thus the final damage distribution are not affected by the orientation of the finite element mesh.

Figure 6.15 shows the load P versus three deformation quantities measured by Schlangen (1993): the deformation parameter δ_2 which was also used for the indirect displacement control, and the crack mouth opening and sliding displacements (CMOD and CMSD respectively). The CMOD and CMSD are defined as the relative horizontal and vertical displacements

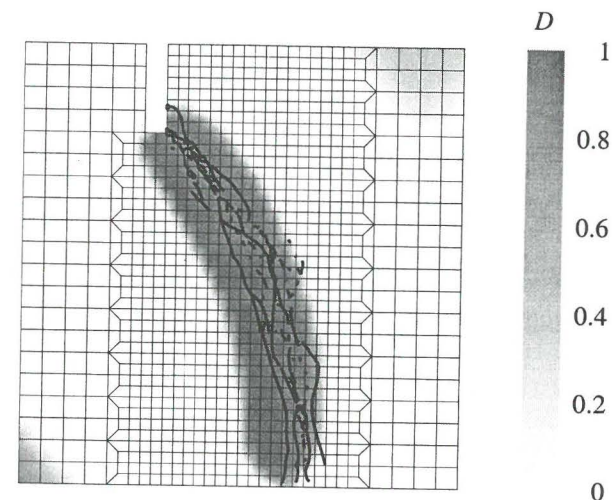


Figure 6.13: Comparison of the final damage distribution and experimental crack patterns.

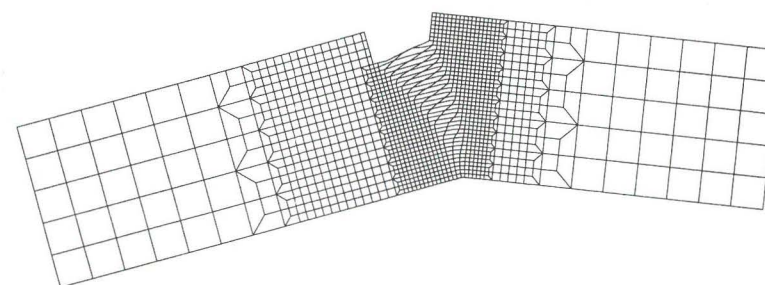


Figure 6.14: Displacements at the end of the fracture process, scaled by a factor 100.

of the notch faces at the top of the beam. The solid curves are the computed load-displacement relations, while the dashed curves represent the three experiments reported by Schlangen (1993). A good agreement is observed, with the numerical curves lying within or close to the band formed by the experimental curves. The computed response is slightly too brittle in the lower half of the softening regime, but since the same trend is observed in all three diagrams it is believed that the fit can be improved by using a different evolution law for the damage variable. The fact that there is no significant discrepancy between the CMOD and CMSD curves suggests that the anisotropy of the local material response, for instance due to sliding friction between crack faces and aggregate interlock, plays a minor role, which is consistent with the experimental and numerical observations by Schlangen (1993).

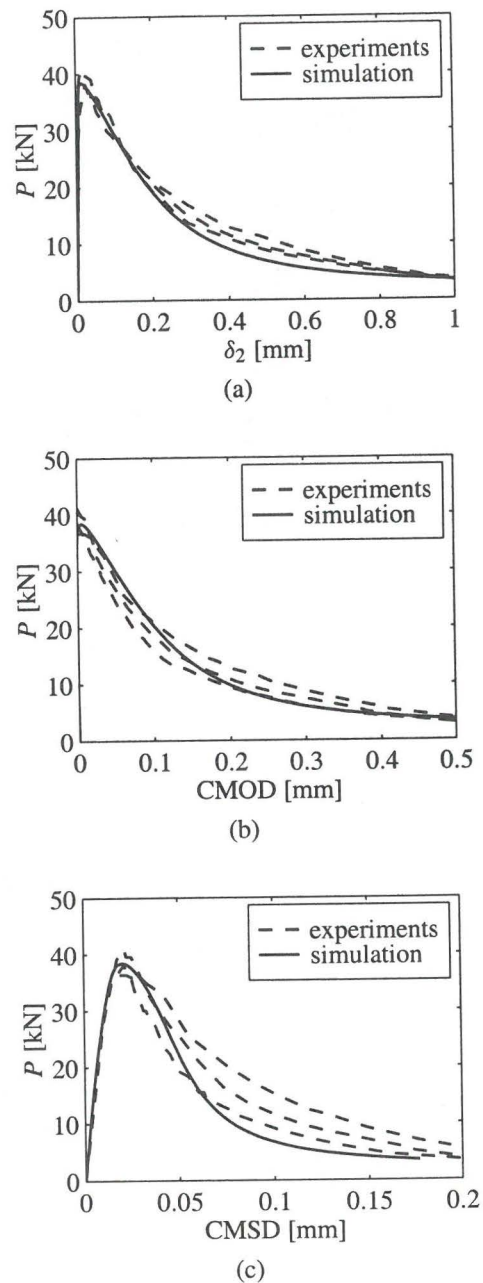


Figure 6.15: Load-deformation curves: P versus (a) δ_2 , (b) CMOD and (c) CMSD.

6.2 Composite fracture

Modelling damage and fracture processes in fibre reinforced polymers is more challenging than modelling concrete fracture in the sense that the larger deformations which are observed in polymer composites may give rise to nonphysical responses if the growth of cracks is not described correctly by the numerical model. The experimental analysis of composite fracture by Geers (1997) provides an excellent basis to study the behaviour of the gradient damage model under these circumstances. In the experiments, compact tension specimens of different sizes were tested almost until complete fracture. The specimens were made of polypropylene, reinforced with 30 wt.% 12.5 mm glass-fibres in a random distribution. The geometry considered here is shown in Figure 6.16, see ASTM standards E399 and E647 (ASTM, 1993) or Geers (1997) for details. The thickness of the specimens was 3.8 mm. Displacements were measured in a square area in front of the notch by optically tracking a marker grid, so that accurate deformation data is available for these experiments.

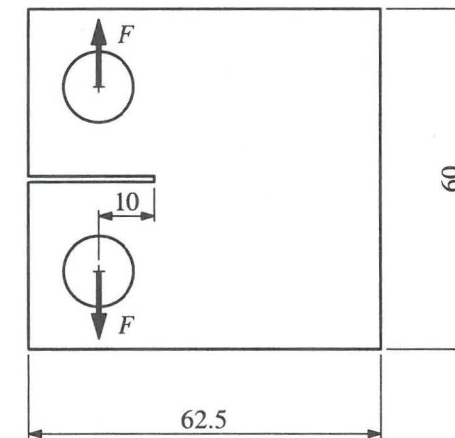


Figure 6.16: Problem geometry of the compact tension experiments (dimensions in mm).

The experiments were modelled by Geers (1997) using a so-called transient-gradient damage formulation, i.e., a gradient damage model with a length scale which depends on the (local) strain state, see also Geers et al. (1998f). This variable length scale was used to avoid pathological growth of damage at the crack faces. Here the standard, constant gradient damage formulation is used and nonphysical damage growth is avoided by removing completely damaged elements from the finite element problem, see Section 5.4. The other components of the damage model have been adopted unaltered from Geers (1997), which means that the Mazars equivalent strain definition (2.16) and the modified power law (2.13) for the damage growth have been used and the model parameters have been set to $E = 3200$ MPa, $\nu = 0.28$, $c = 2$ mm², $\kappa_0 = 0.011$, $\kappa_c = 0.5$, $\alpha = 5$ and $\beta = 0.75$. It is noted that this parameter set may not be optimal for the present model because of the different role of the gradient parameter c .

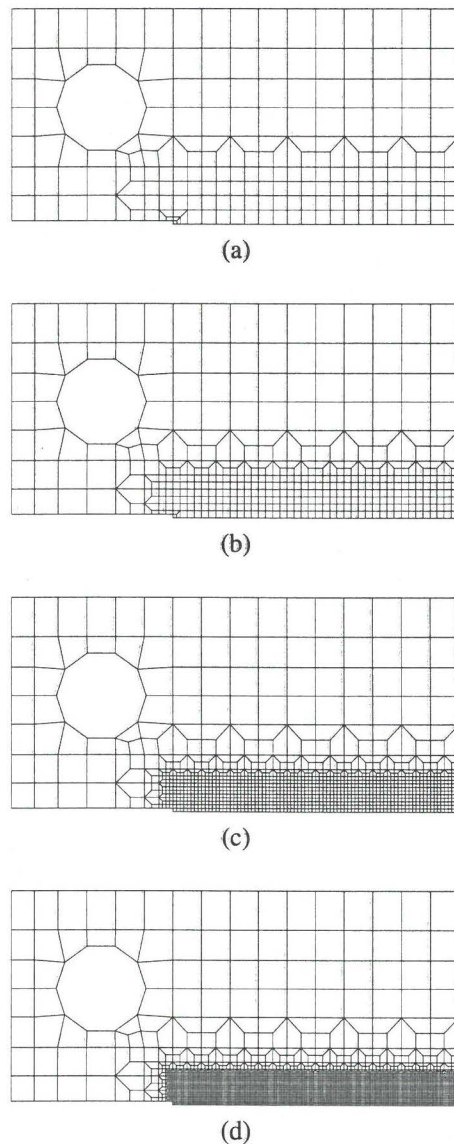


Figure 6.17: Finite element discretisations of the compact tension specimen with element sizes (a) $h = 2$ mm, (b) $h = 1$ mm, (c) $h = 0.5$ mm and (d) $h = 0.25$ mm in the fracture zone.

Because of the symmetry of the problem, only the top half of the specimen has been modelled in the finite element analyses. The appropriate symmetry conditions have been applied at the axis of symmetry. For the nonlocal equivalent strain this condition is identical to the free boundary condition (4.20). Four different finite element meshes have been used, with elements of $h = 2, 1, 0.5$ and 0.25 mm in the fracture zone and a total of 206, 439, 1143 and 3507 elements, respectively (Figure 6.17). The meshes consist of plane-stress elements with bilinear interpolations of the displacements and nonlocal equivalent strain and a constant damage variable. A 2×2 point Gauss integration has been used. The loading force has been applied by nodal forces acting on the two uppermost nodes of the pinhole contour. The average vertical displacement of these two nodes has been used in the indirect displacement control of the loading process. Damage growth has been suppressed in the elements around the top half of the pinhole to avoid fracture in this area.

The global responses obtained with the four discretisations have been plotted in Figure 6.18. This diagram shows the pin force versus the relative vertical displacement of the loading pins, which is defined here as twice the average vertical displacement of the two nodes at the top of the pinhole. The corresponding results for the local damage model have already been given in Figure 3.3. In contrast to the local damage model, the solution of the gradient formulation converges to a stable response with a finite fracture energy upon refinement of the discretisation. The damage distributions at the end of the loading process have been plotted in Figure 6.19 for the four meshes. A relatively large region takes part in the damage process, instead of the vanishing volume in the local damage model. The width of the damage zone is approximately the same in the four discretisations. Moreover, the width of the damage zone is approximately constant along the crack, which indicates that there is no damage growth at the crack faces as the crack opening increases.

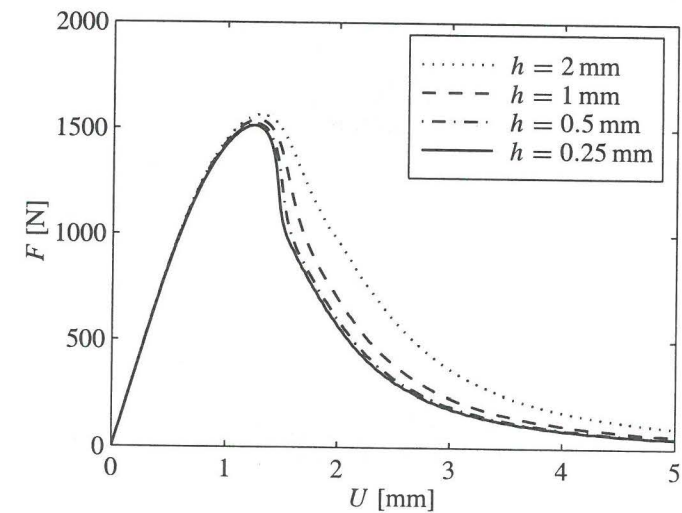


Figure 6.18: Predicted load-displacement response for the four meshes.

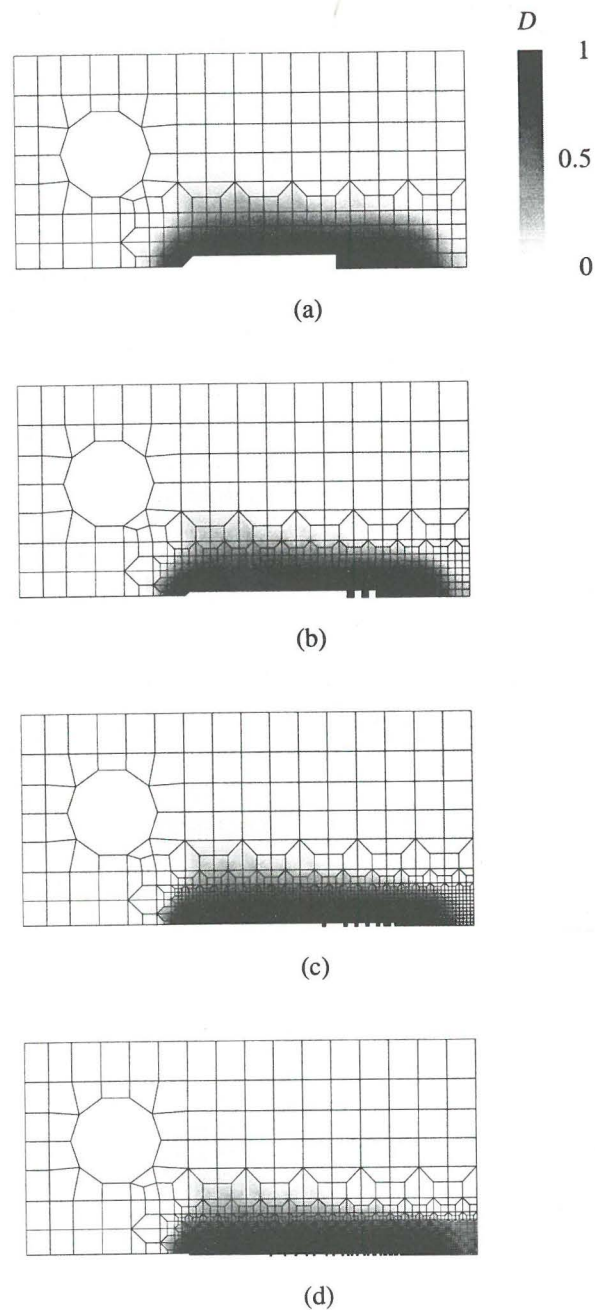


Figure 6.19: Final damage distributions computed with the (a) $h = 2$ mm, (b) $h = 1$ mm, (c) $h = 0.5$ mm and (d) $h = 0.25$ mm meshes.

It has been argued in Section 4.5 that the width of the crack must be zero in the quasi-brittle damage model, because the material adjacent to the projected crack path unloads immediately after the crack tip has passed. This vanishing crack width is represented in the finite element analyses by the smallest possible band of cracked elements. Figures 6.19(b-d), however, show that the crack tip does not always propagate element by element and that elements thus remain in the wake of the crack tip. Since the damage variable is already close to one in these crack bridging elements, they have only a marginal influence on the stress distribution. When the crack opening further increases, these elements successively fail, so that a complete separation of the material is still obtained. The intermittent crack growth is a consequence of the fact that the finite element representation of the crack has a finite width. This means that when an element fails, a finite volume with relatively high equivalent strains no longer contributes to the nonlocal equivalent strain. As a result, the nonlocal equivalent strain at the newly created crack tip decreases by a small amount and its maximum shifts to some distance in front of the crack. If this distance is larger than the size of one element, it may not be the element next in line which fails next, but an element further along the projected crack path. The nonlocal strain in the remaining elements then decreases because a further contribution vanishes, and the damage growth in these elements is therefore temporarily arrested. When the crack opening further increases, however, the nonlocal equivalent strain increases again in these elements, and they still fail.

In Figure 6.20 the load-displacement response obtained with the finest mesh is compared with the experimental data of Geers (1997). Instead of the pin displacement, the more accurate optical displacement measurements have been used in this diagram. For this purpose, two reference points were defined close to the loading pins in the experiments. In the sim-

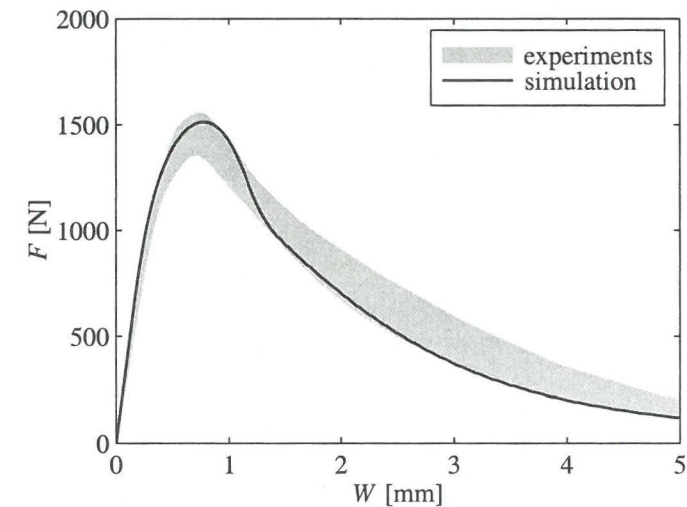


Figure 6.20: Comparison of the numerical and experimental load-displacement responses.

ulation the relative displacement of these points, W , has been determined by interpolation of the nodal displacements. Although the parameter set which has been used in the analyses is probably not optimal for the constant gradient damage model, the predicted load-displacement curve lies almost entirely in the band of experimental responses. The predicted fracture strength is slightly higher than that of the transient-gradient model of Geers (1997), while the post-peak response is somewhat more brittle.

6.3 Metal fatigue

In the fatigue analyses the problem of Figure 6.21 has been considered. The thickness of the specimen is 0.5 mm. A blunt notch has been used in order to have a finite number of cycles to crack initiation, which allows us to study the initiation and propagation of a crack in the same problem. The lower edge of the specimen is fixed in all directions, while fully reversed vertical displacement cycles with an amplitude of 0.0048 mm are forced upon its top edge. The material data that have been used in the analyses are those of 1015 steel and have been taken from Suresh (1991). The fatigue limit of this material, defined for $5 \cdot 10^8$ cycles, is 240 MPa. The damage threshold κ_0 is obtained by dividing this value by Young's modulus $E = 210$ GPa, resulting in $\kappa_0 = 0.00114$. Poisson's ratio has been set to $\nu = 0.3$ and the von Mises equivalent strain (2.28) has been used. The parameter α of the damage evolution function (2.21) has been set to 10. The damage growth curve which is obtained for this value (Figure 2.7) is in reasonable agreement with experimental data (e.g., Lemaitre and Chaboche, 1990; Lemaitre, 1996). The remaining parameters C and β of the evolution law have been solved from expressions (2.26) for the fatigue strength coefficient ($\sigma'_f = 827$ MPa) and the fatigue strength exponent ($b = -0.110$), yielding $C = 6.60 \cdot 10^{21}$ and $\beta = 8.09$. The internal

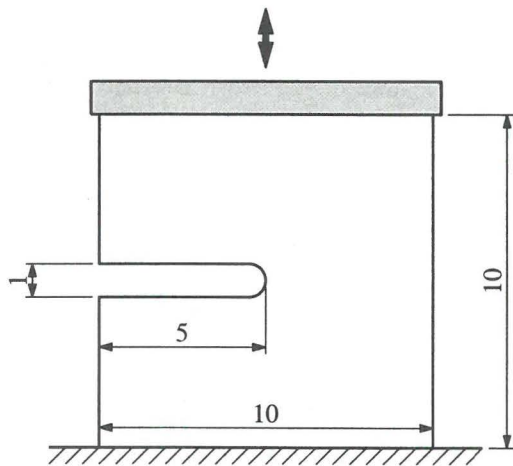


Figure 6.21: Problem geometry and loading conditions of the fatigue problem (dimensions in mm).

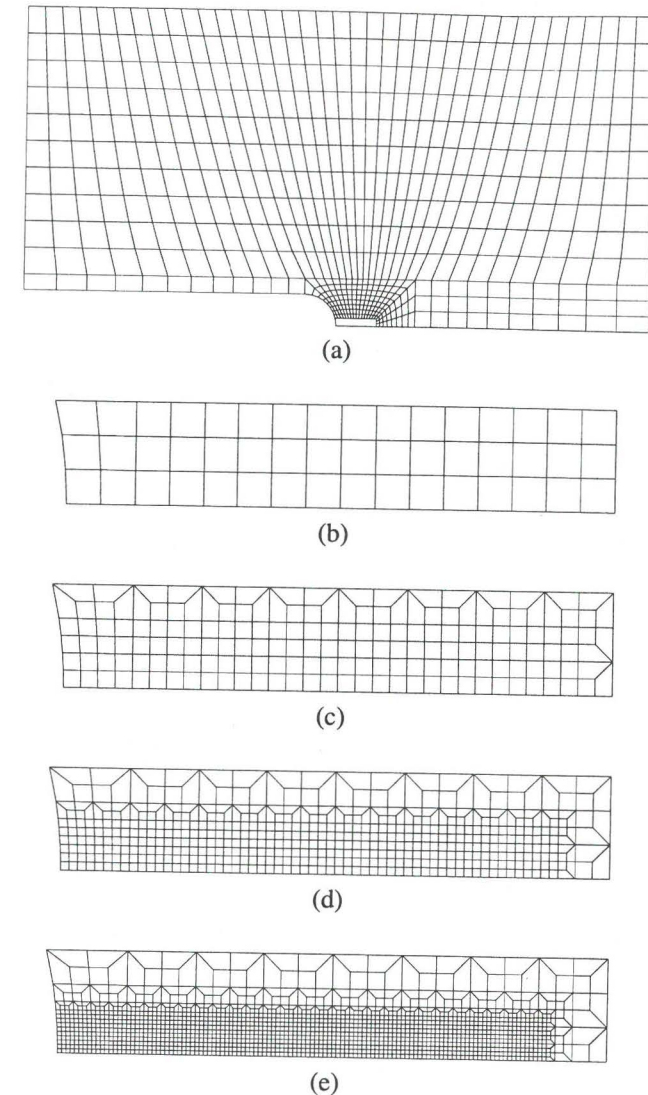


Figure 6.22: Finite element discretisations used in the mesh sensitivity study: (a) entire specimen and refinements with (b) $h = 0.04$ mm, (c) $h = 0.02$ mm, (d) $h = 0.01$ mm, (e) $h = 0.005$ mm.

length has been set to $\sqrt{c} = 0.1$ mm, which is a rough estimate of the maximum grain size in the material.

Because of symmetry only half of the specimen has been modelled in the finite element analyses. The reference mesh contains a regular grid of elements with an edge length $h = 0.04$ mm in an area of approximately 0.65×0.12 mm² at the notch tip, see Figure 6.22(a,b). The discretisation has been successively refined in this area to $h = 0.02, 0.01$ and 0.005 mm (Figure 6.22(c-e)). The resulting discretisations consist of 612, 738, 1065 and 2046 plane-stress elements with bilinear displacement and nonlocal strain interpolations and a constant damage variable. A 2×2 Gauss scheme has been used for the spatial integration. The integration in time has been carried out with the explicit cycle based scheme (5.27), (5.28), with $\vartheta = 0.5$, $\eta = 0.5$ and minimum and maximum increment sizes of 1 and 10^5 cycles.

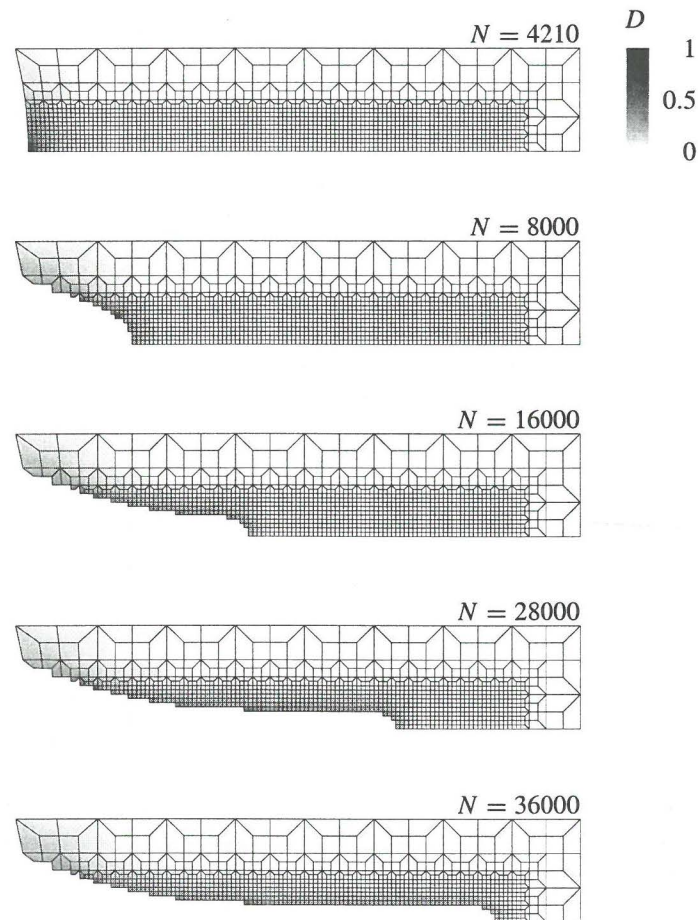


Figure 6.23: Damage and crack growth at the notch tip in the $h = 0.005$ mm mesh.

Figure 6.23 shows the crack initiation and growth process as simulated with the finest of the four meshes. The stress concentration at the notch tip leads to a concentration of damage in this area. At a certain stage a crack is initiated, i.e., the damage variable becomes critical in an element which is then removed from the mesh. For continued cycling the crack grows along the symmetry axis. In contrast to the quasi-brittle analyses of the previous section, the crack has a finite width, which is in agreement with the arguments put forward in Section 4.5. The crack width decreases as the damage zone which was formed before crack initiation is traversed. Beyond this damage zone the crack width becomes stationary at 0.02 mm, which is of the same order as the internal length $\sqrt{c} = 0.1$ mm.

The influence of the finite element discretisation on the crack shape is shown in Figure 6.24, in which the final crack pattern has been plotted for the four discretisations. The

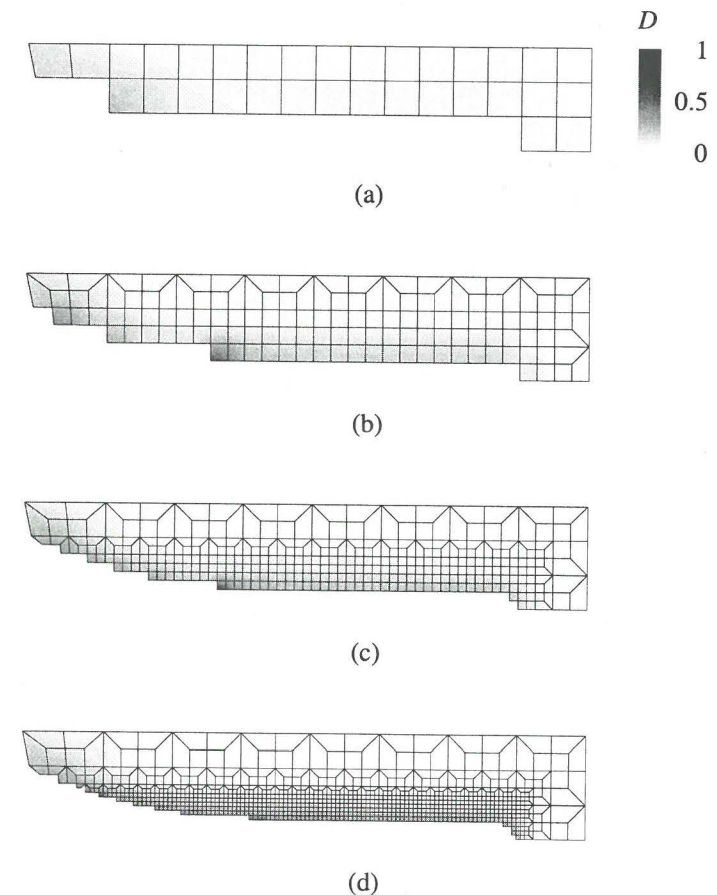


Figure 6.24: Final crack pattern in the (a) $h = 0.04$ mm, (b) $h = 0.02$ mm, (c) $h = 0.01$ mm and (d) $h = 0.005$ mm meshes.

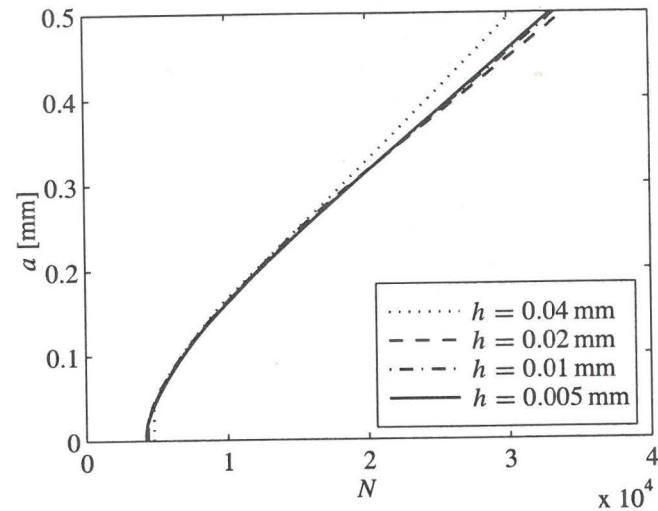


Figure 6.25: Influence of the element size on the predicted crack growth.

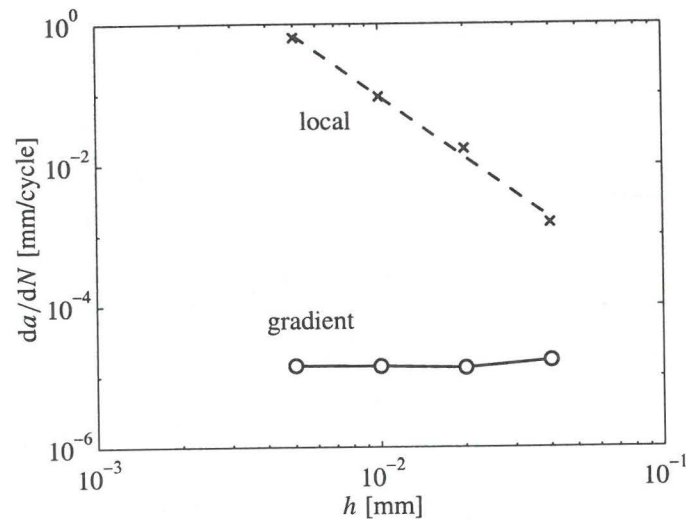


Figure 6.26: Influence of the element size on the steady-state crack growth rate predicted by the local and gradient damage models.

coarsest mesh (Figure 6.24(a)) gives a rather crude approximation of the crack shape and necessarily overestimates the width of steady-state part of the crack because this width is smaller than the element size. But the $h = 0.02$ and 0.01 mm meshes give a good approximation of the crack shape in the finest discretisation. The steady-state width of the crack does not vary between the three finest discretisations. Figure 6.25 shows the length of the crack, a , versus the number of loading cycles N for the four meshes. For an increasingly refined discretisation the growth curves converge to a response with a finite number of cycles to crack initiation and a finite growth rate. The converged initiation life is approximately 4210 cycles. Immediately after its initiation, the crack starts to grow at a relatively high rate. The growth slows down as the damage zone which was formed before crack initiation is traversed until it becomes almost linear beyond this zone. This transition corresponds to the width of the crack becoming constant (Figure 6.23). The steady-state crack growth rate has been plotted versus the element size h in Figure 6.26. The corresponding values for the local damage model, which have already been given in Figure 3.4, have also been plotted in the diagram. Whereas the local model shows a drastic increase of the crack growth rate when the element size is reduced and goes to infinity in the limit $h \rightarrow 0$, the growth rate becomes practically constant at $1.42 \cdot 10^{-5}$ mm/cycle in the gradient model.

Figure 6.27 demonstrates the influence of the internal length \sqrt{c} on the crack growth behaviour. The reference value $\sqrt{c} = 0.1$ mm has been reduced to 0.05 and 0.025 mm. The $h = 0.005$ mm mesh has been used in these analyses. For smaller values of the internal length the crack is initiated sooner (after 814 and 309 cycles, respectively) and it grows faster (approximately $2.51 \cdot 10^{-4}$ and $3.18 \cdot 10^{-2}$ mm/cycle). This trend is caused by the fact that the nonlocal equivalent strain follows the local equivalent strain more closely for smaller

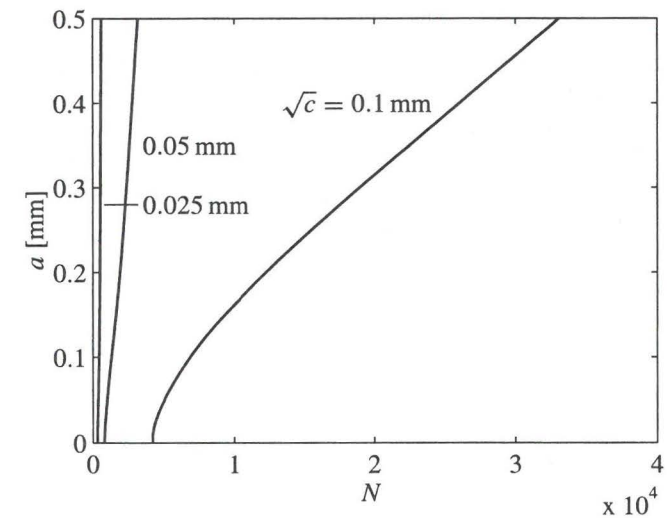


Figure 6.27: Influence of the internal length scale on the crack growth.

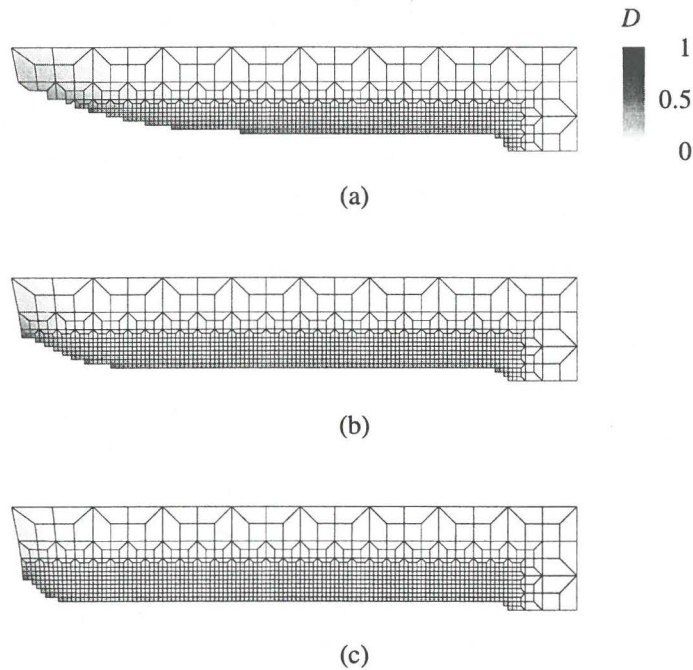


Figure 6.28: Influence of the internal length scale \sqrt{c} on the final damage distribution and crack shape: (a) $\sqrt{c} = 0.1$ mm, (b) $\sqrt{c} = 0.05$ mm and (c) $\sqrt{c} = 0.025$ mm.

length scales. As a consequence, the nonlocal equivalent strain at the notch tip and, after initiation of a crack, at the crack tip is higher, resulting in faster damage growth and thus in faster initiation and growth of the crack. The effect of the length scale on the final crack shape is shown in Figure 6.28. As expected, a smaller length parameter results in a smaller steady-state crack width. Furthermore, this constant crack width is reached after a smaller amount of crack growth as a result of the fact that a smaller area has been damaged before crack initiation.

Chapter 7

Conclusion

The principal objective of the research reported in this thesis was to develop a mathematically consistent continuum damage formulation which can realistically describe fracture processes. A key issue in the development of continuum damage and other continuous fracture models is their ability to correctly describe the localised deformations which are characteristic of fracture problems. If this issue is not properly addressed, the damage process which represents the initiation and growth of cracks tends to localise in a vanishing volume. A perfectly brittle response is then obtained, even if the constitutive relations show a gradual loss of strength. This pathological localisation of damage is usually related to loss of ellipticity of the rate equilibrium equations as a result of material instabilities. When the rate equilibrium equations locally lose ellipticity, discontinuities may arise in the displacement field. Discontinuous displacements imply that the strain field is singular, i.e., that the deformation localises in a vanishing volume. As a consequence, the damage development becomes unstable and a crack is initiated prematurely.

The role of material instabilities and loss of ellipticity in crack growth, however, may sometimes have been overestimated. Singularities at the crack tip may render the damage growth rate singular. The material in front of the crack then fails immediately and in a vanishing volume, even if the rate equilibrium equations do not first lose ellipticity. The crack traverses the remaining cross section at an infinite growth rate and the thickness of the corresponding damage band is zero. This mechanism is not only relevant in time-dependent fracture processes, as suggested by Murakami and Liu (1996), but also in time-independent fracture. Loss of ellipticity may act as a premature initiator of singularities in this situation, but it is the instantaneous crack growth caused by the singular damage rate which renders the fracture process perfectly brittle.

The nonphysical behaviour of the standard models can be effectively removed by the introduction of nonlocality in the constitutive relations. In a strict sense nonlocality means that stresses in a material point are no longer a functional of the deformation history solely in that point – as in standard, local continua – but also of the deformation history in a vicinity of the point. In continuum damage models this concept can be implemented by defining a nonlocal strain measure which is a weighted average of its standard, local counterpart and reformulating the growth of damage in terms of this nonlocal strain. As a result, the localisation of

damage is limited to the scale of the intrinsic length which is introduced by the averaging procedure and which must be related to the microstructure of the material. The damage field thus remains smooth and displacement discontinuities and damage rate singularities are avoided. Crack growth is no longer instantaneous in the enhanced model and a finite, positive volume takes part in the damage process which describes the crack growth, even if the final crack may have a vanishing thickness. This also means that a positive amount of work is needed for the crack growth and that the fracture process is thus no longer perfectly brittle.

A similar effect can be achieved by including nonstandard gradient terms in the constitutive model. In fact, such models can be derived as approximations of the nonlocal formulation. Two forms of this gradient enhancement have been considered in Chapter 4. In the first, so-called explicit approach, second-order strain gradients enter the constitutive model. As a result of the continuity of the deformation field, deformation gradients in a point contain information about the deformation in the surrounding material and therefore introduce a certain nonlocal action. In a mathematical sense, however, the gradients are local quantities and the model is thus local. Indeed, strain variations in a certain point affect the strain gradients – and thus the nonlocal strain and damage – in only an infinitesimal volume around the point.

The situation is subtler in the second, so-called implicit gradient formulation. This model contains gradients of the nonlocal strain instead of the local strain. As a consequence, the nonlocal strain is no longer defined explicitly in terms of the local strain, but as the solution of a partial differential equation in which the local strain appears as a source term. This means that variations of the local strain in a certain point affect the nonlocal strain in the entire domain and thus that the model is truly nonlocal in this sense. Indeed, it has been shown in Chapter 4 that the nonlocal strain which follows from the implicit gradient approach can be written in the integral format of the nonlocal model by formally solving the partial differential equation for the nonlocal strain.

The different character of the nonlocal interactions in the two gradient models has far-reaching consequences for their ability to describe damage localisation and crack growth. The implicit gradient formulation results in smooth solutions without discontinuities or damage rate singularities and shows a qualitative agreement with the corresponding nonlocal model. The response of the explicit model, on the other hand, is fundamentally different and may even be physically unrealistic in some respects. Its applicability to fracture problems is therefore doubtful.

In each of the enhanced damage models the treatment of boundaries must be specified separately. In the nonlocal model the normalisation of the weight function changes in the presence of boundaries. The gradient models require additional boundary conditions for the displacements (explicit gradient model) or the nonlocal strain (implicit gradient model). Homogeneous, natural boundary conditions have been selected for this purpose, but the physical motivation of these conditions is still rather poor. Nevertheless, the treatment of the nonlocality at boundaries may have an important effect on the predicted response. This is particularly true in crack growth problems, where an internal boundary separates the crack from the remaining material. In the gradient models not only the standard dynamic boundary conditions must be applied at this internal boundary, but also the additional boundary conditions required by the gradient enhancement. In the nonlocal model cracked material must be removed from

the weighting volume and the weight function must be renormalised accordingly as the crack grows.

Numerical implementations of the enhanced damage models must reflect the separation of the cracked region from the remaining part of the continuum. This means that the spatial discretisation of the equilibrium problem must be adapted for each increment of crack growth. If this separation is not made rigorously, the damage growth rate may be overestimated and nonphysical damage growth may be predicted at the faces of the crack. The numerical implementation of the implicit gradient model which has been detailed in Chapter 5 is consistent with the underlying continuum model in this respect. Numerical solutions provided by the algorithm have been shown to yield meaningful, mesh objective results. Analyses of quasi-brittle fracture result in stable crack growth and in a finite fracture energy. The predicted damage band is insensitive to the fineness and the orientation of the spatial discretisation, provided that this discretisation is sufficiently fine to describe the strongly heterogeneous deformations in the fracture zone. The fatigue model can describe the formation and growth of high-cycle fatigue cracks. A special time integration scheme has been used to simulate the large numbers of cycles which are characteristic of high-cycle fatigue with an acceptable computational effort. In these analyses cracks have a finite, positive width, which depends on the internal length scale provided by the gradient enhancement, but which is insensitive to the spatial discretisation. Crack growth rates remain finite and are also insensitive to the element size.

Although reliable and useful for development purposes, the numerical implementation which has been used in this thesis is probably not yet suitable for most practical problems. When the location of crack initiation and the direction of crack growth are not known in advance, adaptive spatial discretisation techniques are needed to follow the free boundary which represents the crack and to accurately describe the high deformation gradients at its tip. These requirements are very similar to those of (nonlinear) fracture mechanics and some of the techniques needed may therefore be borrowed from numerical fracture mechanics. Indeed, this 'convergence' of discrete and continuous representations of fracture can be observed not only in their numerical implementations, but also in the underlying theory. In a sense, the continuum damage formulation used in this study already results in a discrete crack. On the other hand, strong discontinuity approaches assume a discrete (fictitious) crack surface, but nevertheless use stress-strain relations from continuum mechanics to model the nonlinearity of the fracture problem (e.g., Oliver, 1996) and can sometimes be regarded as solutions of nonlocal formulations (Planas et al., 1994).

In comparison with the classical fracture mechanics modelling of cracks, continuum damage models and related continuous fracture models are often more complex and have larger parameter sets. Furthermore, the mechanisms represented by these parameters show strong interactions, so that the parameters often cannot be determined independently and an inverse modelling approach is necessary. The nonlocality or gradient enhancement adds a further parameter to these models: the intrinsic length scale which is used to regularise the development of damage. If this length cannot be uniquely determined from the microstructure of the material, it must also be fitted on experimental results. This can be done indirectly, by relating the internal length scale to the difference between homogeneous and heteroge-

neous responses (Bažant and Pijaudier-Cabot, 1989) or to size effects (Pijaudier-Cabot, 1995; Carmeliet, 1996). But a more direct and probably more reliable method is to measure the extent of material damage in experiments, for instance by optical deformation measurements (Geers, 1997; Geers et al., 1998e, 1999b).

The complexity of the constitutive modelling and the number of model parameters further increase when some of the limitations made in this thesis are lifted. The most important of these limitations is probably the lack of permanent deformations. The practical relevance of the damage modelling greatly increases if plastic or viscoplastic terms are added to the constitutive models, since analyses of creep, low-cycle fatigue and ductile fracture then become feasible. Theoretically, the introduction of these terms does not seem to require major changes in the concepts developed here. Indeed, nonlocal damage or damage-like models have already been used to model creep (Saanouni et al., 1989) and ductile fracture (Needleman and Tvergaard, 1998) with a varying degree of success. A second possible extension of the theory is obtained by taking into account the anisotropy exhibited by many engineering materials. This anisotropy may either be intrinsically present in the undamaged material or be introduced by the development of damage. Particularly the latter case may require some reinterpretation since it may involve several damage variables, which generally do not become critical at the same moment.

Despite theoretical, numerical and experimental difficulties, damage mechanics and related local fracture models seem to be gaining interest. An important reason for this development is probably that these models often can be linked more closely to the microstructural processes which govern crack initiation and crack growth in engineering materials than the traditional fracture mechanics approaches. Since the accuracy of existing models can only be improved by including more detail of these processes in the modelling, it is believed that the importance of continuum approaches to fracture will continue to increase in the near future.

Bibliography

- Aifantis, E.C., 1984. On the microstructural origin of certain inelastic models. *J. Eng. Mat. Technol.*, **106**, 326–330.
- Aliabadi, M.H. and Rooke, D.P., 1991. *Numerical Fracture Mechanics*. Kluwer, Dordrecht, The Netherlands.
- Aliabadi, M.H., Cartwright, D.J. and Nisitani, H. (eds.), 1992. *Localized Damage II: Computer Aided Assessment and Control of Localized Damage. Proc. Int. Conf.* Elsevier, London.
- ASTM, 1993. *Annual Book of ASTM Standards*. American Society for Testing and Materials, Philadelphia.
- Atluri, S.N., 1986. *Computational Methods in the Mechanics of Fracture*. North-Holland, Amsterdam.
- Barenblatt, G.I., 1962. The mathematical theory of equilibrium cracks in brittle fracture. *Advances Appl. Mech.*, **7**, 55–129.
- Basquin, O.H., 1910. The exponential law of endurance tests. *Proc. ASTM*, **10**, 625–630.
- Bažant, Z.P., 1991. Why continuum damage mechanics is nonlocal: micromechanics arguments. *J. Eng. Mech.*, **117**, 1070–1087.
- Bažant, Z.P. and Pijaudier-Cabot, G., 1989. Measurement of characteristic length of nonlocal continuum. *J. Eng. Mech.*, **115**, 755–767.
- Bažant, Z.P., Belytschko, T. and Chang, T.P., 1984. Continuum theory for strain-softening. *J. Eng. Mech.*, **110**, 1666–1692.
- Benallal, A., Billardon, R. and Geymonat, G., 1989. Some mathematical aspects of the damage softening rate problem. Mazars, J. and Bažant, Z.P. (eds.), *Cracking and Damage, Strain Localization and Size Effect. Proc. France-US Workshop*, Elsevier, London, 247–258.
- Beran, M.J. and McCoy, J.J., 1970. Mean field variations in a statistical sample of heterogeneous linearly elastic solids. *Int. J. Solids Struct.*, **6**, 1035–1054.
- Berends, A.H., 1996. *Enhanced assumed strain element for fracture*. Internal report 03.21.1.31.20, Faculty of Civil Engineering, Delft University of Technology, Delft, The Netherlands.
- Brekelmans, W.A.M. and de Vree, J.H.P., 1995. Reduction of mesh sensitivity in continuum damage mechanics. *Acta Mechanica*, **110**, 49–56.

- Brekelmans, W.A.M., Schreurs, P.J.G. and de Vree, J.H.P., 1992. Continuum damage mechanics for softening of brittle materials. *Acta Mechanica*, **93**, 133–143.
- Broek, D., 1986. *Elementary Engineering Fracture Mechanics*. 4th edn., Martinus Nijhoff, Dordrecht, The Netherlands.
- Carmeliet, J., 1996. gradient damage and size effects. *Proc. Engineering Mechanics 1996*, ASCE, New York, 1175–1178.
- Chaboche, J.L., 1988. Continuum damage mechanics. Part I – General concepts; Part II – Damage growth, crack initiation, and crack growth. *J. Appl. Mech.*, **55**, 59–64, 65–72.
- Chaboche, J.L. and Lesne, P.M., 1988. A non-linear continuous fatigue damage model. *Fatigue Fract. Eng. Mat. Struct.*, **11**, 1–17.
- Coleman, B.D. and Hodgdon, M.L., 1985. On shear bands in ductile materials. *Arch. Rat. Mech. Anal.*, **90**, 219–247.
- Comi, C., 1998. Computational modelling of gradient-enhanced damage in quasi-brittle materials. *Mech. Cohesive-Frictional Mat.*, **4**, 17–36.
- Comi, C. and Driemeier, L., 1997. On gradient regularization for numerical analyses in the presence of damage. *Proc. IUTAM symposium on Material Instabilities in Solids*.
- Courant, R. and Hilbert, D., 1953. *Methods of Mathematical Physics. Vol. II: Partial Differential Equations*. Wiley, New York.
- de Borst, R., 1986. *Non-linear analysis of frictional materials*. Ph.D. thesis, Delft University of Technology, Delft, The Netherlands.
- de Borst, R. and Mühlhaus, H.-B., 1991. Continuum models for discontinuous media. van Mier, J.G.M., Rots, J.G. and Bakker, A. (eds.), *Fracture Processes in Concrete, Rock and Ceramics. Proc. Int. RILEM/ESIS Conf.*, Chapman & Hall, London, 601–618.
- de Borst, R. and Mühlhaus, H.-B., 1992. Gradient-dependent plasticity: formulation and algorithmic aspects. *Int. J. Num. Meth. Eng.*, **35**, 521–539.
- de Borst, R., Sluys, L.J., Mühlhaus, H.-B. and Pamin, J., 1993. Fundamental issues in finite element analysis of localization of deformation. *Eng. Comp.*, **10**, 99–121.
- de Borst, R., Pamin, J., Peerlings, R.H.J. and Sluys, L.J., 1995. On gradient-enhanced damage and plasticity models for failure in quasi-brittle and frictional materials. *Comp. Mech.*, **17**, 130–141.
- de Borst, R., Benallal, A. and Heeres, O.M., 1996. A gradient-enhanced damage approach to fracture. Pineau, A. and Rousselier, G. (eds.), *Proc. 1st European Mechanics of Materials Conf. on Local Approach to Fracture "86–96"*, *Journal de Physique IV*, vol. 6, 491–502.
- de Borst, R., Benallal, A. and Peerlings, R.H.J., 1997. On gradient-enhanced damage theories. Fleck, N.A. and Cocks, A.C.F. (eds.), *Proc. IUTAM Symposium on Mechanics of Granular and Porous Materials*, Kluwer, Dordrecht, The Netherlands, 215–226.
- de Borst, R., Geers, M.D.G., Kuhl, E. and Peerlings, R.H.J., 1998a. Enhanced damage models for concrete fracture. de Borst, R., Bićanić, N., Mang, H. and Meschke, G. (eds.), *Computational Modelling of Concrete Structures – Proc. EURO-C 1998 Conf.*, Balkema, Rotterdam, 231–248.

- de Borst, R., Geers, M.G.D., Peerlings, R.H.J. and Benallal, A., 1998b. Some remarks on gradient and nonlocal damage theories. Voyiadjis, G.Z., Ju, J.-W. and Chaboche, J.-L. (eds.), *Damage Mechanics in Engineering Materials*, Elsevier, Amsterdam, 223–236.
- de Borst, R., Geers, M.G.D. and Peerlings, R.H.J., 1999. Computational damage mechanics. Carpenteri, A. and Aliabadi, M.H. (eds.), *Computational Fracture Mechanics in Concrete Technology*, Computational Mechanics Publications. To appear.
- de Vree, J.H.P., Brekelmans, W.A.M. and van Gils, M.A.J., 1995. Comparison of nonlocal approaches in continuum damage mechanics. *Comp. Struct.*, **55**, 581–588.
- Dugdale, D.S., 1960. Yielding of steel sheets containing slits. *J. Mech. Phys. Solids*, **8**, 100–108.
- Eringen, A.C. and Edelen, D.G.B., 1972. On nonlocal elasticity. *Int. J. Eng. Sci.*, **10**, 233–248.
- Feenstra, P.H. and de Borst, R., 1996. Composite plasticity model for concrete. *Int. J. Solids Struct.*, **33**, 707–730.
- Fichant, S., Pijaudier-Cabot, G. and La Borderie, C., 1995. Continuum damage modelling with crack induced anisotropy. Owen, D.R.J. and Oñate, E. (eds.), *Computational Plasticity, Fundamentals and Applications. Proc. 4th Int. Conf.*, Pineridge Press, Swansea, U.K., 1045–1056.
- Fleck, N.A. and Hutchinson, J.W., 1993. A phenomenological theory for strain gradient effects in plasticity. *J. Mech. Phys. Solids*, **41**, 1825–1857.
- Frémond, M. and Nedjar, B., 1995. Damage, gradient of damage and principle of virtual power. *Int. J. Solids Struct.*, **33**, 1083–1103.
- Geers, M.D.G., de Borst, R., Peijs, T. and Meuwissen, M.H.H., 1998a. Internal length scales for higher-order damage models in random fibre reinforced composites. Idelsohn, S.R., Oñate, E. and Dvorkin, E.N. (eds.), *Computational Mechanics, New Trends and Applications, Proc. 4th World Congress on Computational Mechanics*, CIMNE, Barcelona.
- Geers, M.D.G., de Borst, R. and Peerlings, R.H.J., 1998b. Inverse characterization of non-local behaviour using digital image correlation. Brillard, A. and Ganghoffer, J.F. (eds.), *Nonlocal Aspects in Solid Mechanics. Proc. EUROMECH colloquium 378*, 143–150.
- Geers, M.G.D., 1997. *Experimental analysis and computational modelling of damage and fracture*. Ph.D. thesis, Eindhoven University of Technology, Eindhoven, The Netherlands.
- Geers, M.G.D., de Borst, R., Brekelmans, W.A.M. and Peerlings, R.H.J., 1997a. Computational damage analysis of short fibre-reinforced composite materials. Oñate, E. and Owen, D.R.J. (eds.), *Computational Plasticity – Proc. 5th Int. Conf.*, CINME, Barcelona, 1176–1185.
- Geers, M.G.D., de Borst, R., Brekelmans, W.A.M. and Peerlings, R.H.J., 1997b. Numerical modelling of failure phenomena in quasi-brittle materials. *Proc. Workshop of the Belgian Society of Mechanical and Environmental Engineering*.
- Geers, M.G.D., de Borst, R. and Peerlings, R.H.J., 1998c. Damage analysis of notched concrete beams loaded in four-point-shear. Mihashi, H. and Rokugo, K. (eds.), *Fracture Me-*

- chanics of Concrete Structures. Proc. FRAMCOS-3, Aedificatio, Freiburg, Germany, 981–992.
- Geers, M.G.D., Peerlings, R.H.J., de Borst, R. and Brekelmans, W.A.M., 1998d. Higher-order damage models for the analysis of fracture in quasi-brittle materials. de Borst, R. and van der Giessen, E. (eds.), *Material Instabilities in Solids*, Wiley, Chichester, U.K., 405–423.
- Geers, M.G.D., de Borst, R., Brekelmans, W.A.M. and Peerlings, R.H.J., 1998e. On the use of local strain fields for the determination of the intrinsic length scale. Bertram, A. and Sidoroff, F. (eds.), *Proc. 2nd European Mechanics of Materials Conf. on Mechanics of Materials with Intrinsic Length Scale: Physics, Experiments, Modelling, and Applications, Journal de Physique IV*, vol. 8, 167–174.
- Geers, M.G.D., de Borst, R., Brekelmans, W.A.M. and Peerlings, R.H.J., 1998f. Strain-based transient-gradient damage model for failure analyses. *Comp. Meth. Appl. Mech. Eng.*, **160**, 133–153.
- Geers, M.G.D., de Borst, R. and Peijs, T., 1999a. Mixed numerical-experimental identification of nonlocal characteristics of random fibre reinforced composites. *Composites Science and Techn.* Accepted.
- Geers, M.G.D., de Borst, R., Brekelmans, W.A.M. and Peerlings, R.H.J., 1999b. Validation and internal length scale determination for a gradient damage model: application to short glass-fibre-reinforced polypropylene. *Int. J. Solids Struct.* Accepted.
- Gradshteyn, I.S. and Ryzhik, I.M., 1994. *Table of Integrals, Series and Products*. 5th edn., Academic Press, Boston.
- Hall, F.R. and Hayhurst, D.R., 1991. Modelling of grain size effects in creep crack growth using a non-local continuum damage approach. *Proc. Royal Soc. London*, **433**, 405–421.
- Hayhurst, D.R., Dimmer, P.R. and Chernuka, M.W., 1975. Estimates of the creep rupture lifetime of structures using the finite element method. *J. Mech. Phys. Solids*, **23**, 335–355.
- Hertzberg, R.W., 1989. *Deformation and Fracture Mechanics of Engineering Materials*. 3rd edn., Wiley, New York.
- Hill, R., 1958. A general theory of uniqueness and stability in elastic-plastic solids. *J. Mech. Phys. Solids*, **6**, 236–249.
- Hill, R., 1962. Acceleration waves in solids. *J. Mech. Phys. Solids*, **10**, 1–16.
- Hillerborg, A., Modéer, M. and Petersson, P.-E., 1976. Analysis of crack formation and crack growth in concrete by means of fracture mechanics and finite elements. *Cement Concr. Res.*, **6**, 773–781.
- Hordijk, D.A., 1991. *Local approach to fatigue of concrete*. Ph.D. thesis, Delft University of Technology, Delft, The Netherlands.
- Hua, C.T. and Socie, D.F., 1984. Fatigue damage in 1045 steel under constant amplitude biaxial loading. *Fatigue Eng. Mat. Struct.*, **7**, 165–179.
- Huerta, A. and Pijaudier-Cabot, G., 1994. Discretization influence on the regularization by two localization limiters. *J. Eng. Mech.*, **120**, 1198–1218.

- Jirásek, M., 1998. Element-free Galerkin method applied to strain-softening materials. de Borst, R., Bićanić, N., Mang, H. and Meschke, G. (eds.), *Computational Modelling of Concrete Structures. Proc. EURO-C 1998 Conf.*, Balkema, Rotterdam, 311–319.
- Kachanov, L.M., 1958. On the time to failure under creep conditions. *Izv. Akad. Nauk. SSSR, Otd. Tekhn. Nauk.*, **8**, 26–31. In Russian.
- Kanninen, M.F. and Popelar, C.H., 1985. *Advanced Fracture Mechanics*. Oxford University Press, New York.
- Krajcinovic, D. and Fonseka, G.U., 1981. The continuous damage theory of brittle materials. Part I: General theory. *J. Appl. Mech.*, **48**, 809–815.
- Kreyszig, E., 1993. *Advanced Engineering Mathematics*. 7th edn., Wiley, New York.
- Larsson, R. and Runesson, K., 1993. Discontinuous displacement approximation for capturing plastic localization. *Int. J. Num. Meth. Eng.*, **36**, 2087–2105.
- Larsson, R. and Runesson, K., 1994. Cohesive crack models derived from localization of damage coupled to plasticity. Mang, H., Bićanić, N. and de Borst, R. (eds.), *Computational Modelling of Concrete Structures. Proc. EURO-C 1994 Int. Conf.*, Pineridge Press, Swansea, U.K., 413–424.
- Lasry, D. and Belytschko, T., 1988. Localization limiters in transient problems. *Int. J. Solids Struct.*, **24**, 581–597.
- Lemaitre, J., 1986. Local approach to fracture. *Eng. Fract. Mech.*, **25**, 523–537.
- Lemaitre, J., 1996. *A Course on Damage Mechanics*. 2nd edn., Springer, Berlin.
- Lemaitre, J. and Chaboche, J.-L., 1990. *Mechanics of Solid Materials*. Cambridge University Press, Cambridge.
- Lemaitre, J. and Doghri, I., 1994. Damage 90: a post processor for crack initiation. *Comp. Meth. Appl. Mech. Eng.*, **115**, 197–232.
- Lemaitre, J. and Plumtree, A., 1979. Application of damage concepts to predict creep-fatigue failures. *J. Eng. Mat. Technol.*, **101**, 284–292.
- Liu, Y. and Murakami, S., 1998. Crack-tip singularity in damaged materials. Voyiadjis, G.Z., Ju, J.-W.W. and Chaboche, J.-L. (eds.), *Damage Mechanics in Engineering Materials*, Elsevier, Amsterdam, 95–114.
- Liu, Y., Murakami, S. and Kanagawa, Y., 1994. Mesh-dependence and stress singularity in finite element analysis of creep crack growth by continuum damage mechanics approach. *Eur. J. Mech. A/Solids*, **13**, 395–417.
- Lublinter, J., Oliver, J., Oller, S. and Oñate, E., 1989. A plastic-damage model for concrete. *Int. J. Solids Struct.*, **25**, 299–326.
- Manson, S.S. and Hirschberg, M.H., 1964. *Fatigue: An Interdisciplinary Approach*. Syracuse University Press, Syracuse, N.Y.
- Marom, E., 1970. Fatigue detection using holographic techniques. Robertson, E.R. and Harvey, J.M. (eds.), *The Engineering Uses of Holography. Proc. Conf.*, Cambridge University Press, Cambridge, 237–247.
- Mazars, J. and Pijaudier-Cabot, G., 1989. Continuum damage theory – application to concrete. *J. Eng. Mech.*, **115**, 345–365.

- Mühlhaus, H.-B. and Aifantis, E.C., 1991. A variational principle for gradient plasticity. *Int. J. Solids Struct.*, **28**, 845–857.
- Mühlhaus, H.-B. and Vardoulakis, I., 1987. The thickness of shear bands in granular materials. *Géotechnique*, **37**, 271–283.
- Murakami, S. and Liu, Y., 1995. Mesh-dependence in local approach to creep fracture. *Int. J. Damage Mech.*, **4**, 230–250.
- Murakami, S. and Liu, Y., 1996. Local approach of fracture based on continuum damage mechanics and the related problems. *Mat. Sci. Res. Int.*, **2**, 131–142.
- Needleman, A., 1988. Material rate dependence and mesh sensitivity in localisation problems. *Comp. Meth. Appl. Mech. Eng.*, **67**, 69–86.
- Needleman, A. and Tvergaard, V., 1994. Mesh effects in the analysis of dynamic ductile crack growth. *Eng. Fract. Mech.*, **47**, 75–91.
- Needleman, A. and Tvergaard, V., 1998. Dynamic crack growth in a nonlocal progressively cavitating solid. *Eur. J. Mech. A/Solids*, **17**, 421–438.
- Oliver, J., 1996. Modelling strong discontinuities in solid mechanics via strain softening constitutive equations. Part I: Fundamentals; Part II: Numerical simulation. *Int. J. Num. Meth. Eng.*, **39**, 3575–3623.
- Oliver, J. and Pulido, D.G., 1998. On the use of strain-softening damage constitutive equations to model cracking of concrete. de Borst, R., Bićanić, N., Mang, H. and Meschke, G. (eds.), *Computational Modelling of Concrete Structures. Proc. EURO-C 1998 Conf.*, Balkema, Rotterdam, 363–372.
- Ortiz, M., Leroy, Y. and Needleman, A., 1987. A finite element method for localized failure analysis. *Comp. Meth. Appl. Mech. Eng.*, **61**, 189–214.
- Ottosen, N.S. and Runesson, K., 1991. Properties of discontinuous bifurcation solutions in elasto-plasticity. *Int. J. Solids Struct.*, **27**, 401–421.
- Paas, M.H.J.W., 1990. *Continuum damage mechanics with an application to fatigue*. Ph.D. thesis, Eindhoven University of Technology, Eindhoven, The Netherlands.
- Paas, M.H.J.W., Schreurs, P.J.G. and Brekelmans, W.A.M., 1993. A continuum approach to brittle and fatigue damage: theory and numerical procedures. *Int. J. Solids Struct.*, **30**, 579–599.
- Peerlings, R.H.J., 1996. *Computational Modelling of Fatigue Failure*. Internal report WFW 96.131, Faculty of Mechanical Engineering, Eindhoven University of Technology, Eindhoven, The Netherlands.
- Peerlings, R.H.J., 1997. *Continuum Damage Modelling of Fatigue Crack Initiation*. Internal report MT 97.037, Faculty of Mechanical Engineering, Eindhoven University of Technology, Eindhoven, The Netherlands.
- Peerlings, R.H.J., de Borst, R., Brekelmans, W.A.M. and de Vree, J.H.P., 1995. Computational modelling of gradient-enhanced damage for fracture and fatigue problems. Owen, D.R.J. and Oñate, E. (eds.), *Computational Plasticity, Fundamentals and Applications. Proc. 4th Int. Conf.*, Pineridge Press, Swansea, U.K., 975–986.

- Peerlings, R.H.J., de Borst, R., Brekelmans, W.A.M. and de Vree, J.H.P., 1996a. Gradient-enhanced damage for quasi-brittle materials. *Int. J. Num. Meth. Eng.*, **39**, 3391–3403.
- Peerlings, R.H.J., de Borst, R., Brekelmans, W.A.M., de Vree, J.H.P. and Spee, I., 1996b. Some observations on localisation in non-local and gradient damage models. *Eur. J. Mech. A/Solids*, **15**, 937–953.
- Peerlings, R.H.J., de Borst, R., Brekelmans, W.A.M. and Geers, M.G.D., 1998a. Gradient-enhanced damage modelling of concrete fracture. *Mech. Cohesive-Frictional Mat.*, **3**, 323–342.
- Peerlings, R.H.J., Brekelmans, W.A.M., de Borst, R. and Geers, M.G.D., 1998b. Softening, singularity and mesh sensitivity in quasi-brittle and fatigue damage. Brillard, A. and Ganghoffer, J.F. (eds.), *Nonlocal Aspects in Solid Mechanics, Proc. EUROMECH Colloquium 378*, 94–99.
- Peerlings, R.H.J., de Borst, R., Brekelmans, W.A.M. and Geers, M.G.D., 1998c. Wave propagation and localisation in nonlocal and gradient-enhanced damage models. Bertram, A. and Sidoroff, F. (eds.), *Proc. 2nd European Mechanics of Materials Conf. on Mechanics of Materials with Intrinsic Length Scale: Physics, Experiments, Modelling, and Applications, Journal de Physique IV*, vol. 8, 293–300.
- Pietruszczak, S. and Mróz, Z., 1981. Finite element analysis of deformation of strain-softening materials. *Int. J. Num. Meth. Eng.*, **17**, 327–334.
- Pijaudier-Cabot, G., 1995. Non-local damage. Mühlhaus, H.-B. (ed.), *Continuum models for materials with Microstructure*, Wiley, Chichester, U.K., 105–143.
- Pijaudier-Cabot, G. and Bažant, Z.P., 1987. Nonlocal damage theory. *J. Eng. Mech.*, **113**, 1512–1533.
- Pijaudier-Cabot, G. and Benallal, A., 1993. Strain localization and bifurcation in a nonlocal continuum. *Int. J. Solids Struct.*, **30**, 1761–1775.
- Pijaudier-Cabot, G. and Burlion, N., 1996. Damage and localisation in elastic materials with voids. *Mech. Cohesive-Frictional Mat.*, **1**, 129–144.
- Pijaudier-Cabot, G. and Huerta, A., 1991. Finite element analysis of bifurcation in nonlocal strain softening solids. *Comp. Meth. Appl. Mech. Eng.*, **90**, 905–919.
- Pijaudier-Cabot, G., Bažant, Z.P. and Tabbara, M., 1988. Comparison of various models for strain-softening. *Eng. Comp.*, **5**, 141–150.
- Ping, O., 1984. The laser speckle spectrum correlation method and its application in damage mechanics. *Advances in Surface Treatments – Technology, Applications, Effects*, Pergamon, Oxford, 233–236.
- Planas, J., Elices, M. and Guinea, G.V., 1994. Cohesive cracks as a solution of a class of nonlocal models. Bažant, Z.P., Bittnar, Z., Jirásek, M. and Mazars, J. (eds.), *Fracture and Damage in Quasibrittle Structures – Experiment, modelling and computer analysis. Proc. US-Europe Workshop*, E & FN Spon, London, 131–144.
- Rabotnov, Y.N., 1969. *Creep Problems in Structural Members*. North-Holland, Amsterdam.
- Rice, J.R., 1976. The localization of plastic deformation. Koiter, W.T. et al. (eds.), *Theoretical*

- and Applied Mechanics. Proc. 14th IUTAM Congress, North-Holland, Amsterdam, 207–220.
- Rots, J.G. and de Borst, R., 1989. Analysis of concrete fracture in 'direct' tension. *Int. J. Solids Struct.*, **25**, 1381–1394.
- Rudnicki, J.W. and Rice, J.R., 1975. Conditions for the localization of deformation in pressure-sensitive dilatant materials. *J. Mech. Phys. Solids*, **23**, 371–394.
- Saanouni, K., Chaboche, J.-L. and Lesne, P.M., 1989. On the creep crack-growth prediction by a non local damage formulation. *Eur. J. Mech. A/Solids*, **8**, 437–459.
- Schlangen, E., 1993. *Experimental and numerical analysis of fracture processes in concrete*. Ph.D. thesis, Delft University of Technology, Delft, The Netherlands.
- Schreyer, H.L. and Chen, Z., 1986. One-dimensional softening with localization. *J. Appl. Mech.*, **53**, 791–797.
- Shah, S.P. and Maji, A.K., 1989. Experimental observation of cracking and damage. Mazars, J. and Bažant, Z.P. (eds.), *Cracking and Damage, Strain Localization and Size Effect. Proc. France-US Workshop*, Elsevier, London, 15–29.
- Simo, J.C., 1989. Strain softening and dissipation: a unification of approaches. Mazars, J. and Bažant, Z.P. (eds.), *Cracking and Damage, Strain Localization and Size Effect. Proc. France-US Workshop*, Elsevier, London, 440–461.
- Simo, J.C., Oliver, J. and Armero, F., 1993. An analysis of strong discontinuities induced by strain-softening in rate-independent inelastic solids. *Comp. Mech.*, **12**, 277–296.
- Sluys, L.J., 1992. *Wave propagation, localisation and dispersion in softening solids*. Ph.D. thesis, Delft University of Technology, Delft, The Netherlands.
- Sluys, L.J., 1997. Discontinuous modelling of shear banding. Oñate, E. and Owen, D.R.J. (eds.), *Computational Plasticity. Proc. 5th Int. Conf.*, Pineridge Press, Swansea, U.K., 735–744.
- Sluys, L.J., 1998. Modelling of crack propagation with embedded discontinuity elements. Mihashi, H. and Rokugo, K. (eds.), *Fracture Mechanics of Concrete Structures. Proc. FRAMCOS-3*, Aedificatio, Freiburg, Germany, 843–860.
- Sluys, L.J. and Berends, A.H., 1998. Discontinuous failure analysis for mode-I and mode-II localization problems. *Int. J. Solids Struct.*, **35**, 4257–4274.
- Sluys, L.J. and de Borst, R., 1994. Dispersive properties of gradient-dependent and rate-dependent media. *Mech. Mat.*, **18**, 131–149.
- Suresh, S., 1991. *Fatigue of Materials*. Cambridge University Press, Cambridge, U.K.
- Triantafyllidis, N. and Aifantis, E.C., 1986. A gradient approach to localization of deformation. I Hyperelastic materials. *J. Elasticity*, **16**, 225–237.
- Tvergaard, V. and Needleman, A., 1995. Effects of non-local damage in porous plastic solids. *Int. J. Solids Struct.*, **32**, 1063–1077.
- van Mier, J.G.M., 1997. Personal communication.
- Williams, J.G., 1973. *Stress Analysis of Polymers*. Longman, London.

- Zauderer, E., 1989. *Partial Differential Equations of Applied Mathematics*. 2nd edn., Wiley, Chichester, U.K.

Samenvatting

Continue-schademechanica kan gebruikt worden om zowel de vorming als de groei van scheuren te beschrijven. In deze theorie wordt microstructurele schade in materialen in een gemiddelde zin gerepresenteerd door een continue variabele. Voor een zekere kritieke waarde van deze schadevariabele verliest het materiaal lokaal zijn samenhang en ontstaat er dus een scheur. Voortzetting van het belastingsproces leidt tot voortplanting van de scheur (gerepresenteerd door het gebied waarin de schadevariabele kritiek is) door middel van schadegroei en herverdeling van spanningen. De snelheid en richting van scheurgroei worden bepaald door de schadegroei in een relatief klein gebied voor de scheurtip, in plaats van door de aparte scheurgroecriteria die in de breukmechanica worden gebruikt.

Numerieke simulaties die gebaseerd zijn op standaard schademodellen blijken echter vaak sterk beïnvloed te worden door de ruimtelijke discretisatie van het probleem. De schadegroei vertoont de neiging zich te concentreren in het kleinste gebied dat nog door de ruimtelijke discretisatie beschreven kan worden. Als gevolg hiervan wordt voor fijnere discretisaties eerder de vorming van een scheur voorspeld, die bovendien sneller groeit. In de limiet van een oneindige ruimtelijke resolutie wordt de dikte van de schadezone nul en plant de scheur zich oneindig snel voort, zonder dat daarvoor arbeid nodig is. Dit in fysisch opzicht onrealistische gedrag wordt veroorzaakt door het feit dat de lokalisering van schade in een vlak niet in overeenstemming is met de veronderstelling van een continue schadeverdeling die ten grondslag ligt aan de continue-schademechanica.

De oorzaken van de lokalisering van schade zijn onderzocht voor schademodellen van quasi-brosse breuk en vermoeiing. Twee effecten spelen een belangrijke rol. Ten eerste kan het stelsel van partiële differentiaalvergelijkingen dat de snelheid van deformatie bepaalt op een zeker moment zijn ellipticiteit verliezen. Als gevolg hiervan kunnen discontinuïteiten ontstaan in het verplaatsingsveld, die leiden tot een singuliere schadegroeisnelheid. De singulariteit van de schadegroei leidt op haar beurt tot de onmiddellijke vorming van een scheur. Ten tweede resulteert de singuliere schadegroei aan de tip van een eenmaal gevormde scheur onmiddellijk in falen van het materiaal voor de scheur. Omdat de singulariteit van de schadegroeisnelheid blijft bestaan wanneer de scheur groeit, treedt onmiddellijk volledige breuk op. Dit effect doet zich niet alleen voor bij voortijdige scheurinitiatie als gevolg van verplaatsingsdiscontinuïteiten, maar ook als de schadevariabele op een stabiele wijze kritiek is geworden.

Verplaatsingsdiscontinuïteiten en singulariteiten in de schadegroei kunnen voorkomen worden door niet-lokaliteit toe te voegen aan de schademodellering. In de niet-lokale schademechanica worden daartoe ruimtelijke gemiddelden geïntroduceerd. Het verbeterde model

dat hieruit voortvloeit resulteert in gladdere schadevelden, waarin de lokalisering van schade beperkt blijft tot de lengteschaal die geïntroduceerd wordt door de middeling. Hierdoor wordt de voortijdige vorming van scheuren voorkomen en blijft de voorspelde scheurgroei snelheid eindig.

Een soortgelijk effect kan bereikt worden door hogere-orde deformatiegradiënten op te nemen in het constitutieve model. Twee van dit soort verbeteringen zijn onderzocht; beide kunnen afgeleid worden als benaderingen van het niet-lokale model. In het eerste type worden tweede-orde rekgradiënten expliciet opgenomen in de spanning-rekrelaties. De tweede aanpak definieert de afhankelijkheid van hogere-orde gradiënten op een meer impliciete wijze, via een partiële differentiaalvergelijking die moet worden opgelost naast de evenwichtsvergelijkingen. Vooral deze laatste, impliciete benadering is in vele opzichten equivalent met het niet-lokale model. In het bijzonder kan worden aangetoond dat het impliciete gradiëntenmodel ook de ruimtelijke interacties over langere afstanden vertoont die karakteristiek zijn voor het niet-lokale model.

Het impliciete gradiëntenmodel kan relatief eenvoudig in een eindige-elementenformulering gegoten worden. Scheurgroei wordt gerepresenteerd door elementen waarin de schade kritiek is geworden te verwijderen uit de discretisatie. Deze aanpassing van de discretisatie is noodzakelijk om onrealistische schadegroei aan het scheuroppervlak ten gevolge van interacties tussen scheur en het omliggende materiaal te voorkomen.

De eindige-elementenformulering is gebruikt om quasi-brosse breuk en vermoeiingsbreuk te simuleren. De berekende schadezones hebben een eindige dikte, die afhangt van de intrinsieke lengteschaal die samenhangt met de gradiënttermen. Het quasi-brosse model laat een stabiele afname van sterkte zien, die goed overeenkomt met experimentele gegevens. Het vermoeiingsmodel resulteert in scheurvorming na een eindig aantal belastingscycli en in scheurgroei met een eindige groeisnelheid. Voor beide breukmechanismen zijn de numerieke analyses niet langer gevoelig voor de ruimtelijke discretisatie.

Dankwoord

Dit proefschrift zou nooit het licht gezien hebben zonder de hulp en ondersteuning van een aantal collega's. Op het gevaar af anderen tekort te doen, wil ik diegenen die daarin voor mijn gevoel verder zijn gegaan dan ik van hun had kunnen verwachten speciaal bedanken. Allereerst denk ik aan mijn begeleiders, René de Borst en Marcel Brekelmans. Zij hebben me in staat gesteld mijn werk te doen zoals dat bij eerste-geldstroom onderzoek naar mijn mening hoort: met veel vrijheid en ruimte voor zijnsprongen. Ik heb mijn best gedaan om het vertrouwen dat hieruit spreekt niet te beschamen.

Dank ook aan Vivian van Gansewinkel en Ivanka Spee, die in het begin van het project een bijdrage hebben geleverd in het kader van stages. Hoewel ze het zich misschien niet altijd gerealiseerd hebben, heeft hun werk veel bijgedragen aan mijn begrip van de materie en daarmee aan dit proefschrift. Marc Geers bedank ik voor de laatste correcties en voor vele vruchtbare discussies, soms op het scherpst van de snede, maar altijd in een plezierige sfeer. Nuttige opmerkingen heb ik ook gekregen van Olaf van der Sluis en van Henk de Vree, onder wiens hoede ik ooit mijn eerste, voorzichtige stappen in de wereld van de schademechanica heb gezet.

Met veel plezier denk ik terug aan de tijd die ik met mijn kamergenoten Peter Kessels en Maykel Verschueren heb doorgebracht onder de nok van W-Hoog. Het was boeiend te praten over elkaars werk, waarin we ondanks onze verschillende werkterreinen allerhande onvermoede parallellen ontdekten. Maar nog boeiender was de verbale communicatie (in de ruimste zin van het woord) over de meest uiteenlopende andere zaken. Zonder deze intermezzo's zouden de afgelopen vier jaar zeker veel minder snel voorbij zijn gegaan.

Op het sociale vlak heeft het schrijven van dit proefschrift meer offers gevraagd dan ik me vooraf had kunnen voorstellen. Vooral gedurende de laatste maanden hebben mijn ouders, familie en vrienden mij minder gezien dan zij en ik wellicht gewild hadden. Diegenen die te maken hebben gehad met lange radiostiltes, of met gezeur over deadlines, achterstand en tegenslagen, wil ik oprecht bedanken voor hun geduld en begrip. Ik beloof mijn best te doen om een en ander snel in te halen.

Ron Peerlings
Weert, december 1998

Curriculum vitae

- 18 maart 1971 geboren te Weert
- augustus 1983 – juni 1989 gymnasium β , Bisschoppelijk College Weert
- september 1989 – november 1994 studie werktuigbouwkunde, Technische Universiteit Eindhoven
- december 1994 – januari 1995 werkzaam aan het Laboratoire de Mécanique et Technologie, ENS de Cachan / CNRS / Université Pierre et Marie Curie, Cachan, Frankrijk
- februari 1995 – januari 1999 assistent in opleiding, faculteit Werktuigbouwkunde, Technische Universiteit Eindhoven

Stellingen

behorende bij het proefschrift

Enhanced damage modelling for fracture and fatigue

1. Klassieke lokaliseringscriteria, gebaseerd op homogene referentietoestanden, kunnen niet zonder meer worden toegepast op de sterk inhomogene deformaties rond scheuren.
 - Rice, J.R., 1976. The localization of plastic deformation. Koiter, W.T. et al. (eds.), *Theoretical and Applied Mechanics. Proc. 14th IUTAM Congress*, North-Holland, Amsterdam, 207–220.
 - Dit proefschrift, Hoofdstuk 3.
2. Bij breukproblemen spelen singulariteiten aan de scheurtip een minstens zo belangrijke rol in de lokaliseringsproblematiek als discontinuïteiten in het verplaatsingsveld; dit geldt niet alleen in de schademechanica, maar ook in plasticiteit.
 - Liu, Y., Murakami, S. and Kanagawa, Y., 1994. Mesh-dependence and stress singularity in finite element analysis of creep crack growth by continuum damage mechanics approach. *Eur. J. Mech. A/Solids*, **13**, 395–417.
 - Dit proefschrift, Hoofdstuk 3.
3. De ‘impliciete’ gradiënt-schadeformulering kan met recht niet-lokaal genoemd worden. De naamgeving van deze en vergelijkbare formuleringen is dan ook verregaand arbitrair.
 - Dit proefschrift, Hoofdstuk 4.
4. Realistische wiskundige beschrijvingen van scheurgroei leiden noodzakelijkerwijs tot vrije-randproblemen. Het niet in acht nemen van dit gegeven kan numerieke moeilijkheden veroorzaken.
 - Dit proefschrift, Hoofdstuk 5.
5. De theoretische en praktische verschillen tussen discrete en continue breukmodelleringen worden vaak sterk overdreven.
 - de Borst, R., Feenstra, P.H., Pamin, J. and Sluys, L.J., 1994. Some current issues in computational mechanics of concrete structures. Mang, H. et al., *Computational Modelling of Concrete Structures. Proc. EURO-C 1994 Int. Conf.*, Pineridge Press, Swansea, U.K., 283–302.
 - Dit proefschrift, Hoofdstuk 7.

6. De ontwikkeling van (niet-destructieve) schadedetectie-technieken is ver achter gebleven bij de theoretische modelvorming van schadeprocessen. Als gevolg hiervan kunnen schademodellen veelal alleen indirect gevalideerd worden.
7. Numerieke methoden behoren te worden aangepast aan het voorliggende wiskundige probleem en niet andersom.
8. Soms is het nodig het wiel opnieuw uit te vinden om de werking ervan goed te begrijpen.
9. Elegante oplossingen zijn vaak ook de beste.
10. 'Principieel' wordt niet alleen op de basisschool regelmatig verward met 'in principe'.

Ron Peerlings

Eindhoven, 23 maart 1999

Bibliotheek

Technische Universiteit Eindhoven

Postbus 90159
5600 RM
Eindhoven



Telefoon (040) 24 72224

9900647